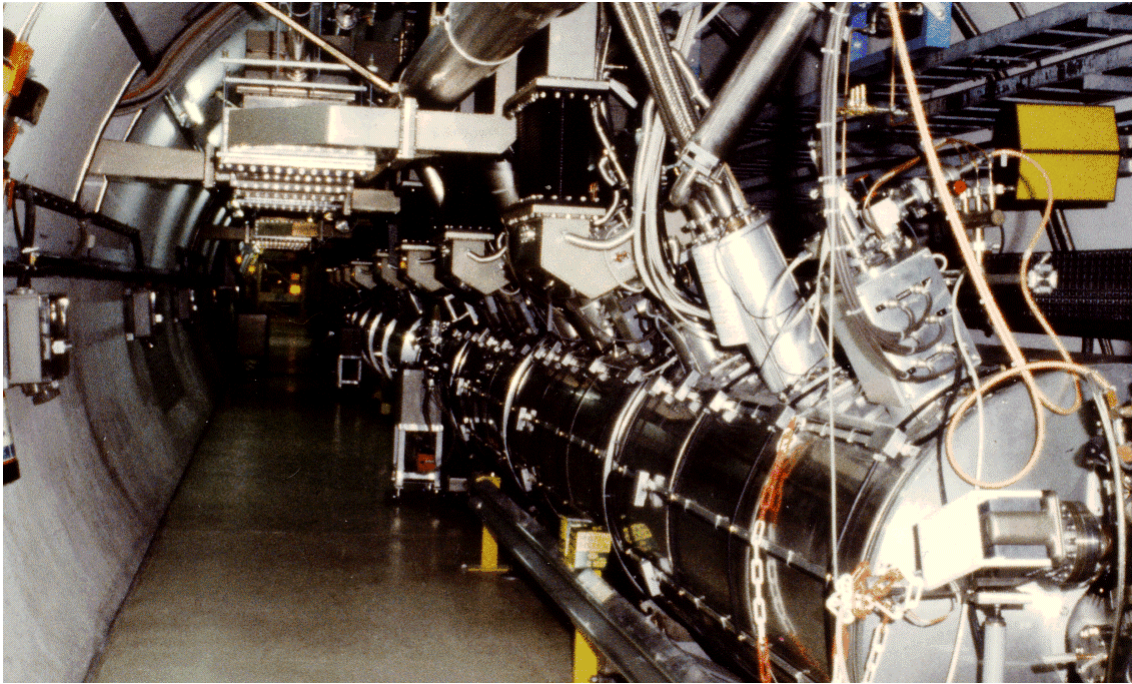


Glossary .....	iv
1. Introduction .....	1
2. Basics .....	3
2.1 Secondary electron emission .....	3
2.1.1 The energy distribution of the emitted electrons .....	3
2.1.2 The secondary electron yield (SEY) .....	4
2.1.3 The SEY as a function of the primary electron energy .....	4
2.1.4 Influence of adsorbed layers of another species on the SEY .....	5
2.1.5 Influence of the work function on the SEY .....	5
2.1.6 Influence of the surface structure on the SEY .....	5
2.2 Air .....	6
2.3 Copper and copper oxidation .....	7
2.4 Vacuum basics .....	9
2.4.1 Kinetic theory of gases .....	9
2.4.2 The mean free path $\bar{l}$ of a gas molecule .....	9
2.4.3 The monolayer time $\tau$ .....	9
2.4.4 Gas flow regimes .....	9
2.4.5 Pumping speed $S$ and throughput $Q$ .....	10
2.4.6 Conductance $C$ .....	10
2.5 Analytical techniques employed to characterise the sample surfaces .....	11
2.5.1 Scanning electron microscopy (SEM) .....	11
2.5.2 Energy dispersive X-ray analysis (EDX) .....	11
2.5.3 Auger electron spectroscopy (AES) .....	12
3. The Experimental System .....	13
3.1 The electron gun .....	15
3.2 The vacuum system .....	16
3.2.1 The pumping system .....	17
3.2.2 Total pressure measurement .....	20
3.2.3 Partial pressure measurement .....	23
4. Experimental Procedures .....	25
4.1 The cleaning of the samples .....	25
4.1.1 Bakeout .....	25
4.1.2 Glow discharge cleaning .....	25

4.2 Gas exposures .....	28
4.2.1 Air exposure.....	28
4.2.2 Pure water vapour exposure.....	28
4.2.3 Pure oxygen exposure.....	29
4.3 Error estimation .....	31
5. Results.....	32
5.1 Influence of an air exposure on the SEY of initially clean copper.....	32
5.2 Influence of a pure oxygen exposure on the SEY of initially clean copper .....	34
5.3 Influence of a pure water vapour exposure on the SEY of initially clean copper.....	35
5.4 Influence of the other gases in air.....	35
5.5 Influence of a pure water vapour exposure on oxidised copper .....	36
5.6 Influence of a bakeout on the SEY .....	36
5.7 Influence of an air exposure at high temperature .....	38
5.8 Influence of an air exposure on the SEY of copper oxidised at 350°C in air .....	40
5.9 Conditioning of the LEP2 power couplers together with copper plated extensions which were heated in air at 350°C .....	41
6. Discussion and Outlook.....	43
References .....	45
Appendix .....	47
Acknowledgments .....	65

## 1. Introduction

Superconducting cavities have been developed to accelerate particles in powerful particle accelerators like the Large Electron Positron collider (LEP) at CERN. They are necessary to provide the high accelerating gradients that are needed to compensate the large energy loss of the particles by synchrotron radiation. Superconducting cavities are also more efficient in converting the mains power to the beam power and, hence, less power consuming than normal conducting cavities /1/.



*Figure 1; Module consisting of four superconducting cavities installed in the LEP tunnel*

The performance of such superconducting radio frequency (RF) resonators can be severely hampered by the phenomenon of multipacting.

Multipacting or resonant electron loading is an avalanche-like electron multiplication that can occur in high vacuum. If multipacting is initiated the growing electron avalanche absorbs the input RF power. Furthermore, the bombarding electrons can desorb high amounts of tightly adsorbed gases from the cavity surface, thus spoiling the cavity vacuum. Finally, the cooled cavity walls can be locally heated up by absorption of a part of the electrons energy, resulting in a transition from the superconducting to the normalconducting state (quench).

Two conditions have to be fulfilled to initiate multipacting:

- the primary electrons are resonant with the RF field, i.e., they hit the same target again after an even number of RF half cycles (one surface multipacting) or they hit another target after an odd number of RF half cycles (two surface multipacting) /2/.
- each impacting primary electron liberates more than one secondary electron, i.e., the secondary electron yield (SEY) of the target material is higher than unity.

Therefore, it is important to know the SEY of the materials used in superconducting cavities in order to avoid, or at least to limit multipacting. Copper is used to coat auxiliary equipment like power couplers, where multipacting is often observed.

The SEY of pure copper can be found in literature. However, secondary electrons are emitted from the upper monolayers of a surface only and the SEY is strongly influenced by surface contamination. The large LEP cavities have to be exposed to air during installation or modification. The gases present in air interact with the surfaces during the time of exposure and, as a consequence, the SEY after exposure differs from the yield of a clean surface.

This work studies the effects which air exposures of different duration have on the SEY of clean and technical, i.e., contaminated copper surfaces at room temperature and at elevated temperatures.

## 2. Basics

### 2.1 Secondary electron emission

When electrically charged particles with sufficient kinetic energy impinge on a solid surface, this surface emits electrons. The emitted electrons are called secondary electrons and the bombarding particles are called primary particles. For this work only the emission induced by primary electrons is of interest.

#### 2.1.1 The energy distribution of the emitted electrons

The energy of emitted secondary electrons varies from very low energies up to the primary electrons energy. A typical energy distribution for all metals is shown in Figure 2.

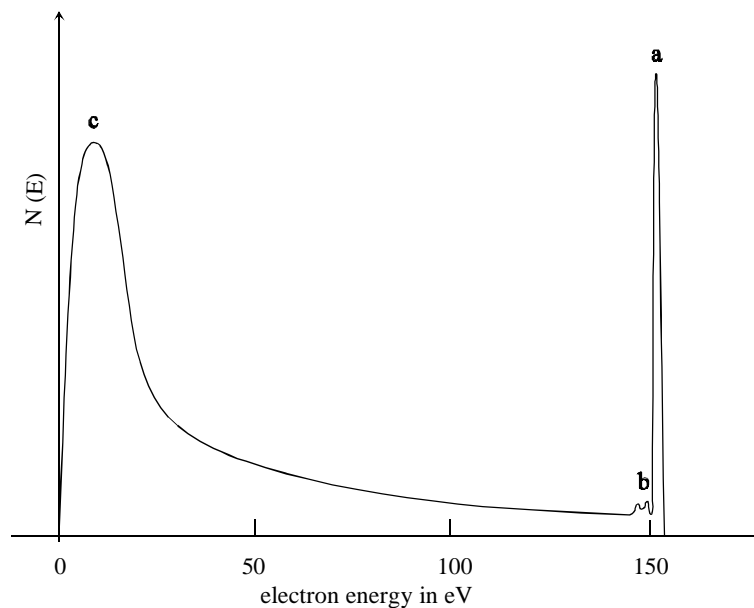


Figure 2; Energy distribution of electrons emitted by silver upon bombardment with 155 eV primary electrons /3/

One distinguishes mainly between three groups of secondary electrons. These are true secondary electrons, inelastically backscattered primary electrons and elastically reflected primary electrons.

The peak indicated by *a* corresponds to elastically reflected primary electrons.

Most emitted electrons have low energies, corresponding to the peak indicated by *c*. These are referred to as true secondary electrons, indicating that they are electrons which originally occupied bound states in the crystal. As it is impossible to determine the origin of individual electrons one usually regards all emitted electrons with an energy below 50 eV as true secondary electrons.

The emitted electrons with energies between 50 eV and the primary energy are then referred to as inelastically reflected primary electrons, i.e., incident electrons which have been backscattered after losing part of their energy in the solid.

The two small peaks near *b* correspond to emitted electrons with discrete energies. They are called Auger electrons and can be used to determine the different atomic species present on a surface (see 2.5.3).

### 2.1.2 The secondary electron yield (SEY)

Different definitions for the SEY exist. The following four coefficients can be found in literature [4]:

- 1)  $\eta$ : backscatter coefficient, i.e., the number of backscattered electrons (energies >50 eV) per incident primary electron.
- 2)  $\delta_s$ : the number of true secondary electrons per incident primary electron.
- 3)  $\delta_t$ : ratio of the true secondary electrons and the number of the primary incident electrons without the backscattered electrons. This coefficient is sometimes called the true yield, because the backscattered electrons are lost for the process of electron emission.
- 4)  $\delta$ : the total number of emitted secondary electrons per incident primary electron, i.e., the secondary electron current  $i_{sec}$  divided by the primary electron current  $i_p$ .

$$\delta = \frac{i_{sec}}{i_p} \quad \text{Equation 1}$$

The first three coefficients are useful for the experimental verification of the theory of secondary electron emission. As far as multipacting is concerned only the total SEY  $\delta$  is relevant and hence this definition will be followed throughout this work.

### 2.1.3 The SEY as a function of the primary electron energy

The SEY of a solid depends on the energy of the primary electrons. Primary electrons with very low energy can only liberate few secondary electrons. On the other hand, high energetic electrons will penetrate deeply into the bulk and deposit most of their energy in regions where the liberated secondary electrons are not able to escape. Between those two cases the maximum SEY  $\delta_{max}$  is found.

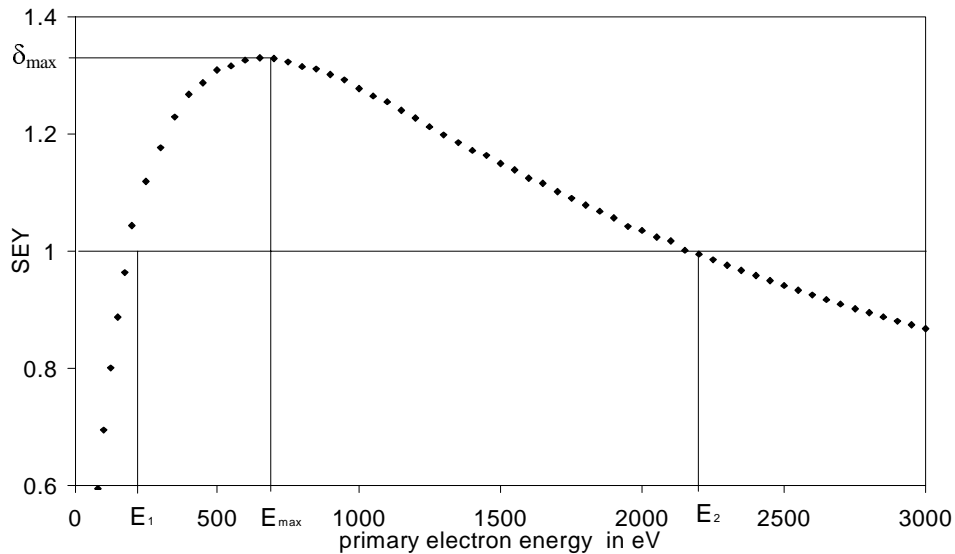


Figure 3; Total SEY  $\delta$  of copper in dependence of the primary electron energy

Figure 3 shows the SEY of copper as a function of the primary electron energy. This curve can be described by the following characteristic values:

- $\delta_{\max}$ : maximum SEY  
 $E_{\max}$ : energy at which  $\delta_{\max}$  is attained  
 $E_1$ : energy below which the SEY is less than unity  
 $E_2$ : energy above which the SEY is less than unity

For metals the maximum SEY varies between 0.5 (lithium) and 1.8 (platin). For copper it is 1.3. The yield of elemental semiconductors is also of the order of unity /5/. The maximum SEY of insulators is considerably higher than that for metals and semiconductors. Quartz, as an example, has a maximum SEY of about 3. For other insulators yields up to 10 have been measured /6/.

#### 2.1.4 Influence of adsorbed layers of another species on the SEY

The maximum escape depth of secondary electrons from metals is estimated as 10 atomic layers /7/. Assuming a thickness of 4 Å for one atomic layer, the emitted electrons origin from the upper 4 nm of the solid. The likeliness for the low energetic secondary electrons to pass through a condensate layer of adsorbed gases is higher. The escape depth of secondary electrons in such layers is about 100 monolayers.

The SEY of a condensate layer can differ strongly from that of the base material. The SEY of water condensed on a silver target at 77 K is about 2.3 /8/. If the condensate layer is only a few atomic layers thick, the proportion of secondary electrons which are emitted there is small compared with the number of secondaries emitted from the base material. On the other hand, the electron emission will be determined by the condensate layer only if it is thicker than the maximum escape depth of the secondary electrons. For a condensate some 10 monolayers thick one can assume a SEY between that of the base material and that of the pure condensate.

However, it is not evident if the change of the SEY is due to electrons which have been liberated in the adsorbed layer or to a change of the work function of the base material.

#### 2.1.5 Influence of the work function on the SEY

The work function of a metal can be changed by the adsorption of atoms of another species onto the base material. The work function of copper for instance can be increased by the adsorption of oxygen and it can be decreased by the adsorption of water vapour.

Electron emission processes like photo-electric emission or thermionic emission depend strongly on the work function of the emitting material. Compared to these processes the influence of the work function on the SEY is much smaller. This can be explained by the fact that the mean energy of the secondary electrons is considerably higher than that of electrons emitted by the other processes.

Effects on the SEY are reported mainly for the adsorption of atoms which decrease the work function /3/. For atoms which increase the work function like oxygen on tungsten it is reported that they have only a slight influence on the SEY.

In a more recent theoretical investigation Hachenberg and Brauer claim that the influence of the surface on the SEY may be neglected in satisfactory approximation /9/.

#### 2.1.6 Influence of the surface structure on the SEY

The surface structure of a material can have a decisive influence on the SEY. Layers consisting of very small crystallites do not present a reflecting surface but are rather optically black. Such

microcrystalline layers have much lower yields than smooth layers [3]. Carbon in the form of soot for example has a SEY of 0.5. The yield of a smooth carbon layer is higher than 1.

The small SEY of a microcrystalline layer can be explained as follows. Once a secondary electron passes through the surface of a smooth layer it meets no more obstacles and hence it contributes to the SEY. On the other hand, secondary electrons which have been liberated in a labyrinthine structure are likely to face other microcrystals and a big fraction will be absorbed before they can escape from the surface. This is illustrated in Figure 4.

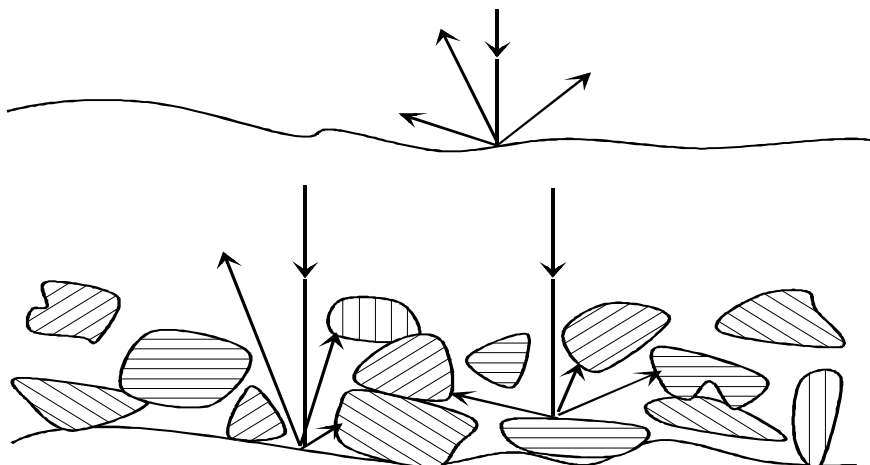


Figure 4; Influence of the surface roughness on the SEY. From a smooth surface the emitted electrons are more likely to escape than from a rough surface.

## 2.2 Air

At sea level air consists mainly of 791 mbar  $N_2$ , 212 mbar  $O_2$ , 9.4 mbar Ar and 0.3 mbar  $CO_2$ . It also contains gaseous pollutants like  $SO_2$ ,  $NH_3$ , NO or ozone which can have a strong impact on corrosion processes.

Water vapour is another constituent of air and it is the most detrimental for vacuum applications. Furthermore, it is essential to the formation of an electrolyte solution that supports electrochemical corrosion reactions. The concentration of water vapour in the atmosphere is usually expressed in terms of the relative humidity. This is defined as the ratio of the actual partial pressure of the water vapour in the atmosphere compared to that which would saturate the atmosphere at the same temperature. Most corrosion processes depend strongly on the relative humidity. The relative humidity of common indoor atmospheres is about 60%. In other environments like storage huts or the housing of large accelerators it can be much more critical.

The behaviour of the water molecules is strongly influenced by their shape. The two hydrogen atoms are attached to the oxygen atom in such a way to make an angle of  $104.5^\circ$ . This makes the water molecule a dipole because the electrons are closer to the oxygen atom. Hence, the oxygen corner of the molecule has a slightly negative charge and the hydrogen ends are slightly positively charged. The negative part of one water molecule attracts the positive part of another molecule, which causes a comparatively strong sticking of the molecules to each other. This is the reason for the unusual properties of water. It has a very high heat capacity and the ability to dissolve many different substances. It is also responsible for the high vapour pressure of  $H_2O$  at room temperature (23 mbar at  $20^\circ C$ ) compared to gases with a similar mass.



## 2.3 Copper and copper oxidation

Copper is the metallic, chemical element of atomic number 29. It has the electronic configuration 2.8.18.1. Loss of the outermost electron gives the cuprous ion  $\text{Cu}^+$ , and a second electron may be lost in the formation of the cupric ion  $\text{Cu}^{2+}$ .

Cu consists of the two stable isotopes Cu63 (69.1%) and Cu 65 (30.9%) and has an atomic weight of 63.5. The melting point of pure copper is 1083°C and its boiling point is 2563°C.

Copper is frequently used for many technical applications, mainly because of its excellent thermal and electrical conductivity, its good workability and its high corrosion resistance. For ultra high vacuum applications Cu is favourable because of its low gas solubility (relatively low outgassing) and its vacuum tightness which allows the employment of relatively thin-walled apparatus.

After the extraction of copper from its ores it is available as low purity crude copper with about 2% impurities. The crude copper can then be refined by electrolysis (electrolytic copper). To purify Cu electrolytically, the impure Cu is made the anode in an electrolytic cell. A thin sheet of already purified Cu acts as the cathode. With a suitable electrolyte and appropriate operating conditions very pure ETPC (electrolytic tough pitch copper) can be deposited on the cathode.

ETPC contains some oxygen, chiefly as  $\text{Cu}_2\text{O}$ . Oxygen lowers the melting point, the strength and the conductivity of the pure copper. It also leads to fine cracks if heated in  $\text{H}_2$  atmosphere ('hydrogen sickness'). This is due to  $\text{H}_2$ , which readily diffuses into heated Cu and combines with the oxygen present to water vapour:



The water vapour has a low diffusion rate in copper and so builds up pressures of several thousand bar in the bulk, leading to microscopic cracks /10/.

The amount of oxygen can be reduced by heating the copper in a carbon monoxide atmosphere. CO is not soluble in Cu but combines readily with the oxygen at the copper surface. This phenomenon is utilised to produce the so called OFHC (oxygen-free high-conductivity) copper. OFHC copper is immune against the hydrogen embrittlement (as long as it has not been oxidised by heating it in air or oxygen).

For ultra high vacuum equipment, which usually has to be bakeable, OFHC copper can be used. OFHC-regular contains less than 0.05% impurities. Particularly suitable for high vacuum applications is OFHC-certified, which contains less than 0.02% impurities. The purest grade of copper commercially available is GFHP (gas-free high purity) copper with a minimum copper content of 99.993%.

The vapour pressure and the rate of evaporation of copper are relatively high. Therefore, the operating temperature of vacuum equipment should not exceed 550°C.

Copper can be oxidised to cuprous oxide ( $\text{Cu}_2\text{O}$  or copper(I)-oxide) and to cupric oxide ( $\text{CuO}$  or copper(II)-oxide).

The reddish  $\text{Cu}_2\text{O}$  is a p-type semiconductor formed by the chemical process:



Pure  $\text{CuO}$  is black and it can be formed when powdered copper is heated in air or oxygen:



Bulk copper under the same conditions forms a mixture of CuO and Cu<sub>2</sub>O. At room temperature in dry air a thin, invisible film of Cu<sub>2</sub>O is formed. At temperatures higher than 250°C the surface tarnishes. Then it consists of an adherent inner layer of Cu<sub>2</sub>O and a comparatively thin outer layer of the black CuO. At higher temperatures the amount of CuO existing is determined by the pressure of oxygen /11/.

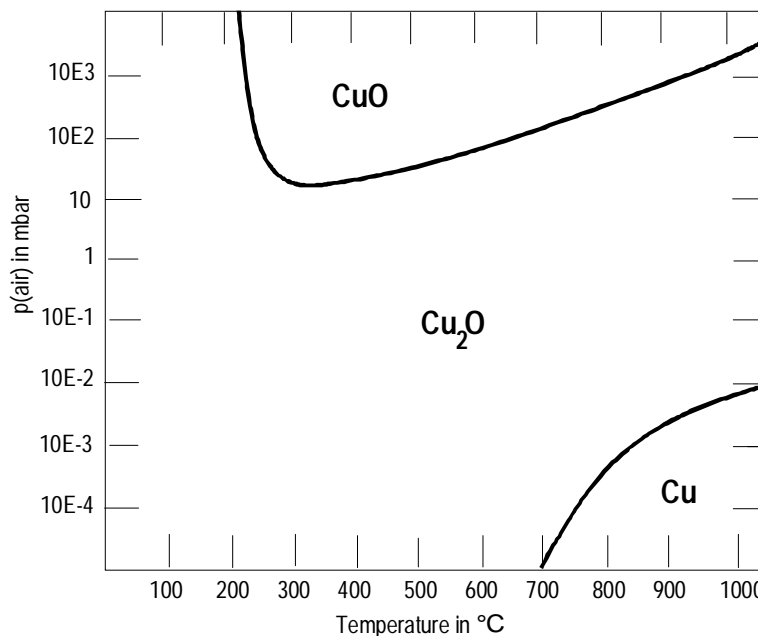


Figure 5; Temperature/pressure regions of formation of Cu<sub>2</sub>O and CuO /12/

Figure 5 shows the dependence of the oxygen pressure and temperature on the oxide film composition. The oxygen pressure/temperature curves enclose the regions in which CuO or Cu<sub>2</sub>O is the outermost oxide of the film. The decomposition pressure of CuO at 1000°C corresponds approximately with the partial pressure of oxygen in air. Therefore, at temperatures above 1000°C only Cu<sub>2</sub>O is formed in air.

For the corrosion reaction to proceed, copper ions and electrons have to migrate through the Cu<sub>2</sub>O layer, which is predominantly responsible for protection /13/. Hence, the rate of oxidation decreases with the thickness of the Cu<sub>2</sub>O layer.

At temperatures up to 100°C the oxide film grows linearly with the logarithm of time and above 400°C the oxidation of Cu follows the parabolic law /14/.

In dry air at atmospheric pressure and room temperature Cu is not attacked superficially. However, in moist air containing carbon dioxide Cu initially darkens because of the build up of a thin layer of black CuO. After several years a bluish green layer of basic copper carbonate called patina is formed.

An oxidation of Cu by pure water vapour takes not place even at high temperatures up to 1000°C /15/.

Besides heating copper in air, cuprous oxide can be formed for example by anodic oxidation of copper or by reactive sputtering of copper in gas mixtures including oxygen.

Because of its comparatively low dissociation pressure cuprous oxide can be used as oxidiser in a catalytic pump for hydrogen pumping. In such a pump molecular hydrogen is dissociated by means of a hot metal filament (atomising catalyst) and the atomic hydrogen is absorbed on a

cuprous oxide layer where it is oxidised to  $\text{H}_2\text{O}$ . The water vapour is desorbed and condenses finally on a liquid nitrogen trap. A  $\text{Cu}_2\text{O}$  temperature of  $200^\circ\text{C}$  has been found to be sufficient to rapidly desorb the produced  $\text{H}_2\text{O}$  from the cuprous oxide [16].

## 2.4 Vacuum basics

### 2.4.1 Kinetic theory of gases

For calculations in vacuum technology one assumes the gas molecules as pointlike particles which only interact elastically and are not able to condense at the ambient temperature. Such a gas is called a perfect gas and it can be described by the perfect gas law:

$$p \cdot V = N \cdot k \cdot T \quad \text{Equation 5}$$

where  $p$ ,  $V$  and  $T$  correspond to the gas pressure, volume and absolute temperature respectively.  $N$  is the number of molecules and  $k$  is Boltzmann's constant.

The result of continual elastic collisions and exchange of energy of the residual gas molecules is the Maxwell-Boltzmann velocity distribution. The mean velocity  $\bar{c}$  (arithmetic mean value) of a gas particle can be calculated:

$$\bar{c} = \sqrt{\frac{8R \cdot T}{\pi \cdot M}} \quad \text{Equation 6}$$

with the molar mass  $M$  and the molar gas constant  $R$ .

### 2.4.2 The mean free path $\bar{l}$ of a gas molecule

The mean free path  $\bar{l}$  is the distance which every molecule travels on the average between two collisions with other particles. It is a function of the particle diameter  $2r$  and the number density of molecules  $n$ . In good approximation it can be calculated as:

$$\bar{l} = \frac{1}{\pi \sqrt{2} \cdot n \cdot (2 \cdot r)^2} \quad \text{Equation 7}$$

### 2.4.3 The monolayer time $\tau$

The time which is needed for the formation of a monomolecular or monatomic layer on a substrate surface is called the monolayer time  $\tau$ .

$$\tau = \frac{4 \cdot a}{n \cdot c} \quad \text{Equation 8}$$

With the assumption that every particle arriving at this surface sticks to it,  $\tau$  is proportional to the number of free places  $a$  on the surface and inversely proportional to the number of molecules hitting the surface per unit time and hence the pressure.

### 2.4.4 Gas flow regimes

Whenever there is a directed net movement of gas in a system under the influence of pumps, the gas flows. Three different regimes of gaseous flow exist. These are viscous flow, Knudsen flow

and molecular flow. The kind of flow depends on the geometry of the vacuum system as well as the pressure, temperature and type of the present gas.

The molecular flow occurs at low gas densities when the mean free path of the gas molecules is greater than the diameter of the conducting tube. In this region the gas molecules have virtually no influence on each other and their motion is strictly random.

Viscous flow prevails in rough vacuum when the mean free path of the gas molecules is much smaller than the dimensions of the vacuum system. The mutual interactions of the particles with each other determine the character of this regime so that the flow is limited by its viscosity. At low gas velocities the flow is laminar where parallel flow lines may be imagined. At higher velocity the flowing gas layers are no longer parallel but cross each other. This condition is called turbulent flow.

At pressures where the mean free path of the molecules is similar to the dimensions of the vacuum enclosure, the flow of the gas is governed by viscosity as well as by molecular phenomena. This regime is called Knudsen flow or intermediate flow.

The expressions rough-, medium- and high vacuum are related to the flow regimes viscous-, Knudsen- and molecular flow respectively.

#### 2.4.5 Pumping speed $S$ and throughput $Q$

The pumping speed  $S$  is defined as the volume  $V$  of gas passing through a pump per unit time  $t$ .

$$S = \frac{dV}{dt} \quad \text{Equation 9}$$

The throughput  $Q$  describes the gas load which is removed by a pump per unit time. It is defined as the product of the pumping speed and the pressure  $p$  at the pump inlet, i.e.,

$$Q = S \cdot p \quad \text{Equation 10}$$

#### 2.4.6 Conductance $C$

The throughput of gas through any conducting element is proportional to the difference between the pressures at the entrance and at the exit of the conducting element.

$$Q = C(p_2 - p_1) \quad \text{Equation 11}$$

The constant  $C$  in this equation is called the conductance between the two points where  $p_1$  and  $p_2$  were measured. Hence, the conductance is a figure which describes the likeliness for the gas molecules to travel through a vacuum enclosure according to its geometry. Therefore, short pipes with large cross sections have a high conductance.

In the molecular flow regime the conductance is independent of the pressure. In the viscous flow region the conductance is a function of the pressure and its effective value is larger than that in the molecular flow regime.

For a tube which length  $l$  is big compared with its inner diameter  $d_i$ , the conductance for gas molecules with a mean velocity  $\bar{c}$  can be calculated:

$$C = \frac{\pi}{12} \cdot \frac{d_i^3}{l} \cdot \bar{c} \quad \text{Equation 12}$$

When conductances are joined in series, the system conductance  $C_{\text{sys}}$  is given by:

$$\frac{1}{C_{\text{sys}}} = \frac{1}{C_1} + \frac{1}{C_2} + \frac{1}{C_3} + \dots \quad \text{Equation 13}$$

One can imagine a perfect pump as a conductance with an inlet pressure  $p$  and an outlet pressure of zero. The pumping speed of such a pump  $S$  is then equal to its conductance and it is determined by its effective cross section only. If this pump is joined to a vacuum vessel via a vacuum pipe with a conductance  $C$ , the effective pumping speed  $S_{\text{eff}}$  can be calculated:

$$\frac{1}{S_{\text{eff}}} = \frac{1}{S} + \frac{1}{C} \quad \text{Equation 14}$$

## 2.5 Analytical techniques employed to characterise the sample surfaces

### 2.5.1 Scanning electron microscopy (SEM)

A commonly used tool to investigate surface structures is the SEM. The samples have to be placed in a high vacuum chamber and an electron beam is scanned over the chosen surface area.

Several signals resulting from this primary electron bombardment can be detected and imaged. The most common image mode detects the low energetic secondary electrons (in 2.1.1 referred to as true secondary electrons). They originate from a surface depth no larger than several Å. The signal is captured by a so called Everhart-Thornley detector which consists basically of a scintillator-photomultiplier combination. The detector output serves to modulate the intensity of a cathode ray tube, which is rastered in synchronism with the primary beam.

Contrast variation can be caused by the difference in secondary electron emission of the materials present on the investigated surface. The topological contrast, however, has much more influence on the image. Different incident angles of the primary electrons result in variations of the secondary electron emission. At edges the volume from which secondary electrons can escape is particularly high and as a result edges appear brightest on the screen.

The image magnification is the ratio of scan lengths on the cathode ray tube to that on the specimen. If the area on the screen is kept constant, the magnification is determined by the size of the surface area above which the primary beam is scanned.

The resolution of the SEM is mainly limited by the minimum spot size of the primary beam which can be achieved with a sufficiently high signal to noise ratio. The highest with a SEM attainable lateral resolution is about  $50 \text{ Å} / 17^\circ$ . Apart from the high resolution, the great depth of focus is a major advantage of the SEM.

Backscattered electrons can also be detected for imaging. The probability of backscattering increases with the atomic number  $Z$  of the sample material. Therefore, contrast can develop between regions of the sample that differ widely in  $Z$ . Since the escape depth for high energetic backscattered electrons is much greater than for low energetic secondary electrons, there is much less topographical contrast in such images.

### 2.5.2 Energy dispersive X-ray analysis (EDX)

X-rays are another signal emitted by the samples in a SEM under electron bombardment. Besides bremsstrahlung, a discrete spectrum of characteristic X-rays can be detected in order to identify the emitting atoms. Characteristic X-rays are emitted, when an electron from an outer shell

lowers its energy by filling an electron vacancy in an inner shell, which has been created by interaction of the atom with a primary electron. If the number of X-rays of a certain energy is counted, the concentration of atoms in a specimen can be determined.

An X-ray detector registers the emitted photons and delivers pulses with a voltage amplitude proportional to the photon energy. These pulses are amplified and then sorted according to their amplitude by a multichannel analyser. This analyser also counts and stores the number of pulses within given increments of the voltage range. The result is an X-ray spectrum, characteristic for the elements present on the investigated sample area.

Lowenergetic photons are absorbed by the window which protects the X-ray detector from contamination. For this reason, it is difficult to detect elements with a low  $Z$ . With a standard detector only elements with an atomic number higher than 10 can be registered /18/. The spectral resolution of energy dispersive X-ray analysis systems is limited to about 150 eV.

### 2.5.3 Auger electron spectroscopy (AES)

Instead of characteristic X-rays, electrons with a characteristic energy can be emitted by excited atoms when they decay to their ground state. These are called Auger-electrons and they can serve to identify the emitting atoms. The processes of Auger transition and X-ray emission go on simultaneously. In the low- $Z$  elements, the probability is greater that an Auger transition will occur, whereas X-ray emission is favoured for elements with a high  $Z$ .

When the Auger transitions occur within a few angstroms of the surface, the Auger electrons may be ejected from the surface without loss of energy and contribute to the total spectrum of ejected electrons at a distinct characteristic energy (see 2.1.1). The Auger peaks appearing in the energy distribution  $N(E)$  are small compared with the background current and the use of  $N(E)$  is in general inadequate for analytical purposes. Instead the differential distribution  $dN(E)/dE$  is recorded. The differentiation can largely eliminate the background and makes the peaks more easy to identify.

The sensitivity of the Auger technique is determined by the transition probability of the Auger transitions involved, the incident beam current and energy and by the collection efficiency of the analyser. With a 3 keV, 50  $\mu\text{A}$  beam and a high sensitivity cylindrical mirror analyser, the limit of detection for the elements varies between approximately 0.02 and 0.2 atomic percent with scanning rates of 1 eV per second /19/. Apart from hydrogen and helium all elements can be detected by AES.

Since the escape depth of the Auger electrons is only a few atomic layers, AES has a high depth resolution. A depth profile can be obtained if the sample surface is continuously removed by sputter etching and the Auger peaks for the elements of interest are monitored simultaneously.

### 3. The Experimental System

The measurements were carried out with the apparatus shown in principle in Figure 6. It consists basically of an electron gun, a collector for the emitted electrons, a revolving sample holder and the vacuum equipment that is necessary to achieve a base pressure in the low  $10^{-10}$  mbar region.

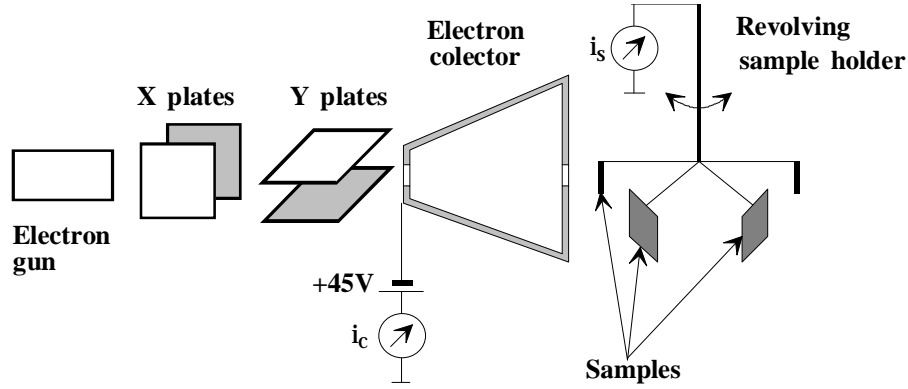


Figure 6; Experimental set-up for the measurement of the total SEY  $\delta$

The revolving sample holder allows to charge the experiment with up to 14 samples.

The electrons are accelerated in the electron gun to energies between 60 eV and 3 keV. They are then guided by electrostatic deflection plates through a hole in the collector onto the sample. The collector is biased at +45V with respect to ground in order to capture all secondary electrons which are emitted by the sample and also to re-capture secondary electrons which are emitted by the collector itself. Only a small fraction of backscattered electrons can escape.

The sample current  $i_s$  and the collector current  $i_c$  are measured simultaneously. The collector current equals the secondary electron current provided, the backscattering current is negligible compared to the true secondary current. Two current amplifiers Keithley 427 are used as electrometers and the signals are digitised by an AD-converter. The data acquisition is realised with a PC driven by LabVIEW.

The total SEY is calculated as follows:

$$\delta = \frac{i_c}{i_c + i_s} \quad \text{Equation 15}$$

where the sum of the sample current  $i_s$  and the collector current  $i_c$  represents the beam current  $i_b$ .

$$i_b = i_s + i_c \quad \text{Equation 16}$$

Before the measurements a special program optimises the voltage at the deflection plates for every primary energy in order to have the maximum possible beam current reaching the samples.

The SEY of a material can be changed by primary electron bombardment, particularly if the surface contains adsorbed layers of a foreign species [20]. To avoid this, low primary electron currents of typically  $5 \cdot 10^{-9}$  A and a pulse length of 300 ms are used to have a sufficiently high signal to noise ratio without affecting the SEY by primary electron bombardment. With an estimated beam area of  $1 \text{ mm}^2$  the electron dose for one measurement is  $1.5 \cdot 10^{-9} \text{ C/mm}^2$ .

The Keithley current amplifiers have an accuracy of 1% in the relevant range. As a result of this uncertainty and the calculation of the SEY, which is specific for the used set-up, the random error of the SEY measurements is strongly depending on the SEY itself. The deviation of the calculated  $\delta$  values in the worst case, i.e., the measured collector current is the true current  $i_{c,true} - 1\%$  and the measured sample current is the true current  $i_{s,true} + 1\%$ , is plotted as a function of the real SEY in Figure 7. The highest  $\delta$  value which was measured during this work is 2.5. In the worst case this yield differs 0.08 from the real SEY.

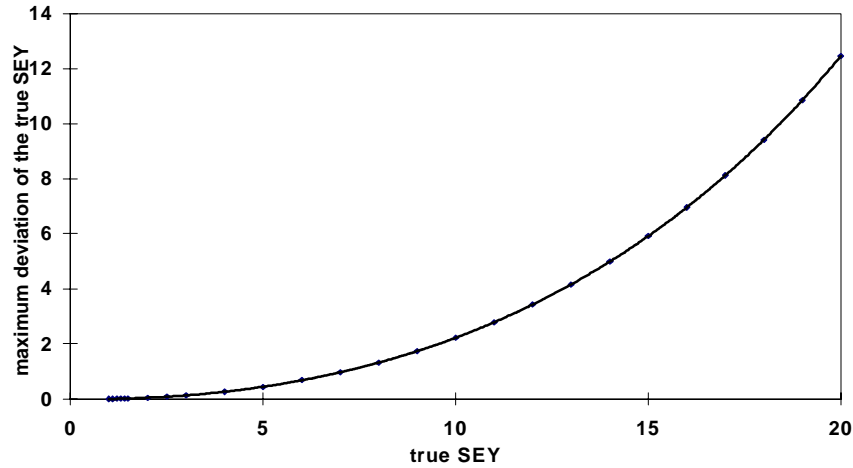


Figure 7; Maximum deviation of the true total secondary electron yield as a function of the true yield itself

Some insulators give SEY values higher than 10 and for condensed noble gases like argon or xenon values above 40 have been measured. For such high SEY values the random error of the used set-up would not be tolerable anymore. In those cases the primary electron current has to be measured directly, e.g., with a positively biased dummy sample which is removed after the primary electron current has been measured. The disadvantage of this kind of measurement is that electron beam instabilities can falsify the results.



### 3.1 The electron gun

A thermionic electron gun, Riber CER 306, provides the electrons which are accelerated to the desired energy and focused onto the sample surfaces. The gun consists basically of the electron emitting cathode, the Wehnelt cup, the anode, an electrostatic lens and two pairs of deflection plates which guide the electron beam.

The electrons are ejected from the cathode by thermionic emission, i.e., the electrons from the Fermi level of the cathode material overcome the work function by thermionic excitation. The cathode is made from a tungsten wire, which is bent into a hair-pin. Its emission current density  $j$  can be determined with the Richardson law

$$j = A_R \cdot T^2 \cdot e^{\frac{-\Phi}{k \cdot T}} \quad \text{Equation 17}$$

where  $A_R$  represents the Richardson factor.  $T$  is the absolute temperature of the filament,  $\Phi$  the work function of the cathode material and  $k$  is Boltzmann's constant. Tungsten has a Richardson factor  $A_R = 60 \text{ Acm}^{-2}\text{K}^{-2}$  and its work function  $\Phi = 4.53 \text{ eV}$  [21].

Unlike secondary electron emission, thermionic electron emission is strongly influenced by the work function of the emitting material (see 2.1.5). As a result, the emission current changes if the work function is changed due to absorbed gases. This was observed during injection of oxygen in the vacuum system at  $10^{-6}$  mbar during operation of the electron gun (absorbed oxygen increases the work function of tungsten). The electron beam current was reduced almost by a factor 2, whereas the SEY of the investigated samples was not changed. The stability of the emission current of the hot cathode is an important feature of electron guns (and of hot cathode gauges). For both applications one can only expect reliable measurements once the filament temperature has become stable and after an equilibrium of adsorbing and desorbing molecules has been established.

The electrons are accelerated in the electric field between the negatively biased cathode and the grounded anode. A maximum potential difference of 3 keV can be applied, resulting in a maximum primary electron energy of 3 keV.

The introduction of a so-called Wehnelt cup which is negatively biased with respect to the cathode allows to concentrate the electron emission within a small area of the filament tip. The Wehnelt voltage is regulated together with the focusing lens and the deflection plates during beam adjustment for every primary electron energy. A special program co-ordinates the different voltages such that the beam current which reaches the sample has a maximum value.

The maximum electron beam current of the Riber CER 306 electron gun is 150  $\mu\text{A}$ . The beam diameter is typically 1 mm. It depends on the Wehnelt voltage and on the distance between the gun and the target.

### 3.2 The vacuum system

SEY measurements can easily be falsified by surface contamination of the samples. To avoid this it is necessary to carry out the measurements in ultra high vacuum at pressures where the monolayer time is several hours (see 2.4.3). A schematic view of the vacuum system is shown in Figure 8. It consists basically of the vacuum vessel, the vacuum pumps and the gauges for total and partial pressure measurement.

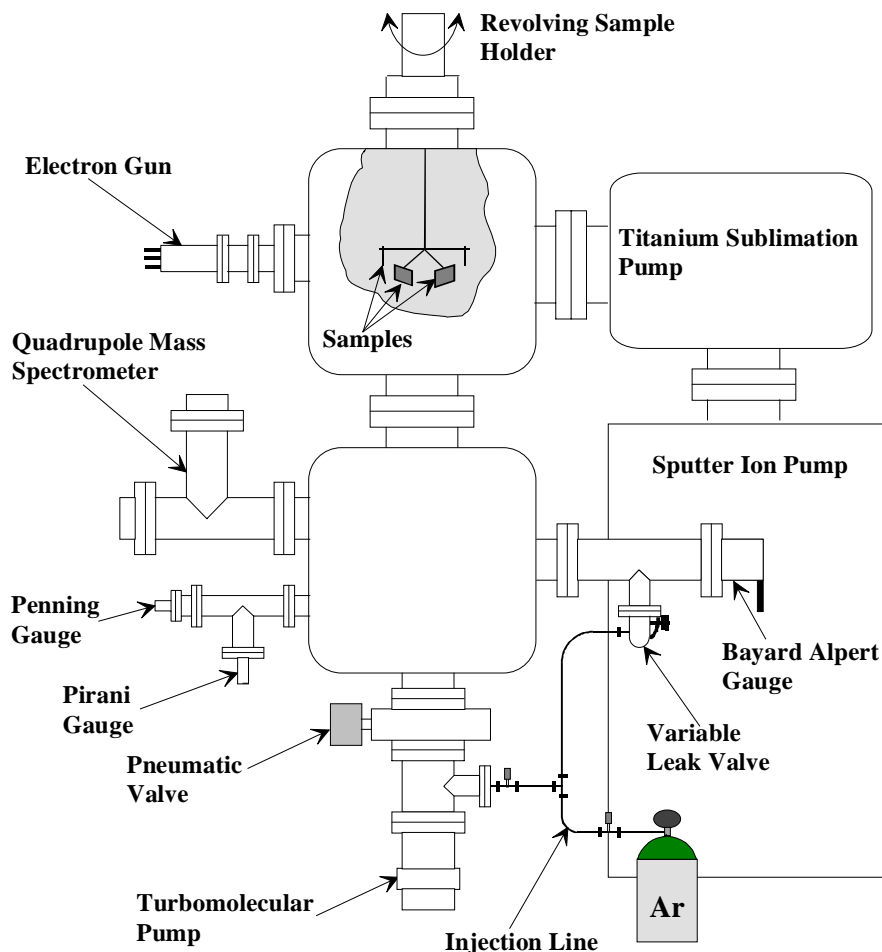


Figure 8; Schematic view of the vacuum system

The vacuum vessel is made of stainless steel and only metallic seals are used to allow a bakeout of the vessel at 350°C.

Pumping is provided by a sputter ion pump and a titanium sublimation pump. A turbomolecular pump, which is backed by an oil-sealed rotary vane pump, serves mainly to evacuate the system from atmospheric pressure to  $10^{-7}$  mbar and it is usually valved off after bakeout.

Three kinds of gauges are used to monitor the total pressure over 13 orders of magnitude. From atmospheric pressure to  $10^{-2}$  mbar a Pirani gauge is used. In the medium and high vacuum range the pressure is measured with a Penning gauge, and a Bayart-Alpert gauge is used for precise measurements in the ultra high vacuum range.

For partial pressure measurements a quadrupole mass spectrometer with a secondary electron multiplier is used.

### 3.2.1 The pumping system

#### 3.2.1.1 Turbomolecular pump

Turbomolecular pumps are mechanical pumps, which work in the molecular flow region, where the mean free path of the molecules is larger than the geometrical dimensions of the pump itself. Therefore, those pumps usually require a backing pressure of some  $10^{-3}$  mbar.

The pump consists mainly of rotor- and stator disks which are arranged alternately. The rotor is turning with high frequency and gas particles which are hit by the rapidly moving rotor surfaces receive an additional impulse in the required flow direction /22/. Due to the appropriate configuration of rotor- and stator blades, the transmission of molecules from the low pressure to the high pressure side is larger than for the inverse direction.

One rotor and one stator make one compression stage. In order to achieve a high compression ratio a turbomolecular pump consists of several stages. The compression ratio for different gases is also dependent on the size and the mean velocity of the gas molecules. The higher the blade speed is relative to the velocity of the gas molecules, the better the gas is pumped and consequently the compression ratio is lowest for  $H_2$ . For the pumping process the blade angle, blade spacing and the ratio of the molecular velocity to the blade speed are of major importance.

The pumping speed is determined by the conductance of the inlet rotor and by the transmission probability of the gases through the pump. The rotor axis diameter is typically half the inlet diameter and as a result the pumping speed is in principle limited to 75% of the conductance of the pump inlet. However, only some 40% of all nitrogen molecules entering the flange of a turbomolecular pump are finally removed from the vacuum system /22/. Except hydrogen, the pumping speed is about the same for all gases because conductance is inversely proportional to the square root of the molecular weight and the transmission probability is roughly directly proportional to the square root of the molecular weight.

The blade speed has at least to be similar to the molecular velocity in order to influence the molecules direction effectively. This makes it necessary to rotate the blades with a frequency of up to  $90000 \text{ min}^{-1}$ , depending on the rotor diameter. The corresponding speed of the blade tips of modern pumps is higher than 300 m/s.

An important feature of a turbomolecular pump is the kind of bearing which keeps the rotor in its proper position. The most common bearings are oil or grease lubricated ball bearings and magnetic bearings. Turbomolecular pumps with magnetic bearings cause less vibrations than those with mechanical ball bearings because the rotor is mechanically isolated from the pump body. This makes them more suitable for vibration sensitive applications like scanning electron microscopes. They are also favourable if a hydrocarbon free vacuum is required. On the other hand, pumps with magnetic bearings are much more sensitive for mechanical shock and improper venting and they are more expensive than pumps with ball bearings.

Turbomolecular pumps can pump an unlimited quantity of gas without becoming saturated. They are also convenient because they have a constant pumping speed in the molecular flow region (as long as backstreaming gases can be neglected) and no 'remembered' gases are released during operation. The residual gas composition of a clean, baked vacuum system pumped by a turbomolecular pump is dominated by  $H_2$ .

A turbomolecular pump with ball bearings, Balzers TPU 060, is used to evacuate the vacuum chamber until the getter pumps can be operated. The nominal pumping speed for air is 56 l/s. A splinter shield reduces the pumping speed by 15% to 48 l/s.

The mean velocity of air ( $M = 29$ ) at a temperature of 293 K is 462 m/s (equation 8). The conductance for air of the connecting tube DN63 with an inner diameter of  $d_i = 70$  mm and a length of  $l = 200$  mm can be calculated as 207 l/s. Equation 14 holds only for tubes which length is big compared to their diameter. As this is not the case, the calculated conductance has to be corrected by a factor  $\psi = 0.6$  ( $\psi$  is a correction factor for short tubes as a function of  $l/d_i$ ) [23]. Hence, the conductance of the connecting tube is 124 l/s and the effective pumping speed for air of the turbomolecular pump  $S_{\text{eff}} = 35$  l/s (equation 16).

### 3.2.1.2 Rotary-vane pump

A two stage, oil sealed rotary vane pump Alcatel 2004 A with a pumping speed of 4.8 m<sup>3</sup>/h provides the backing pressure of about  $10^{-2}$  mbar, which is necessary to operate the turbomolecular pump.

This type of pump belongs to the group of positive displacement pumps. These are pumps in which a volume filled with gas is cyclically isolated from the pump inlet, and then transferred to the outlet after the gas has been compressed.

For a rotary vane pump this is achieved by means of an eccentrically placed, slotted rotor, which turns in a cylindrical stator. In the slots are sliding vanes which are kept in continuous contact with the stator walls under the action of springs. The gas to be pumped is drawn into the stator via the pump inlet and then compressed and expelled through an exhaust valve. A lower base pressure can be attained with two-stage pumps, where the exhaust from the first stage is connected to the inlet of the second stage. The ultimate pressure of oil sealed pumps is limited in principle by the vapour pressure of the pump oil, which serves also as lubricant and provides the heat transfer from the rotor and stator to the pump casing.

Mineral oils are flammable and they are oxidised during pumping of enriched oxygen atmospheres which makes them lose their lubricating properties. Gases containing more than 30% oxygen can therefore not be pumped with rotary vane pumps containing mineral oils.

### 3.2.1.3 Titanium-sublimation pump

The titanium-sublimation pump as well as the sputter-ion pump are getter pumps. In such pumps the gas molecules are mainly retained by chemical combination with an internal getter-surface. Titanium and tantalum are the most common getter materials. As the capacity of a getter-surface is limited, fresh getter films have to be deposited before the pump is saturated. The titanium-sublimation pump differs from the sputter-ion pump basically in the deposition of an active getter film.

The most common sublimation pump consists of a resistively heated titanium-molybdenum filament from which titanium is sublimated as a getter film onto any surrounding surfaces.

The pumping speed of this kind of pump can be very high and it depends on the surface area and the temperature of the titanium layer. Therefore, some pumps allow cooling of the active surfaces with liquid nitrogen (cryosublimation pumps). The specific pumping speed of active titanium surfaces at a temperature of 77 K is about 10 ls<sup>-1</sup>cm<sup>-2</sup> for N<sub>2</sub>, O<sub>2</sub> and CO and about 40 ls<sup>-1</sup>cm<sup>-2</sup> for H<sub>2</sub>.

The sublimation pump is used as a simple, additional pump in ultra-high-vacuum, where it can provide an additional high pumping speed for all active gases. Noble gases are practically not pumped. In the used set-up a complete getter film is deposited after bakeout of the whole vacuum system and also when the pumping speed is reduced because of saturation of the titanium layer.

The titanium-sublimation pump and the sputter ion pump are completely sealed from the atmosphere and no backing pump is needed once the operating pressure of the getter pumps has been achieved. These pumps are therefore immune against vacuum contamination due to power outages or mechanical failures.

#### 3.2.1.4 *Sputter-ion pump*

A Leybold triode sputter ion pump with a pumping speed of 200 l/s for N<sub>2</sub> is the main pump of the vacuum system. Sputter ion pumps are also based on the gettering action of freshly deposited titanium layers but unlike sublimation pumps they employ a Penning discharge to deposit an active surface. These pumps employ a Penning discharge to deposit an active getter film. The electrical discharge occurs between the cylindrical anode and two planar cathodes at a potential of several thousands of volts in an axial magnetic field of 1000 to 2000 Gauss.

The magnetic field forces the electrons to follow a flat, spiral path, thus greatly increasing the path length. This assures an efficient ion formation down to pressures of  $10^{-12}$  mbar.

Sputter ion pumps usually consist of a stainless steel vessel, containing an array of many anodes adjacent to each other. A titanium cathode is mounted opposite each end of the anodes. Once a discharge is started by cosmic rays or field emitted electrons, it is maintained by secondary electrons released from the cathode. The created ions are less influenced by the magnetic field and are accelerated onto the titanium cathodes, where they continuously sputter cathode material. The sputtered titanium condenses mainly on the anode surfaces where it provides a fresh getter film. Chemically active gases react with this surface and form chemical compounds, which have a low vapour pressure at room temperature.

Inert gases like helium, neon and argon are only pumped if they reach the cathode as energetic ions and are implanted in the getter, or if they are buried under atoms which are chemisorbed by the getter. The weakly bound noble gases can be again released under continuous ion bombardment. Hence, the pumping speed of a diode ion pump for noble gases, in particular for argon, is very low. In addition to the poor argon pumping speed, simple diode sputter ion pumps which are continuously pumping argon exhibit regular pressure bursts, at time intervals of several minutes.

Therefore, another pump design, the triode pump, is applied to assure a stable argon pumping. An additional electrode in the form of a grid is incorporated between the anode and the outer plate electrodes. The sputter yield is higher for ions impacting at a sloping angle as it is for ions impacting perpendicularly. Thus, ions which strike the grid electrode are effective in sputtering material onto the outer plate electrodes, and ions which have been neutralised there are effectively buried underneath the sputter deposited material. Sputter etching at the plate electrodes is less effective, because the ions arriving there tend to impact perpendicularly.

Even though the pumping speed for argon of sputter ion pumps is lower than the pumping speed for other gases, the presence of argon can considerably increase the pumping speed for light gases like H<sub>2</sub>. This is due to the high sputter yield of the argon ions which results in an enhanced deposition of fresh titanium. Consequently, after the argon glow discharges the pressure in the vacuum vessel dropped rapidly once the sputter ion pump started to operate.

Sputter ion pumps cannot be started at pressures higher than  $10^{-3}$  mbar, because the ion current at high pressures is large and causes heating of the pump. As a consequence, previously pumped gas is desorbed, leading to a further pressure- and current rise. This run-away process leads to a glow

discharge between the electrodes, and again to a higher pressure, and finally to the destruction of the power supply.

The life time of a sputter ion pump is also strongly dependent on the operating pressure. The pump should therefore not be continuously operated at pressures higher than  $10^{-6}$  mbar.

### 3.2.2 Total pressure measurement

#### 3.2.2.1 Pirani gauge

For pressure measurements in the rough vacuum region a Pirani gauge, Balzers TPR 018 is used. Pirani gauges use the influence of the pressure of a gas on its thermal conductivity.

A thin filament is heated by an electric current. The heat is given off by radiation, conduction of the gas molecules and conduction at the ends of the filament. The temperature like the resistance of the filament drop with higher pressures due to a higher heat conduction because of the higher gas density.

The filament is used as a resistor in a Wheatstone bridge. If the resistance of the filament changes, the bridge will be unbalanced and a voltage difference can be measured. The meter is calibrated in pressure units. Another possibility is to keep the temperature of the filament constant and to measure the change of the heating current.

The pressure range of a Pirani gauge is limited because in the rough vacuum region the heat transfer is hardly dependent on the pressure. Its lower limit is the molecular flow region, when the mean free path of the molecules becomes longer than the diameter of the gauge head. The heat is then transferred mainly by radiation which is also independent of pressure.

Pirani gauges give reliable measurements between 10 and  $10^{-1}$  mbar. The accuracy of the TPR 018 in this range is given as  $\pm 25\%$ . At higher or lower pressures are not very accurate. Like all pressure gauges described in this chapter the pressure reading is dependent on the kind of gas.

#### 3.2.2.2 Bayard-Alpert gauge

For precise pressure measurements in the high and ultra-high vacuum range the experiment is equipped with a modulated Bayard-Alpert gauge, Balzers CERN IMG 020. Bayard-Alpert gauges like Penning gauges are ionisation gauges. Residual gas molecules are ionised by interaction with electrons which have a kinetic energy higher than the ionisation potential of the gas molecules. The created ions are detected and the ion current  $i_+$  is related to the pressure  $p$  by

$$i_+ = \sigma \cdot i_- \cdot \bar{L} \cdot p \quad \text{Equation 18}$$

where  $i_-$  is the electron current (i.e. emission current of a hot cathode) and  $\bar{L}$  is the mean path length which an electron travels before it strikes the anode.  $\sigma$  represents the probability of any electron to create an ion that is collected on the cathode. If all generated ions are detected,  $\sigma$  is the ionisation cross section.

For a given gas in a specific geometry  $\sigma \cdot \bar{L}$  is a constant and

$$s = \frac{i_+}{i_-} \cdot \frac{1}{p} \quad \text{Equation 19}$$

The proportionality constant  $s$  is called the gauge sensitivity and has the units of  $\text{mbar}^{-1}$ . Sometimes the electron current  $i$  is included in the definition of the sensitivity  $s'$

$$s' = \frac{i_+}{p} \quad \text{Equation 20}$$

In this case  $s'$  has the units of amperes per mbar.

Different types of ionisation gauges are characterised by the source of the ionising electrons and the geometric configuration of the gauge electrodes. Hot cathode ionisation gauges use the thermionic emission of a cathode as the electron source (see 3.1).

The most commonly used gauge for precise pressure measurements in ultra high vacuum is the inverted triode hot cathode gauge which was developed by Bayard and Alpert. Unlike conventional triode gauges, the Bayard-Alpert gauge has its cathode placed outside the grid. The emitted electrons are accelerated by an electrostatic field towards the grid, which has a positive potential of about 150 V with respect to the cathode. The ion collector is centred inside the grid and it is set at a negative potential of some -25 V relative to the cathode.

As the grid consists of thin wire, it is likely that the electrons will pass through the grid and they will travel in the same direction until they reach a point where the potential is the same as that of the cathode. From that point they will turn back and oscillate through the grid. On their way the electrons are ionising residual gas molecules until they finally strike a grid wire. The positive ions which are generated between the grid and the ion collector are captured and produce an ion current. This current is a function of the gas density and can be used to determine the gas pressure.

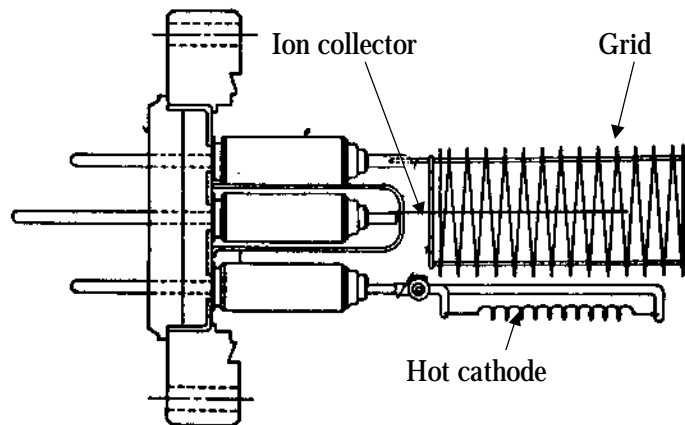


Figure 9; Design of an inverted triode hot filament gauge (Bayard-Alpert gauge) /24/

The electrons impinging on the grid create soft X-rays. These X-rays cause photoemission of electrons from the ion collector and this electron current is indistinguishable from the ion current reaching the ion collector. Thus, a low pressure limit of the gauge occurs when the photoemitted electron current becomes significant compared to the ion current. This limit is referred to as the

X-ray limit of the gauge. A conventional triode gauge is limited to pressures above  $10^{-8}$  mbar because of the X-ray limit. In modern Bayard-Alpert gauges the X-ray current is reduced, mainly because of the small surface area of the ion collector, so they can measure pressures as low as  $10^{-10}$  mbar.

#### *Modulated Bayard-Alpert gauge*

The modulated Bayard-Alpert gauge extends the measurable pressure range by a further order of magnitude to less than  $10^{-11}$  mbar. An additional electrode, the modulator, is placed in the gauge, close to the ion collector. The modulator can be switched from grid potential to the ion collector potential. If the modulator is set to grid potential the apparent ion current  $i_1$  detected by the ion collector is the sum of the true ion current  $i_+$  and the X-ray current  $i_0$ .

$$i_1 = i_+ + i_0 \quad \text{Equation 21}$$

When the modulator is set at the same potential as the ion collector, some ions are detected by the collector and the rest is detected by the modulator. The X-ray current which contributes to the total collector current is not influenced by a changed modulator potential. Thus, the apparent collector current  $i_2$  is

$$i_2 = \alpha \cdot i_+ + i_0 \quad \text{Equation 22}$$

where  $\alpha$  is the fraction of the true ion current which is detected by the ion collector and not by the modulator. The true ion current can then be calculated with the two observables  $i_1$  and  $i_2$ .

$$i_+ = \frac{i_1 - i_2}{1 - \alpha} \quad \text{Equation 23}$$

The parameter  $\alpha$  can be determined by operating the gauge at a pressure where  $i_0$  is negligible.

With an emission current  $i_e$  of 10 mA the used Bayard-Alpert gauge Balzers CERN IMG 020 has a sensitivity of about  $26 \text{ mbar}^{-1}$  for nitrogen. Its measuring range at  $i_e = 10 \text{ mA}$  is between  $10^{-7}$  mbar and  $7 \cdot 10^{-12}$  mbar which can be extended to lower pressures by reducing the emission current. During the measurements the gauge was therefore operated with an emission current of 1 mA in order to measure pressure up to  $10^{-6}$  mbar. The sensitivity of the gauge is then assumed to be  $2.6 \text{ mbar}^{-1}$ .

Hot cathode gauges are sensitive to chemical attack and bombardment of positive ions. Therefore, for rough applications in the medium and high vacuum range cold cathode gauges are preferred if their limited accuracy is tolerable.

#### **3.2.2.3 Penning gauge**

A Penning gauge, Balzers IKR 020, serves for total pressure measurement in the high vacuum region. The measurement principle of this gauge is similar to that of the hot cathode gauge, i.e., residual gas molecules are ionised by electron impact and the resulting ion current is measured. In a certain range this electric current is a linear function of the pressure.

The Penning gauge is a cold cathode gauge, i.e., it has no thermionic electron source. The free electrons are created by means of a gas discharge in a so-called Penning cell (see 3.2.1.4). Two parallel connected cathodes enclose the anode. A potential difference of about 3.3 kV is maintained between the anode and the cathodes, and in addition a magnetic field of a few hundred gauss is introduced perpendicular to the electrodes by a permanent magnet.



An electron emitted by the cathode is accelerated towards the anode in the electric field but it is trapped by the magnetic field and a stable electron current on a circular path can be established at pressures below  $10^{-4}$  mbar. Thus, the mean path length of the electrons and their ionisation ability increase significantly and it is possible to maintain the discharge at very low pressures. The positively charged ions do not form a stable circular current as the radii of their orbits are larger because of their comparatively high mass. They reach the cathode and produce a current proportional to the gas density.

The sensitivity of the gauge is dependent on the kind of gas. Pressure gauges are usually calibrated for air or  $N_2$  and hence the relative sensitivity for air or  $N_2$  is one. Helium has the highest ionisation potential. Hence, the pressure indicated by an ionisation gauge is significantly lower and the pressure reading of the IKR 020 has to be multiplied by a factor of 5.9 in order to obtain the true He-pressure. Heavy gases have a lower ionisation potential than  $N_2$ . In a pure argon atmosphere for example, the pressure reading has to be multiplied by 0.8. For  $O_2$ , and CO the relative sensitivity of the gauge is one and for  $H_2$  it is 2.4.

A contamination of the cathode increases the ion induced secondary electron emission. This secondary electron current can not be distinguished from the ion current and results in a higher pressure reading. Furthermore, the secondary electrons contribute to the circular, ionising electron current, thus increasing the sensitivity of the gauge.

The measuring range of the IKR 020 is about  $10^{-3}$  mbar to  $10^{-10}$  mbar. The upper limit is set by the appearance of a glow discharge, where the ion current is less dependent on the pressure. At low pressures the pressure range of the Penning gauge is limited because field emission currents become significant. The sensitivity of Penning gauges is typically 1 A/mbar at  $10^{-5}$  mbar. The accuracy of the IKR 020 is given by the manufacturer as +60% and -50%.

### 3.2.3 Partial pressure measurement

Partial pressure analysers are basically ionisation gauges in which the generated ions are resolved in a mass spectrum according to their mass to charge ratio. The residual gas composition in a clean vacuum system is usually not very complex. On the other hand the partial pressures of the single gases can be very low. Therefore, special mass spectrometers have been designed which have a high sensitivity but also a limited mass resolution. These spectrometers are often referred to as residual gas analysers.

The operation of a mass spectrometer can be divided in three functional steps. The first step is the ionisation of a fraction of the residual gas molecules in an ion source. These ions are then accelerated by an electrical field and focused onto the entrance aperture of an analyser. In the second step the ions are separated according to their electrical charge to mass ratio. Finally, the ions are detected by a Faraday cup or by a secondary electron multiplier.

Ionisation of a small fraction of the residual gas molecules is realised by low energetic electron bombardment. The electron energy is decisive for the number of ions which is created of a certain species and also for the kind of created ions. The ionisation cross section is highest for electron energies between 50 eV and 150 eV, depending on the kind of gas. Therefore, the electrons which are emitted by a hot cathode are accelerated towards a positively biased grid typically to about 100 eV. Besides multiple charged ions also cracking products are produced which can result in a complex spectrum.

A suitable system of electrodes guides the ions into the mass separator which consists of 4 cylindrical rod electrodes. During the measuring operation, a variable RF voltage is applied to the

rod electrodes and a DC voltage is superimposed on the RF voltage. Depending on the resulting electrical field, only ions with a specific mass to charge ratio reach the ion detector while others are filtered out.

The ions can be detected with a simple Faraday cup. In this case the lowest measurable partial pressure  $p_{i,min}$  is given by

$$p_{i,min} = \frac{i_{+,min}}{s_i} \quad \text{Equation 24}$$

where  $i_{+,min}$  is the smallest measurable ion current and  $s_i$  is the sensitivity of the analyser for a certain gas species. Typically the sensitivity is about  $10^{-4}$  A/mbar and  $i_{+,min}$  is some  $10^{-15}$  A resulting in an ultimate detectable partial pressure  $p_{i,min} = 10^{-11}$  mbar. In ultra high vacuum this is not sufficient and it is necessary to use a secondary electron multiplier instead of a Faraday cup.

The ions which reach the secondary electron multiplier liberate electrons from the cathode. These electrons are accelerated onto a cascade of several dynodes where they create an electron avalanche.

The amplification of the secondary electron multiplier  $A$  is determined by the number of electrons which are emitted from the cathode by one impacting ion  $\eta_I$ , the number of dynodes  $d$ , and the total SEY  $\delta$  of the dynode surfaces for the chosen primary electron energy.

$$A = \eta_I \cdot \delta^d \quad \text{Equation 25}$$

The energy of the electrons impacting on the dynodes can be varied by changing the secondary electron multiplier voltage, i.e., the potential difference between the dynodes. This potential difference is typically some 150 V. The total amplification is strongly increased if this potential is increased. Thus, after calibration of the residual gas analyser, the secondary electron multiplier voltage must not be changed if quantitative measurements are required. However, the SEY of the dynodes is also reduced with the time of operation, particularly if the electron accelerating voltage is high. The quadrupole mass analyser Balzers QMA 120 is equipped with a secondary electron multiplier with 17 dynodes. Its amplification at 2.5 kV is higher than  $10^6$ .

Besides the low partial pressures which can be measured, a major advantage of the secondary electron multiplier is the strong reduction of the time needed for one scan. The feasible fast scan rates make it advantageous to control the spectrometer with a computer. The QMA 120 is controlled by a personal computer run by LabVIEW. This makes it possible to display only distinct masses and to monitor the intensity of single peaks as a function of time. Furthermore, mass spectra can be evaluated by special software which includes the cracking pattern of the gases commonly found in vacuum systems.

The ultimate pressure in the vessel after bakeout is typically  $5 \cdot 10^{-10}$  mbar. At this pressure the residual gas consists roughly of 90%  $H_2$ , 5%  $CH_4$ , 3%  $CO$ ,  $H_2O$ ,  $CO_2$ , and Ar.

The residual gas analyser is also used for leak detection of the whole vacuum system. For this reason it is permanently tuned into mass 4 and the helium partial pressure is monitored during helium is offered outside the vacuum chamber as the search gas.

## 4. Experimental Procedures

Reproducible SEY measurements require sample surfaces in a well defined state and the sample preparation is hence of utmost importance. In this chapter the cleaning process of the samples is described together with the different gas exposure techniques which were employed. The measuring procedure is described in chapter 3.

### 4.1 *The cleaning of the samples*

The definition of cleanliness always depends on the application of a surface within a vacuum system. For general vacuum applications one may consider a surface clean if the remaining molecules are tightly bound to it and, hence, give a low thermal outgassing rate at room temperature /25/.

Secondary electron emission is strongly surface dependent /26/. As a consequence, one needs another definition of cleanliness for SEY measurements. The sample surfaces should be atomically clean, i.e., only a few percent of a monolayer of foreign molecules are acceptable on the surface.

Three types of contamination must be removed from the copper samples in order to have a clean surface which allows reliable SEY measurements. One is adsorbed gases. The second is the oxide layer. The third is crystal damage, including implanted argon ions which may originate from the glow discharge cleaning of the samples /27/.

#### 4.1.1 Bakeout

If the contaminating atoms or molecules have a higher vapour pressure than the base material, they can be removed by heating the material. The atoms gain energy by thermal agitation and are more likely to escape from the surface so that they can be pumped. The degassing rate increases with temperature.

Ultra high vacuum, i.e. , pressures lower than  $10^{-7}$  mbar, can hardly be achieved without baking. After bakeout the degassing rate of the surfaces at room temperature is small enough that with a suitable pumping system low pressures can be reached. However, that does not mean that the surfaces are free of contaminants. Several tens of monolayers of contaminants can remain after a 350°C bakeout /28/.

Baking is particularly efficient to get rid of adsorbed water.

#### 4.1.2 Glow discharge cleaning

Strongly bound contaminants or oxide layers, which can not be desorbed by baking, can be removed by particle bombardment. If the bombarding particles are energetic enough, individual atoms can acquire enough energy via collision processes to escape from the surface /29/. This process is called sputtering. One distinguishes between two principal sputtering applications. Sputter etching has the primary objective to remove material from the target surface. If the re-deposition of these atoms onto another surface is the primary goal, the process is called sputter deposition. The heavier the bombarding particles, the more effective is the sputtering process. Furthermore, the projectiles should not react with the surfaces (nonreactive sputtering). Argon is therefore used, also because it is cheaper than the heavier noble gasses. The effectiveness of the sputtering process can be expressed by the sputtering yield, i.e., the number of atoms ejected from the target per incident ion. The sputtering yield of 500 eV Ar-ions on copper is 2.35 /30/.

The ionisation and the acceleration of the argon towards the samples is achieved by means of a glow discharge, in the simplest case a dc discharge. Hereby, the samples act as the cathode and are biased to -1 kV with respect to the grounded vessel which represents the anode.

To initiate a self-sustaining dc diode discharge, argon is injected in the vessel. In order to have as pure argon as possible the vessel is continuously pumped during argon injection. The sample to ground current can be regulated by changing the gas pressure. A current of 25 mA at about  $5 \cdot 10^{-2}$  mbar has been chosen to have an ion current density of about 0.5 mA per  $\text{cm}^2$  on the sample surfaces. After 15 minutes the induced dose is  $2.8 \cdot 10^{18}$  ions/ $\text{cm}^2$ .

It is necessary to bake the whole vacuum system before the discharge in order to minimise contaminants released from the chamber walls due to electron impact.

Besides the desired sputter etching also some re-deposition of sputtered material from the samples as well as from the sample holders occurs during the glow discharge. This may result in a changed surface topography as shown in Figure 10.

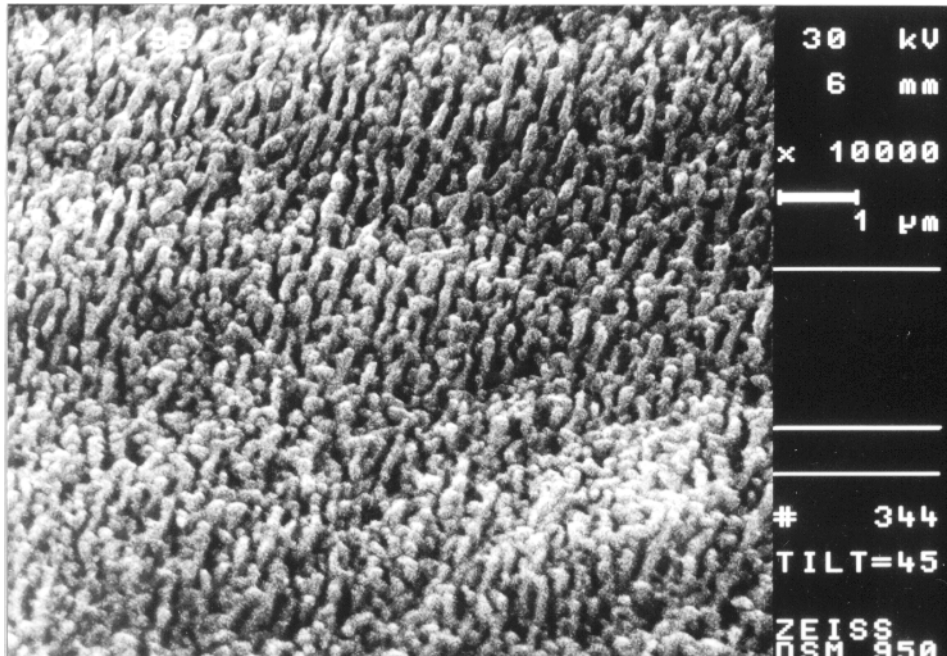


Figure 10; Scanning electron microscope image of a modified surface after 250 min sputter etching (ion dose =  $10^{20}/\text{cm}^2$ , ion current = 25 mA, dc voltage = 1 kV,  $p = 5 \cdot 10^{-2}$  mbar).  $\delta_{\text{max}}$  of this surface after the glow discharge was 0.5. (magnification = 10 000x)

The development of such a topography is sometimes referred to as cone growth. However, the cones are not growing but result from selective etching of distinct areas of the surface. This effect has been attributed to the angular dependence of the sputter yield and on surface impurities which have a lower sputter yield than the base material [31]. Impurities can be sputtered material from the sample holders which are backscattered from the gas phase onto the samples. Copper has a comparatively high sputter yield and is therefore an ideal base material for the creation of cones.

The closely spaced needles produce so much light scattering that the surface resembles black velvet. But they are also influencing the secondary electron emission of the surfaces. This was observed after 45 minutes dc glow discharge at 1 kV with a current density of about 0.5 mA/ $\text{cm}^2$ . The maximum SEY  $\delta_{\text{max}}$  decreased from 1.3 to about 1.2 and the primary electron energy  $E_m$  at

which  $\delta_{\max}$  occurs was shifted to lower energies. Those changes continued with time of the glow discharge and were also strongly dependent on the position of the samples in the vessel.

After 250 minutes glow discharge  $\delta_{\max}$  dropped down to 0.5, which is about the same as for soot /3/. Figure 11 shows the potential of such a treatment to produce surfaces with a  $\delta_{\max}$  well below unity. This is of course detrimental to valuable SEY measurements of materials and the samples have to be changed before the measurements are influenced by the surface structure.

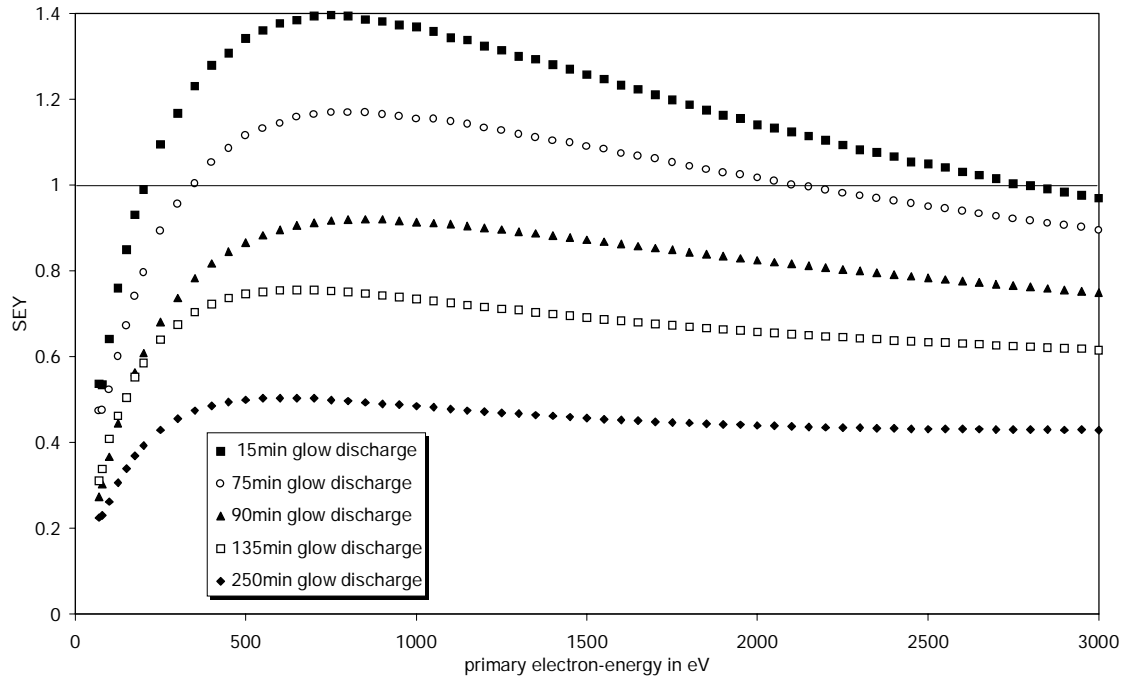


Figure 11; Influence of the surface structure on the SEY. Secondary electron emission is strongly reduced after continuous sputter etching (ion dose after 250 minutes glow discharge =  $10^{20}/\text{cm}^2$ ).

A frequently used method to produce atomically clean surfaces is to employ several cycles of argon bombardment combined with thermal treatment. Hereby, the argon bombardment removes the surface contamination. Resulting surface damage and imbedded argon are then eliminated by annealing /27/. The annealing temperature for copper should be  $450^\circ\text{C}$ . A higher temperature would cause a strong segregation of sulphur to the surface /32/. It is reported that carbon remains very often as a final contaminant on the copper surface after ion bombardment and annealing /33/.

This procedure can not be applied with the used experimental set-up because the samples can only be heated by radiation of the hot vacuum chamber. The highest achievable sample temperature is therefore  $350^\circ\text{C}$  and cycles of argon bombardment and annealing can not be realised.

Two methods have been tried to clean the samples. At first a glow discharge at 1 kV,  $5 \cdot 10^{-2}$  mbar argon pressure and an ion current of 25 mA was started when the vacuum system and the samples were at room temperature. Before the glow discharge the vacuum system had been baked 24 hours at  $350^\circ\text{C}$ . After this procedure the measured  $\delta_{\max}$  was about 1.4.

In a second try a glow discharge with the same parameters was initiated after a 24 hours bakeout at  $350^\circ\text{C}$ , but with the whole vacuum system still at  $350^\circ\text{C}$ . After the glow discharge the vessel temperature was kept at  $350^\circ\text{C}$  for one hour and then cooled to room temperature. This

procedure resulted in a  $\delta_{\max}$  of 1.3, which corresponds to the value found in literature for pure copper.

Unfortunately, with the used set-up it can not be verified if the samples are really atomically clean or not. The bombardment of the hot samples is probably advantageous because it is more effective and less imbedded argon remains after the following one hour heating at 350°C. On the other hand, the partial pressure of water in the hot chamber after 24 hours baking at 350°C is still some  $10^{-6}$  mbar and one could assume that the water reacts with the hot sample surfaces.

However, after both procedures an oxygen exposure of only  $5 \cdot 10^{-4}$  s · mbar following the glow discharge decreased  $\delta(E_p)$  about 0.05. This indicates that the samples had not been strongly oxidised before the exposure. If they would have been oxidised, the oxide layer would have acted as a protective film, strongly decreasing the rate of oxidation (see 2.4) and hence minimising the change in secondary electron emission. It is also reported that pure water vapour does not react with copper even at temperatures as high as 1000°C /15/.

## 4.2 Gas exposures

A frequently used unit to quantify exposed gas doses in surface sciences is the Langmuir.  $1 \text{ L} = 1 \text{ s} \cdot 1.33 \cdot 10^{-6} \text{ mbar}$ . This quantity only considers the offered gas without taking into account the sticking probability of the specific gas on the surface.

### 4.2.1 Air exposure

Initially the samples were exposed to air inside the vacuum vessel. Therefore, the vessel was vented with unfiltered laboratory air to atmospheric pressure and the exposed dose was determined by measuring the time during which the chamber was vented. The venting valve was kept open during the exposure.

Once it became clear that this exposure differs from an air exposure in the laboratory, outside the vessel, the sample holder was always dismantled from the vacuum vessel and placed in the laboratory together with the samples. This procedure took about 20 minutes during which the samples still remained inside the chamber.

The temperature and the relative humidity in the laboratory during the air exposures were not stable. An average temperature of 20°C and a mean relative humidity of 60% are estimated.

### 4.2.2 Pure water vapour exposure

To produce as pure water vapour as possible a separate vacuum vessel was filled with distilled water. This vessel was evacuated upon the water with a dry, three stage diaphragm pump (vacuubrand MD4T). The pressure inside this vessel was monitored with a Pirani gauge. After a short while the vapour pressure of water (23 mbar at 20°C) was achieved. During continuous pumping the pressure dropped to about 15 mbar because the liquid was cooling down.

The outside vessel was connected with a flexible line to a leak valve, which allows to change its conductance, in order to regulate the flow inside the main vacuum vessel. The water vapour was then continuously injected through the leak valve. At the same time pumping of the vessel was provided by the turbomolecular pump and the leak valve was adjusted to reach the desired equilibrium pressure inside the vessel, i.e., to expose the inside samples to a distinct dose of water vapour in mbar·s (at room temperature). This “dynamic” exposure is advantageous because contamination of the water vapour due to degassing of the chamber walls is kept low. However,

to expose the copper samples to higher doses in a reasonable time, a  $\text{H}_2\text{O}$  partial pressure of some 10 mbar was needed. This could only be achieved with a “static” exposure. Hereby, the valve between chamber and turbomolecular pump was closed and the leak valve was kept open until the wanted pressure in the vessel was achieved. Impurities from the chamber walls may in this case be neglected because the pressure during exposure was at least 8 orders of magnitude higher than the pressure in the vessel before exposure.

The residual gas in the vacuum vessel was analysed with a quadrupole mass spectrometer (Balzers QMG 112). Before injection  $p_{\text{tot}}$  was about  $5 \cdot 10^{-8}$  mbar and the spectrum was dominated by  $\text{H}_2$ . During injection at a total pressure of  $5 \cdot 10^{-6}$  mbar  $\text{H}_2\text{O}$  was clearly dominating the residual gas. Peaks were seen at masses 18, 17, 16 and 1 due to the ions  $\text{H}_2\text{O}^+$ ,  $\text{OH}^+$ ,  $\text{O}^+$  and  $\text{H}^+$  respectively which were formed from water by electron impact in the ion source [34]. Mass 2 ( $\text{H}_2^+$ ) was hardly visible in the spectrum. Figure 12 shows the residual gas spectrum in the vacuum chamber during  $\text{H}_2\text{O}$  injection.

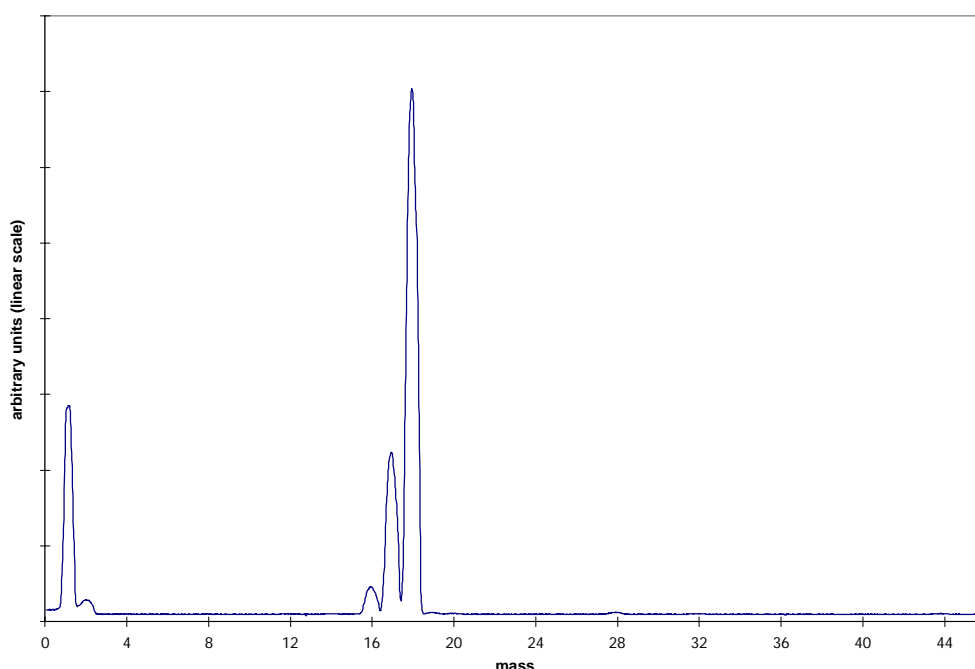


Figure 12; Residual gas spectrum (linear scale) during dynamic  $\text{H}_2\text{O}$  injection at a total pressure of  $5 \cdot 10^{-6}$  mbar

A total pressure monitoring during injection is sufficient to determine the exposed dose of  $\text{H}_2\text{O}$ , because for injection pressures higher than  $10^{-5}$  mbar other gases than  $\text{H}_2\text{O}$  can be neglected in the residual gas. In this pressure region a Penning gauge is used. Injection pressures higher than  $10^{-2}$  mbar are monitored with a Pirani gauge.

After the leak valve has been closed to end a “dynamic” exposure, the pressure in the vessel drops more than two orders of magnitude within a minute. For an injection duration of some 10 minutes this additional dose can be neglected and only the time during which the valve is open has to be considered.

#### 4.2.3 Pure oxygen exposure

At low injection pressures up to the pressure limit of the sputter ion pump (about  $10^{-6}$  mbar) oxygen was injected dynamically, i.e., during injection the vacuum vessel was continuously pumped by the sputter ion pump. Oxygen was admitted to the system from a high purity oxygen

bottle through a variable leak valve. For this kind of injection other gases than  $O_2$  are not relevant in the residual gas spectrum.

After closing the leak valve the pressure in the vessel drops two orders of magnitude in less than a minute. Hence, the exposed dose of  $O_2$  can easily be determined by measuring the total pressure during injection and the injection time.

At higher pressures this is not possible anymore because the sputter ion pump can not be operated. Pumping via the turbomolecular pump of an oxygen enriched atmosphere risks combustion of the primary pump oil and an explosion of the primary pump itself and is therefore excluded [35].

For exposure at pressures up to  $10^{-2}$  mbar all pumps were switched off and  $O_2$  was injected up to the desired pressure. Then the leak valve was closed. Because oxygen is a very reactive gas it is efficiently getter pumped by the chamber walls. The pressure in the vessel drops again after the leak valve has been closed. It took about 15 minutes to reduce the pressure from  $10^{-3}$  mbar to  $3 \cdot 10^{-6}$  mbar and about two hours to reduce the pressure from  $10^{-2}$  mbar to  $3 \cdot 10^{-6}$  mbar. At this pressure the sputter ion pump could be started again and the pressure dropped within several seconds to the low  $10^{-8}$  mbar region.

Shortly after  $O_2$  injection one can assume to have pure oxygen in the vessel. But after some time other “remembered” gases which have been previously pumped by the chamber walls and the sputter ion pump desorb and are replaced by the more reactive oxygen. This leads to a continuous decrease of the oxygen partial pressure and an increase of the contribution of other gases to the total pressure. A spectrum taken at a total pressure of  $10^{-6}$  mbar (15 minutes after oxygen injection at  $10^{-3}$  mbar) is shown in Figure 13.

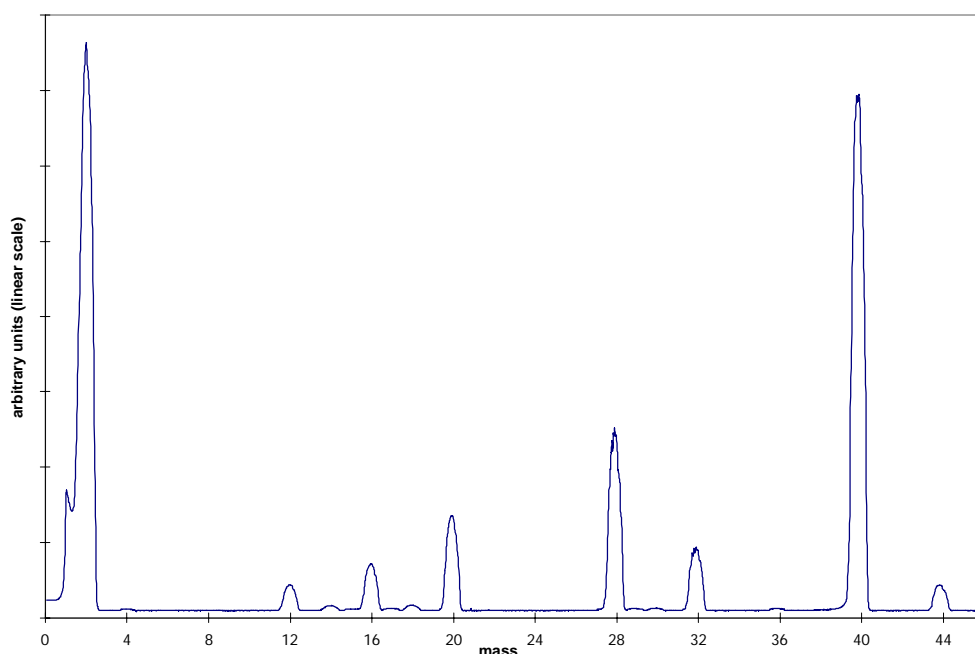


Figure 13, Residual gas spectrum 15 min after static injection of  $O_2$  at  $10^{-3}$  mbar ( $p_{tot} = 10^{-6}$  mbar). The partial pressure of  $O_2$  (mass 32) has been reduced from  $10^{-3}$  mbar to less than  $10^{-7}$  mbar by the pumping action of the chamber walls.

The spectrum is dominated by hydrogen and argon (argon is frequently injected into the vessel at high pressure during glow discharge cleaning).



For a precise determination of the dose it would be necessary to monitor the  $O_2$  partial pressure from injection until it is negligibly low. This was not possible because the used quadrupole mass spectrometer can not operate at pressures higher than  $10^{-5}$  mbar. The exposed dose of  $O_2$  after this kind of exposure is rather a rough estimation than an exact value.

The samples at room temperature are saturated with oxygen after an exposure of  $10^9$  L /36/. With an oxygen partial pressure of  $10^{-3}$  mbar this dose would be reached after 15 days. To realise the exposure in a more reasonable time the oxygen was injected at 1 mbar. After one hour nitrogen was injected up to a total pressure of 5 mbar so that the mixture could be pumped via the turbomolecular pump. As the chamber walls are soon saturated with oxygen at such high pressure, the exposed dose can be calculated by the injected oxygen partial pressure and the total exposure time.

### 4.3 Error estimation

The sample preparation is the major uncertainty of the SEY measurements. Initially the glow discharge cleaning was carried out when the vacuum vessel and the samples were at room temperature and  $\delta_{\max}$  of such prepared samples was about 1.4. Later the samples were sputter cleaned at  $350^\circ\text{C}$  because sputter etching at higher temperature is more effective. The obtained  $\delta_{\max}$  value after this procedure is 1.3, which corresponds with the value found in literature. (The actual temperature of the samples during glow discharge is not known but it might be considerably higher than the bakeout temperature as the total power which is injected during the discharge is 25 W and most of it will be converted into heat on the sample surfaces.)

The scanning electron images showed that a damaged surface remains after the sputter cleaning. This can already affect the measurements. Since an in-situ surface analysis is not possible one can not exclude a remaining contamination after the cleaning process, i.e., the exact surface state after the glow discharge is not known. In particular the results regarding the influence of a changed work function on the SEY have to be treated with care because of the unknown surface state.

The uncertainty of the Bayard-Alpert gauge limits the accuracy of the exposed dose of oxygen during dynamic exposure. An accuracy of  $\pm 50\%$  for this gauge is estimated and other factors of uncertainty may be neglected.

During static oxygen exposure the oxygen contribution to the total pressure varied strongly. Hence, for a precise determination of the exposed dose it would be necessary to monitor the oxygen partial pressure during the whole exposure, which is not possible with the used gas analyser. The measured doses above  $10^4$  L are therefore rather estimations than exact values.

The accuracy of the exposed water dose during dynamic exposure is also limited by the exactness of the pressure gauge. In this case a Penning gauge was used which accuracy is given by the manufacturer as  $+60\%$  and  $-50\%$ . During static exposure the pressure was monitored with a Pirani gauge which has an accuracy at 10 mbar of  $\pm 25\%$ .

As has been pointed out in chapter 3, the maximum random deviation of the measured SEY from the true yield is less than 0.1.

## 5. Results

### 5.1 Influence of an air exposure on the SEY of initially clean copper

The SEY of pure copper changes after air exposure at room temperature. For exposures of a few minutes  $\delta_{\max}$  decreases to about 1.2 and  $E_{\max}$  is shifted from 700 eV to less than 400 eV. After further air exposure the SEY increases steadily.

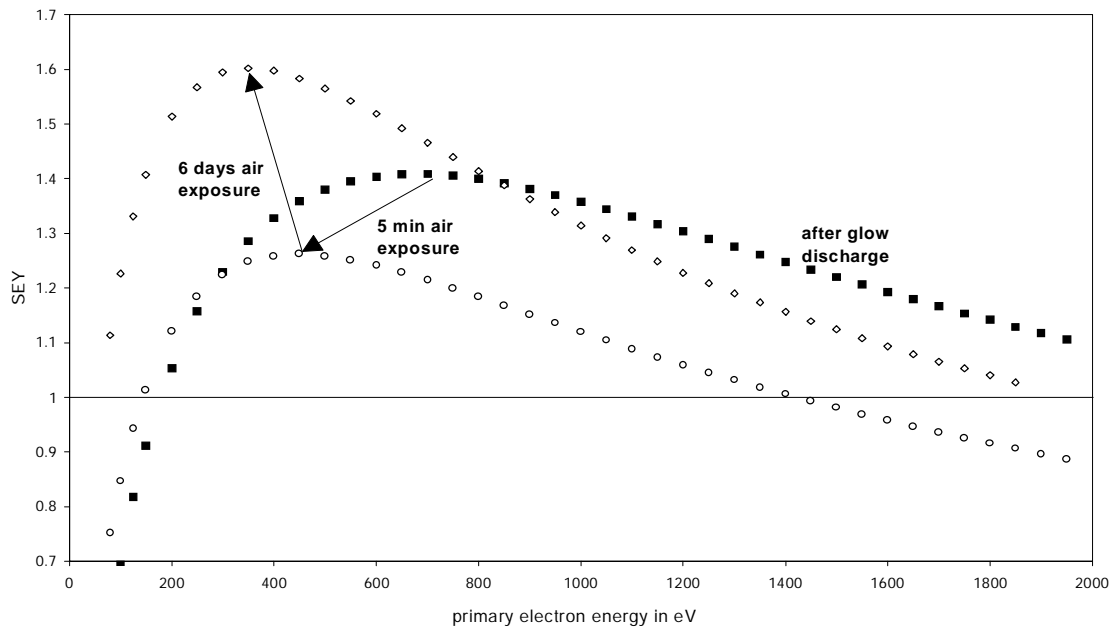


Figure 14; Total SEY  $\delta$  of sputtercleaned copper, after 5 minutes and 6 days air exposure inside the vacuum vessel as a function of the primary electron energy. The initial decrease of  $\delta_{\max}$  is characteristic for copper. The primary energy  $E_{\max}$  at which  $\delta_{\max}$  is obtained is shifted from 700 eV to 400 eV.

There is a significant difference in the change of the SEY after air exposures inside the vacuum vessel and outside the vessel. An air exposure outside the vessel causes higher  $\delta_{\max}$ -values as an exposure inside the vessel. After 6 days  $\delta_{\max}$  of an initially clean copper surface was 1.6 and 1.9 after an air exposure inside and outside the vacuum vessel respectively.

Figure 15 gives for both cases  $\delta_{\max}$  as a function of the air exposure time at atmospheric pressure. After about 100 minutes the SEY increases with a logarithmic rate.

The different impact of air exposures outside and inside the vacuum vessel on the SEY is an important hint which can help to figure out what makes the SEY to increase. Three possible reasons are proposed:

- 1) Reactive pollutants like NO could be less concentrated inside the vacuum chamber because of the pumping action of the chamber walls. If those pollutants would influence the SEY, a different yield after exposures inside and outside the vessel could appear.

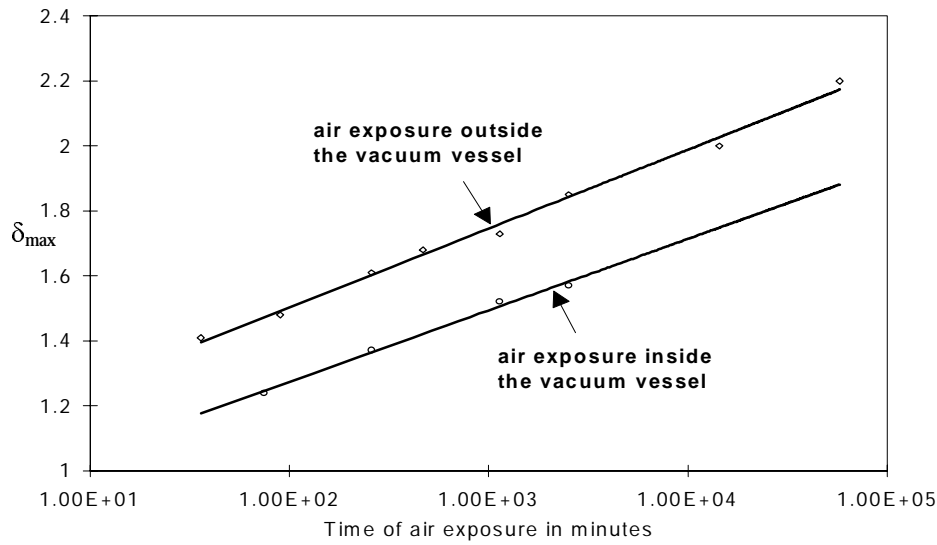


Figure 15; Difference of the maximum SEY  $\delta_{\max}$  of initially clean copper after different doses of air inside and outside the vacuum vessel

- 2) A measurement of the dew point temperature inside the chamber as a function of the time after breaking the vacuum showed that the humidity is at least in the first two hours lower than in the ambient air. Hence, the comparatively low SEY after short exposures could be attributed to the lower humidity. Figure 16 shows the dew point temperature inside and outside the vessel as a function of the time after braking the vacuum. The humidity sensor was not calibrated and quantitative values can not be given. Nevertheless, it can be seen that the water vapour concentration inside the vessel approaches the value of the outside air in a logarithmic rate. It made no difference if the venting valve was kept open during the humidity measurements or if it was closed immediately after braking the vacuum.

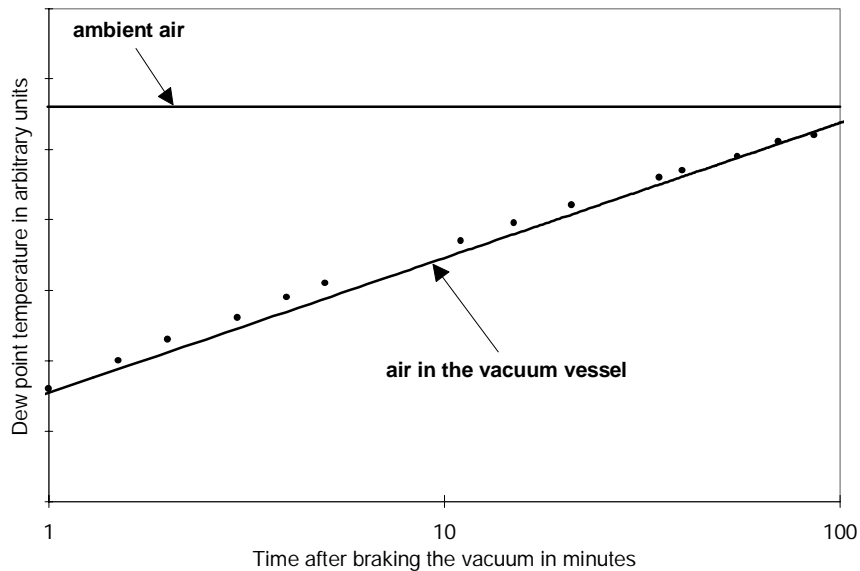


Figure 16; Dew point temperature in the vacuum chamber as a function of the time after braking the vacuum

- 3) The concentration of dust inside the vacuum vessel is probably lower than it is in the laboratory and therefore dust was also under suspicion to increase secondary electron emission. However, the SEY of samples which were exposed to air in a clean room class 100 did not differ from that of samples which were exposed to not filtered air for the same time.

## 5.2 Influence of a pure oxygen exposure on the SEY of initially clean copper

An oxygen exposure of 10 L did not change  $\delta(E_p)$  measurably. After an oxygen exposure of 100 L  $\delta(E_p)$  was slightly decreased. The secondary electron emission continued to decrease with higher doses of oxygen. An  $O_2$  exposure of  $10^9$  L decreased  $\delta_{max}$  to a value less than 1.2.

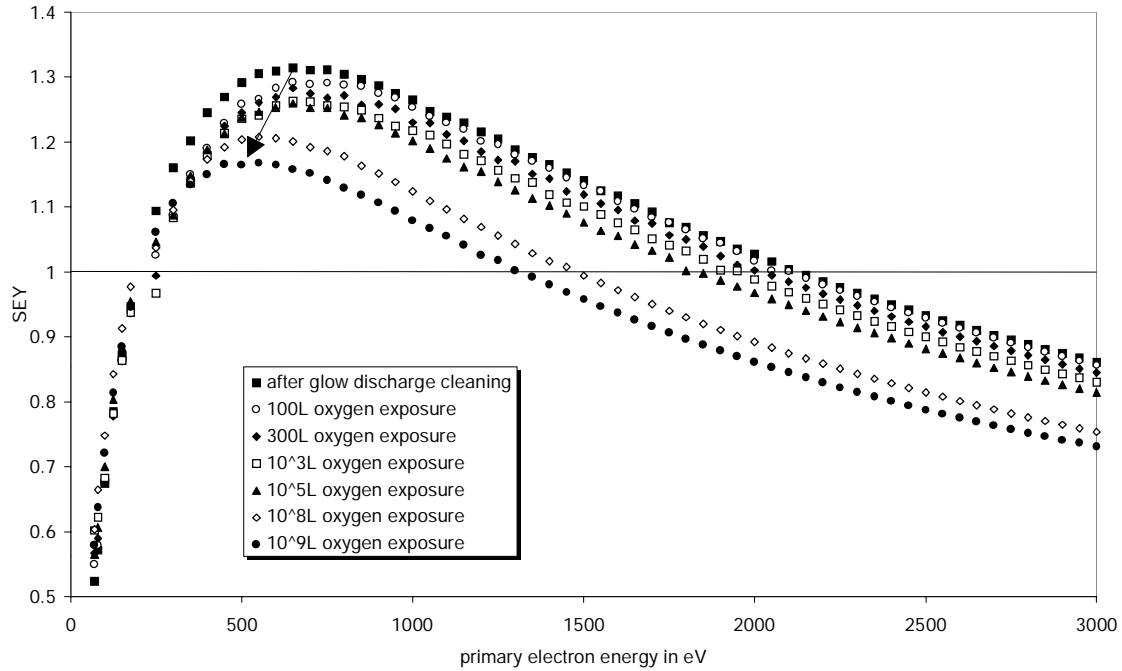


Figure 17; Total SEY  $\delta$  after different doses of oxygen as a function of the primary electron energy. The SEY decreases with the exposed dose of  $O_2$ .

Wagner and Spicer report that the copper work function increases about 0.3 eV after an oxygen exposure of 10 L, which corresponds with one monolayer absorbed oxygen /36/. After further exposure the work function increases only slightly.

One can therefore assume that the SEY of copper is not significantly influenced by a change of the work function due to the adsorption of oxygen, because no change of the SEY was observed after 10 L oxygen exposure (see 2.1.5).

The decrease of the SEY after oxygen exposure is rather due to the building up of a  $Cu_2O$  layer which has a lower SEY than pure copper. Higher doses of oxygen increase the thickness of the oxide layer and, consequently, its contribution to the secondary electron emission gets higher compared with the contribution of pure copper.

Wagner and Spicer assume that after an  $O_2$  exposure of about  $10^9$  L the oxidation of copper at room temperature is essentially complete. After that exposure they estimate an oxide layer of about 8 to 20 atomic layers,  $Cu_2O$  being the dominant oxide. An elemental depth profile of a copper surface, oxidised at room temperature, indicated an oxide layer of 15 Å which corresponds to about 5 atomic layers.

### 5.3 Influence of a pure water vapour exposure on the SEY of initially clean copper

An exposure of water vapour increases the SEY. No initial decrease of  $\delta(E_p)$  has been observed. After a dose of 81 hours·11mbar  $\delta_{\max}$  was about 1.5.

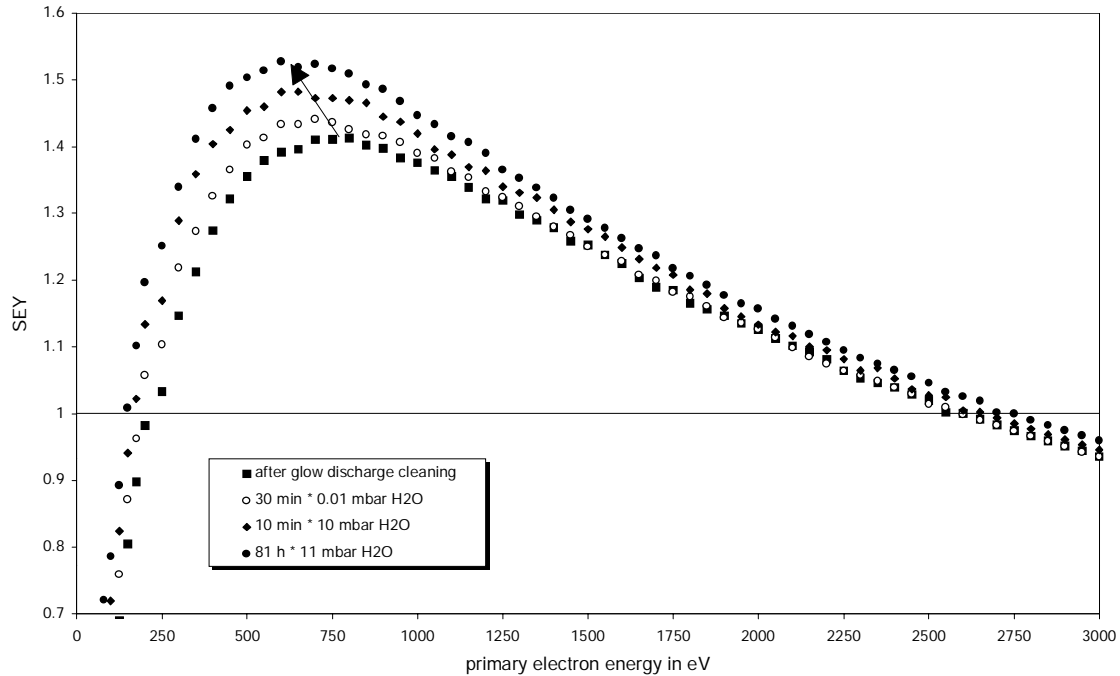


Figure 18; Total SEY  $\delta$  after different doses of  $H_2O$  as a function of the primary electron energy. The SEY increases with the exposed dose of  $H_2O$ .

The SEY is also dependent on the time between the exposure and the measurement. It decreases slightly with the duration of pumping.

An air exposure with a similar dose of water vapour increases the SEY much more than a pure water exposure does (a water partial pressure of 14 mbar, corresponding with 60% relative humidity at 20°C in the laboratory air, is estimated). A dose of 81 hours·11mbar pure water increases  $\delta_{\max}$  from 1.4 to about 1.5. After 60 hours air exposure,  $\delta_{\max}$  of an equally prepared sample is about 1.9.

Heras and Viscido report that the work function of polycrystalline copper decreases 0.73 eV due to water adsorption at 77 K [37]. Hence, one can conclude that a work function change of copper due to adsorbed water hardly influences the SEY, because no initial change of  $\delta(E_p)$  was measured after the first adsorbed monolayers of water.

### 5.4 Influence of the other gases in air

Copper samples were exposed to pure molecular nitrogen, carbon dioxide and argon at a pressure of 1 mbar for 1 day. As expected no influence on the secondary electron emission of pure copper or of oxidised copper was observed.

### 5.5 Influence of a pure water vapour exposure on oxidised copper

15 days pure water exposure at 10 mbar of an oxidised sample increased  $\delta_{\max}$  of differently prepared samples always about 0.15. This is clear evidence that the strong impact of an air exposure on the SEY can only be partly due to the humidity in air and to the resulting physisorption of water on the oxide surface.

On the other hand, for samples which were exposed to air for 45 minutes and during this time dipped into distilled water for 10 minutes  $\delta_{\max}$  increased from 1.4 to 2.4. The maximum SEY of samples which were not put into water during the 45 minutes air exposure was only increased from 1.4 to less than 1.7.

As pure water can hardly increase the secondary electron emission but water in the presence of the other gases in air strongly increases the SEY, it is assumed that the presence of water molecules on the copper surface increases the sticking probability for other gases. The adsorbate which is causing the high SEY after long air exposures could therefore be a mixture of different gases present in air.

### 5.6 Influence of a bakeout on the SEY

Figure 19 shows the influence of various surface treatments on the SEY of the OFHC-copper samples. At first the samples were investigated as received after the standard chemical cleaning procedure for vacuum equipment at CERN. Afterwards the system was baked at 100°C, 200°C, 300°C and 350°C and  $\delta(E_p)$  was measured after every step. Finally  $\delta(E_p)$  was measured after the samples were sputter-cleaned at 350°C during the dc glow discharge described in 4.1.2. The curves show the strong influence of contamination on  $\delta(E_p)$ .

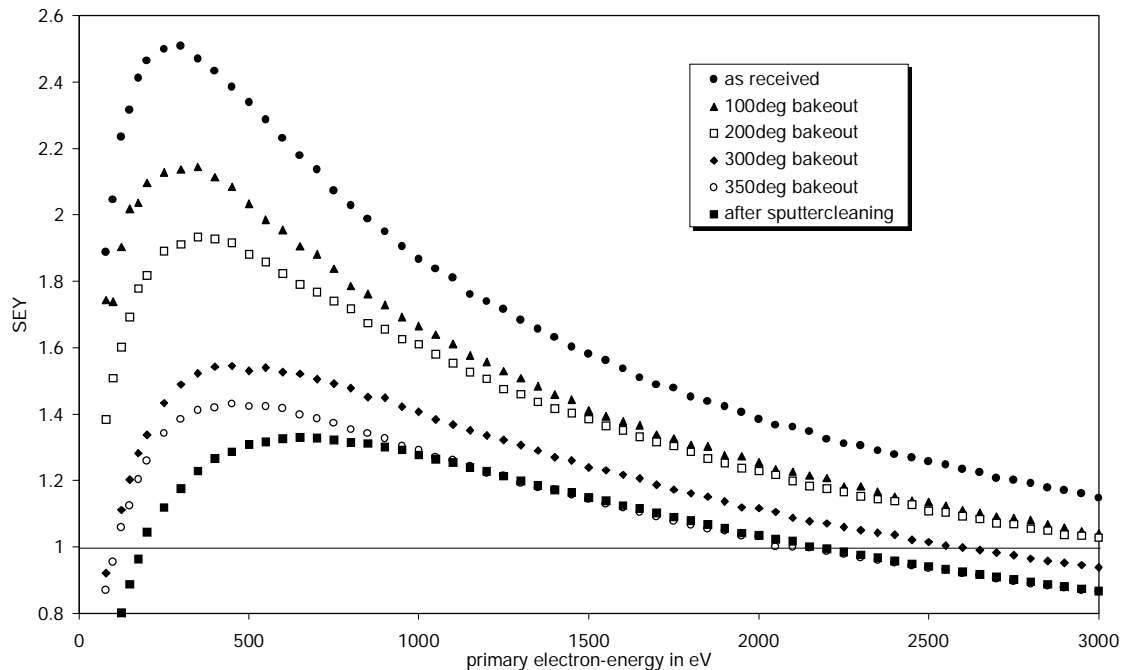


Figure 19; Influence of different levels of surface contamination on the SEY. Removal of adsorbents results in a reduction of secondary electron emission and in a shift of  $E_{\max}$  to higher primary electron energies.

A 350°C bakeout decreases the SEY significantly.  $\delta_{\max}$  of a copper sample as received from the chemical cleaning was reduced from 2.5 to 1.4. The same sample was again baked at 350°C, but

this time it was first sputter-cleaned and then exposed to air for 14 days before the bakeout. This procedure decreased  $\delta_{\max}$  to 1.2.

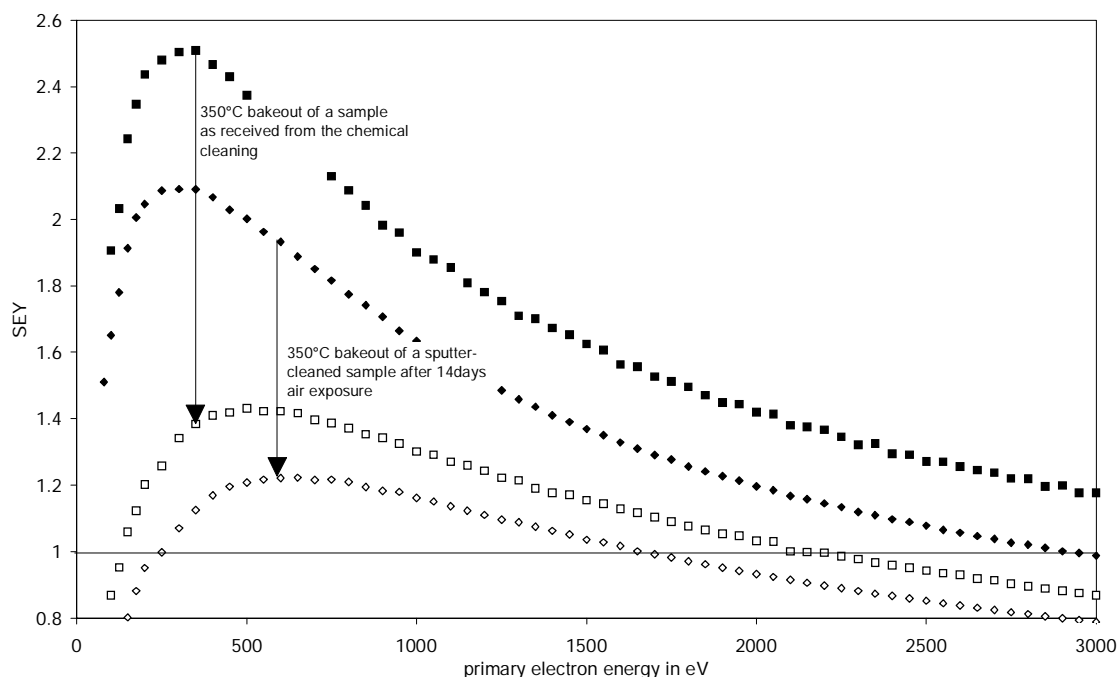


Figure 20; Difference of the secondary electron emission after a 350°C bakeout of a sample as received and after a 350°C bakeout of a sample which had been sputtercleaned and then exposed to air for 14 days

After a 350°C bakeout  $\delta_{\max}$  was lower than 1.25 for samples that were exposed either to air or to pure water vapour, provided they had been sputter-cleaned before the exposure and that the air exposure did not last longer than 20 days. The secondary electron emission of those samples did not change after consecutive oxygen exposure.

This indicates a remaining oxidised surface after the 350°C bakeout following a pure water exposure. This was surprising because it is reported that pure water vapour does not react with the hot copper surface. Possibly the samples were oxidised by some oxygen originating from water molecules which had been dissociated on the hot chamber- or getter pump surfaces during the bakeout.

The maximum SEY of an initially sputtercleaned copper sample, which was exposed to air for 50 days, was decreased to 1.4 by a 350°C bakeout.

Similarly,  $\delta_{\max}$  of the samples as received from chemical cleaning could only be reduced to values between 1.4 and 1.5. This indicates that several monolayers of a contaminant with a SEY higher than that of copper remain on the sample surface after bakeout.

The Auger electron spectrum of a sample as received which was baked at 350°C is shown in Figure 21. The spectrum gave a surface composition of 53% copper, 36% carbon, 10% oxygen and traces of chlorine.

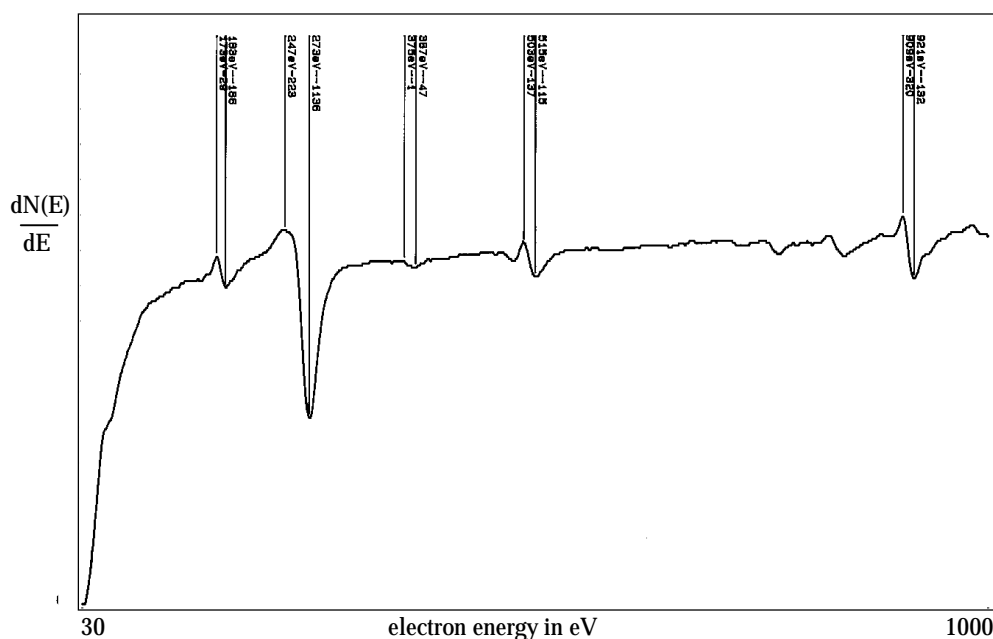


Figure 21; Auger electron spectrum of copper as received from the chemical cleaning after an ex-situ 350°C bakeout. The peaks at 185 eV, 275 eV, 517 eV and 921 eV are characteristic for chlorine, carbon, oxygen and copper respectively.

The sample had to be exposed to air after dismounting it from the vessel until it was brought into the vacuum chamber of the Auger electron spectrometer. Some of the detected species could have been adsorbed during this exposure. Nevertheless, the high amount of carbon is striking. Much less carbon was found on samples which had been sputtercleaned before the unavoidable air exposure. Atomic carbon has a lower SEY than copper but some of the carbon could belong to adsorbed hydrocarbons which possibly cause a higher secondary electron emission.

### 5.7 Influence of an air exposure at high temperature

Several copper samples were exposed to air between 5 and 60 minutes at a temperature of 350°C. After this procedure  $\delta_{\max}$  is about 1.15. A following 350°C bakeout under vacuum, decreases  $\delta_{\max}$  to about 1.05. The energy interval in which the SEY exceeds unity is also considerably decreased from 150 eV-1850 eV after glow discharge cleaning to 250 eV-950 eV after heating in air and bakeout at 350°C. The reduced secondary electron emission of the samples which were heated in air could be attributed to 3 different surface characteristics:

- 1) The low SEY could be due to the formation of a thin layer of CuO, which is reported to appear at 350°C (see 2.3). However, Auger analysis of a sample heated in air gave an oxygen concentration in the bulk of 17%. It is not clear why only so little oxygen was detected, but if the results are correct this would indicate an understoichiometric content of oxygen even for Cu<sub>2</sub>O. Furthermore, the oxygen concentration of the investigated sample was constant in the upper 5300 Å. It is therefore unlikely that a CuO film which is thick enough to influence the SEY remains on the samples at room temperature.
- 2) The reduction of secondary electron emission could also result from an increased thickness of the oxide layer provided that some of the secondary electrons initially originate from not oxidised copper. The elemental depth profile of the samples showed that the thickness of the oxide layer is only 15 Å after oxidation at room temperature, whereas it is 700 Å and 5300 Å



after heating the copper 5 minutes and 60 minutes at 350°C in air respectively. Nonetheless, the thickness of 15 Å corresponds with about 5 monatomic layers and it is assumed that most emitted secondary electrons originate from these layers. Furthermore, the  $\delta_{\max}$  value of Cu<sub>2</sub>O measured by Bruining is 1.19-1.25 [3] which is not in accordance with the obtained 1.05.

- 3) Besides the surface composition also the surface structure could be changed after air exposure at high temperature and consecutive bakeout. Cracks might appear after this procedure which could change the surface structure such that secondary electron emission is reduced afterwards (see 2.1.6).

The components of superconducting cavities can usually not be baked at temperatures as high as 350°C. Therefore, copper samples were heated in air only to 150°C and afterwards baked at this temperature for 6 hours. In Figure 22 the resulting  $\delta(E_p)$  distribution is compared with the SEY values obtained after a 24 hours bakeout at 150°C and the values which were measured after 24 hours baking at 350°C.

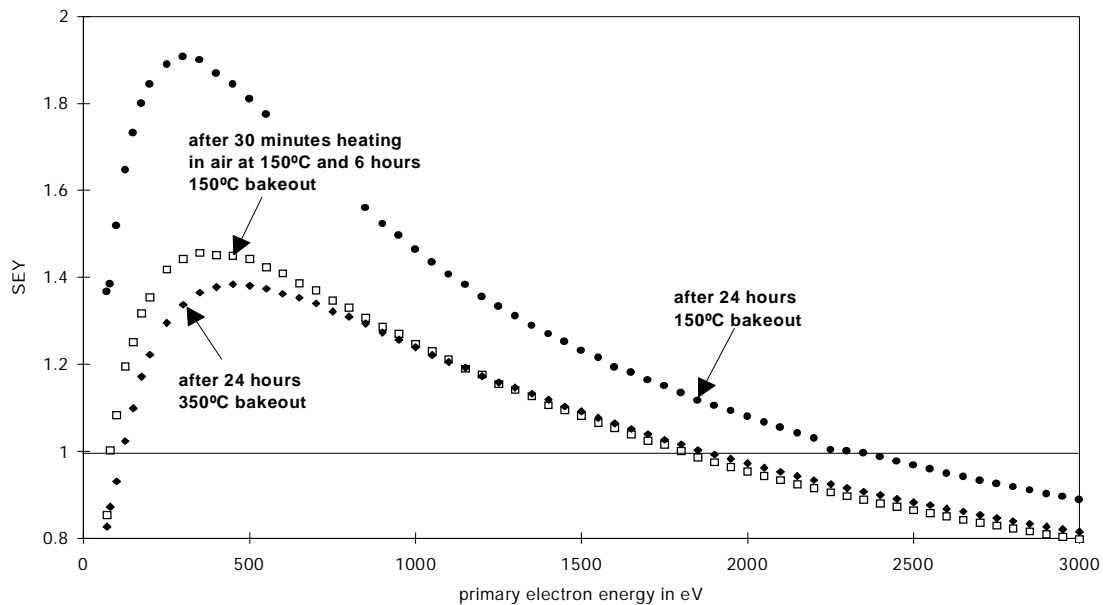


Figure 22; Comparison of secondary electron emission after 3 different treatments of copper surfaces: a) 24 hours 150°C bakeout b) 150°C exposure to air with consecutive 150°C bakeout for 6 hours c) 24 hours 350°C bakeout

The heating at 150°C in air combined with a 150°C bakeout under vacuum reduces the SEY much more than a simple bakeout at the same temperature does. Besides a modification of the bulk copper, it seems that the contaminating layers are favourably affected during the heating in air process. Hence, for copper equipment of superconducting cavities that can only be heated to moderate temperatures, an air exposure at such temperatures might be advantageous.

For general vacuum applications it would be interesting to compare the outgassing rate of a copper surface heated in air and baked at 150°C with one that had only been baked at 150°C under vacuum. As there is a strong correlation between secondary electron emission and surface contamination, the reduced SEY indicates less absorbed species on the copper surface after the heating in air process. As a result, the thermal outgassing rate during conditioning might be reduced after this procedure.

### 5.8 Influence of an air exposure on the SEY of copper oxidised at 350°C in air

A copper sample which was exposed to air for 5 minutes at 350°C (thick oxide layer) was baked at 350°C under vacuum together with a sample as received (thin oxide layer). Both samples were then exposed to air. Figure 23 compares the  $\delta_{\max}$  values which were obtained after different times of air exposure.

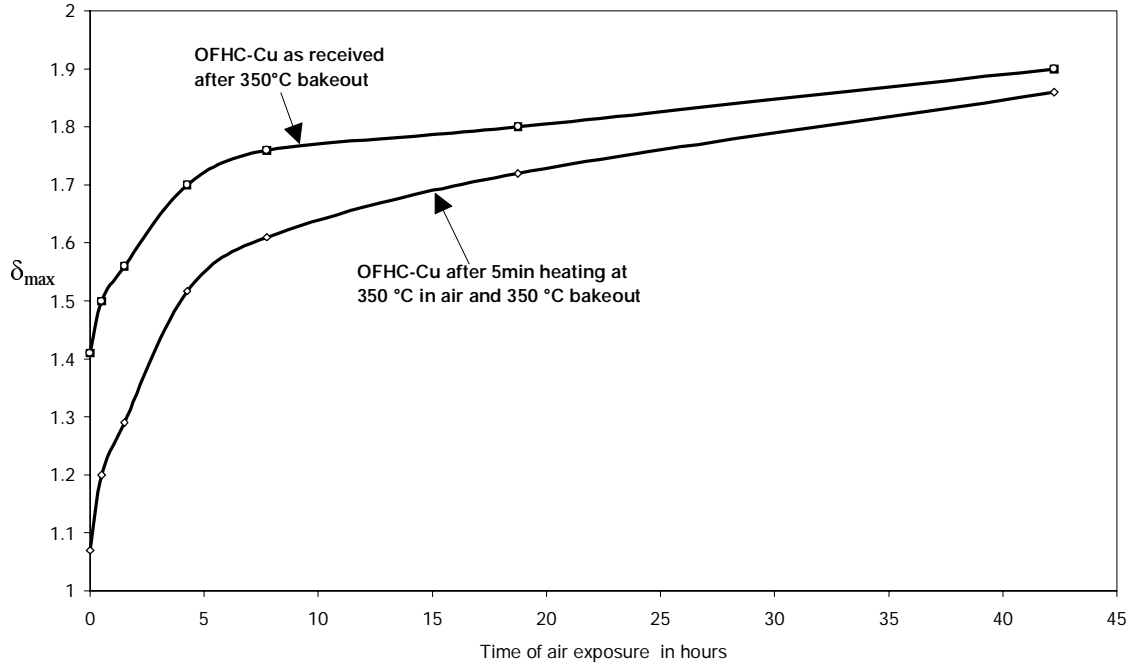


Figure 23; Different maximum SEY  $\delta_{\max}$  of strongly oxidised copper after 350°C bakeout and of copper as received after 350°C bakeout as a function of the air exposure time at atmospheric pressure outside the vacuum vessel

For multipacting not only  $\delta_{\max}$  is of interest but also the energies  $E_1$  and  $E_2$  where the SEY goes beyond and below unity. Figure 24 shows the characteristic SEY versus primary electron energy curves of the two samples.

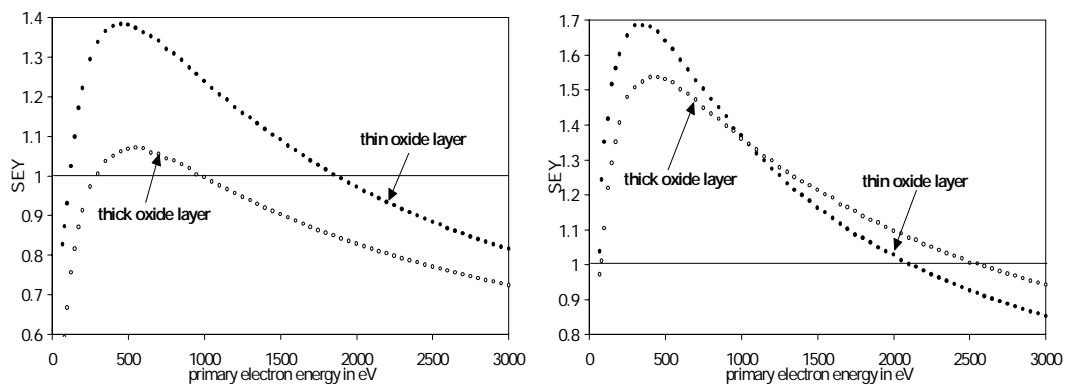


Figure 24; SEY of a thick copper oxide layer compared with the SEY of a sample oxidised at room temperature after a 350°C bakeout

SEY of the same samples after 4 hours air exposure

With increasing air exposure time, the difference in secondary electron emission of the two samples becomes smaller. After 4 hours air exposure the SEY of the strongly oxidised sample is

higher for primary electron energies above 1 keV. After two days air exposure  $\delta_{\max}$  of the strongly oxidised sample is only slightly lower than that of the sample which had been oxidised at room temperature and primary electrons with an energy higher than 500 eV cause a higher SEY of the strongly oxidised sample. A 50 days air exposure increased  $\delta_{\max}$  of a strongly oxidised sample to 2.3, whereas  $\delta_{\max}$  of a sample oxidised at room temperature was only 2.1.

Those results underline that it is not sufficient to consider only the initial state of a surface. Gases which interact with the surface, in particular air, can have a decisive influence on the occurrence of multipacting, and an initially favourable surface can turn out to be detrimental after air exposure.

### ***5.9 Conditioning of the LEP2 power couplers together with copper plated extensions which were heated in air at 350°C***

It is a delicate operation to apply high powers to vacuum RF devices for the first time. Large amounts of gases are adsorbed on the surfaces which can be abruptly desorbed if the power is raised too quickly. The resulting pressure rise can lead to discharges which are able to destroy the RF device. Besides thermal desorption, electron induced desorption due to the occurrence of multipacting is responsible for this behaviour. To avoid damage of the RF structures the whole cavity has to be conditioned before high power levels can be achieved without risking the sudden release of large amounts of gas.

Conditioning is hence a controlled gas desorption. The RF power is slowly increased and as soon as the pressure reaches a certain threshold the RF power is reduced until the a low pressure is re-established by the vacuum pumps. Sharp pressure rises are usually induced by multipacting. In most cases the SEY decreases when contaminating layers are removed and consequently multipacting discharges tend to eliminate themselves /38/. This can however be an expensive and time consuming procedure. In addition to the conditioning of the entire cavity, the power couplers of the LEP2 cavities are pre-conditioned separately at room temperature in order to clean the couplers as much as possible before they are grouped with the cavities. Therefore, two couplers are mounted on a conditioning bench in a clean room class 100 together with the so-called "extensions".

The extension is basically a double walled stainless steel tube of 53 cm length which can be cooled with gaseous helium flowing between the two walls. Its function is to limit the heat flow into the cavity surrounding liquid helium bath. The inner surface of the extension represents the outer tube conductor of a coaxial line and it is plated with copper.

During pre-conditioning the RF power is at first pulsed with different pulse lengths and repetition rates. Then the power is cyclically increased and decreased and finally a constant RF-power of about 180 kW is applied. After pre-conditioning the clean copper surfaces are exposed to an inert gas atmosphere ( $N_2$ ) in order to limit the detrimental impact of the unavoidable air exposure before the couplers and extensions are finally mounted to the cavities.

Each power coupler is equipped with a pressure gauge and an electrode which detects secondary electron currents. If the pressure reading exceeds  $5 \cdot 10^{-7}$  mbar the RF power is automatically reduced. The registration of the secondary electron currents allows to correlate pressure bursts to multipacting and it is also possible to determine in which of the two coaxial lines multipacting appears. Multipacting is observed at distinct power levels and it is of the single point type with electron orbits starting and ending on the outer conductor of the coaxial line /39/, i.e., the inner, copper plated tube of the extension. The strongest multipacting arises at an input power of about

180 kW and the energy of the corresponding primary electrons has been calculated as about 400 eV.

In an attempt to decrease the SEY of the extensions and to evaluate its influence on RF pre-conditioning of the couplers, two extensions were prepared with the procedure described in chapter 5.7, i.e., they were exposed to air at 350°C and baked at 350°C under vacuum. Unfortunately, the copper film of one extension partly fall off after this procedure and the extension could not be used. The couplers were therefore mounted on the conditioning bench together with the remaining extension and one extension which was chemically cleaned and high pressure rinsed but not heated in air (standard extension). By mistake the whole assembly was then baked at 150°C for 72 hours under vacuum instead of 24 hours as it is the normal procedure before pre-conditioning. The air exposure time of the strongly oxidised extension before it was mounted on the conditioning bench was only 2 hours.

During pre-conditioning the following observations were made:

- Pulsing (1 ms pulse length and a repetition rate of 100 ms) initially increased the pressure from about  $10^{-10}$  mbar to  $2 \cdot 10^{-7}$  mbar. After 7 hours pulsing a RF power of 250 kW could be achieved. Usually it takes about 20 hours pulsing to reach this power level.
- After the pulsing period the RF power was cycled up and down between 0 and 250 kW. Electron activity was initially observed on both couplers at 180 kW. After some hours only the standard extension showed electron activity.
- The constant power test at 180 kW could be carried out without difficulties and no electron activity was observed on both couplers. After the constant power test the RF power was once more cycled up and down. At 180 kW there was again strong electron and vacuum activity, exceeding even the interlock levels. Electron activity was only detected on the standard extension.
- In order to test the strongly oxidised extension only, the standard extension was positively biased to 2.5 kV thus suppressing multipacting. After this measure the RF power could be cycled up and down without the occurrence of multipacting and only a low vacuum activity due to thermal outgassing was observed.

The whole pre-conditioning procedure lasted about 3 days instead of 7 days which are usually needed to pre-condition the couplers.

## 6. Discussion and Outlook

The effect of an air exposure on the SEY of pure polycrystalline copper at room temperature is at least partly caused by the reaction with oxygen and the adsorption of water vapour.

The oxidation of the copper surface is a comparatively fast process that is complete after some seconds of air exposure. At room temperature only  $\text{Cu}_2\text{O}$  is formed which has a lower SEY than pure copper. The initial decrease of  $\delta_{\text{max}}$  of pure copper to about 1.2 after air exposure is hence due to the oxide formation. Technical copper surfaces that were not cleaned in-situ are always oxidised and no initial decrease of the SEY can be expected for such surfaces.

After the fast oxidation a comparatively slow process increases the SEY steadily until, after about 8 days,  $\delta_{\text{max}}$  reaches values higher than 2. It is not yet understood what is responsible for this strongly increased secondary electron emission. Water vapour seems to play an important role in this process, but pure water vapour can only increase  $\delta_{\text{max}}$  to 1.5 and 1.6 for oxidised copper and clean copper respectively. A co-adsorption of two or more gases present in air could be responsible for the high SEY after long exposures. The assumption that water plays a crucial role is backed by the fact that an initially clean sample which was put into distilled water for 10 minutes during a 45 minutes air exposure gave a  $\delta_{\text{max}}$  of 2.4.

The strong difference between air exposures inside and outside the vacuum vessel is astonishing. Three possible reasons are suggested:

- The humidity inside the vessel in the first two hours after braking the vacuum is lower than it is in the laboratory. For short air exposures this could be the reason for a different SEY after exposure in- and outside the vessel. However, the strong difference after long exposures can hardly be attributed only to the humidity.
- Reactive pollutants in air like  $\text{NO}_2$  could influence the SEY and they could be less concentrated inside the vessel because they are pumped by the walls. Therefore, it would be interesting to expose copper samples to pure  $\text{NO}_2$  in order to figure out the influence of such gases on the SEY.
- The concentration of dust inside the vessel is probably lower than outside. This could explain the different SEY, provided dust affects secondary electron emission. Samples which were protected with aluminium foil and a plastic bag during air exposure seemed to have a less increased SEY than samples that were exposed to the same dose of air without any protection. This phenomenon could be related to a possible impact of dust on the SEY and should be confirmed by some long term exposures. On the other hand the dust filtered air in a clean room class 100 resulted in the same SEY as an equal dose of not filtered air.

A bakeout of copper equipment that has been exposed to air is always advantageous and the bakeout temperature should be as high as possible. For a sample as received,  $\delta_{\text{max}}$  was reduced from 2.5 to 1.9 and 1.4 after a  $150^\circ\text{C}$  and a  $350^\circ\text{C}$  bakeout respectively. Dust can hardly be removed from a surface by a bakeout and therefore one can conclude that dust by its one does not strongly increase the SEY. However, the combination of dust and some other contaminant might result in an increased SEY.

Heating copper in air combined with a consecutive bakeout under vacuum reduces secondary electron emission. Baking the samples 5 minutes at  $350^\circ\text{C}$  in air and a following  $350^\circ\text{C}$  bakeout under vacuum decreased  $\delta_{\text{max}}$  to a value close to unity, thus providing a surface which is unlikely

to cause multipacting problems. This behaviour is not yet understood but it could be attributed to 3 different surface properties:

- A thin film of CuO could remain after the heating in air process and this film could possibly have a lower secondary electron emission than Cu<sub>2</sub>O.
- The Cu<sub>2</sub>O layer thickness increases during air exposure at elevated temperatures. If this layer has a SEY which is close to unity it could be the reason for the low SEY after air exposure at 350°C.
- The surface structure could be changed after the treatment.

Some copper samples which were exposed to air at high temperature gave  $\delta_{\max}$  values of about 0.95 after they had been sputter cleaned but it is not clear if this low yield is attributed to the surface material or to a changed surface topography. This should be further investigated with different sputtering gases. Light gases like helium might allow an in-situ sputter cleaning of the whole cavity which would certainly be an ideal solution as far as multipacting is concerned. It would also be interesting to examine the secondary electron emission of oxide layers which have been produced by reactive sputtering of copper in gas mixtures containing oxygen.

It is reported that a velvety porous Cu<sub>2</sub>O layer can be formed by anodic oxidation of copper and subsequent heat treatment under vacuum /39/. Such a layer could have a low SEY for both reasons, the surface material as well as the surface structure. An investigation of anodically oxidised copper samples is underway, but results have not yet been obtained.

The pre-conditioning of the LEP2 power couplers together with a strongly oxidised extension was encouraging. The strongly oxidised extension was easier to pre-condition than the standard extension and multipacting did not re-appear after the constant power test. However, the results give not a clear answer whether pre-conditioning is simplified by the tested surface treatment. Firstly the baking procedure of the conditioning bench differed from the standard procedure, i.e., the bakeout lasted longer than usual, and secondly the treated extension had been separately baked at 350° before it was mounted on the conditioning bench while the standard extension had not been baked before.

In addition it is not evident that couplers and extensions which can be pre-conditioned easily will make a good performance during conditioning of the cold cavity. In this case during conditioning desorbed species from a warm surface area can be re-adsorbed onto a cold surface, causing a high SEY there /40/. The condensate layer can become so thick, that all secondary electrons originate from this layer and the SEY of the base material has practically no influence any more.

Therefore, further extensions will be prepared in order to test their influence not only on pre-conditioning but also on conditioning. If anodic oxidation is suitable to reduce secondary electron emission this technique will be applied. Afterwards the extensions will follow exactly the same cleaning and rinsing procedure of the standard extensions before they are tested during pre-conditioning and conditioning of the entire cavity.

In the final phase of LEP2 the accelerator will be equipped with 272 superconducting RF cavities. For other projects like TESLA, the planned superconducting linear collider, much more cavities (about 2000) will be needed and clearly the conditioning time of the couplers and cavities has to be limited. A strong oxidation of copper might be a simple and effective method to provide surfaces with a low SEY which could possibly reduce multipacting problems.

## References

- /1/ W. Weingarten, "Superconducting Cavities-Basics", CERN Accelerator School-Superconductivity in Particle Accelerators, Hamburg, (1995)
- /2/ D. Proch, D. Einfeld, R. Onken, N. Steinhauser, "Measurement of Multipacting Currents of Metal Surfaces in RF Fields", DESY Internal Report M-95-08, (1995)
- /3/ H. Bruining, "Physics and Applications of Secondary Electron Emission", Pergamon Press, London(1954)
- /4/ N. Hilleret, "Coefficient d'émission électronique secondaire de l'extrudal après divers traitements", CERN, Technical Note, (1983)
- /5/ A. J. Decker, "Secondary Electron Emission", Solid State Physics, Vol. 3, (1958)
- /6/ J. Barnard, J. Bojko, N. Hilleret, "Measurements of the Secondary Electron Emission of Some Insulators", CERN, Internal Note
- /7/ I. Buchholz, "Zur Lage des Maximums der Ausbeutekurve bei der Sekundärelektronen-emission", Z. Physik, (1969)
- /8/ J. Barnard, J. Bojko, N. Hilleret, J. M. Jimenez, "Secondary Electron Emission from Various Technical Materials", 7th Workshop on RF Superconductivity, Gif sur Yvette, (1995)
- /9/ O. Hachenberg, W. Brauer, "Secondary Electron Emission from Solids", Heinrich-Hertz-Institut, Berlin, (1981)
- /10/ Werner Espe, "Materials of High Vacuum Technology", Vol. 1, Pergamon Press, Oxford
- /11/ Henry. Leidheiser, "The Corrosion of Copper, Tin and Their Alloys", John Wiley and Sons, New York
- /12/ G. Honjo, J. Phys. Soc. Japan, 4, 330, (1949)
- /13/ "Corrosion of Copper and Copper Alloys", ASM Handbook, Vol. 13, (1987)
- /14/ Herbert Uhlig, "Korrosion und Korrosionsschutz", Akademie-Verlag, Berlin, (1970)
- /15/ Gmelins Handbuch der Anorganischen Chemie, 60 (Kupfer), Verlag Chemie GmbH, Weinheim, (1955)
- /16/ Yoshio Murakami, "Hydrogen Pumping by a New Catalytic Pump", Journal of Vacuum Science and Technology, Vol. 10, (1973)
- /17/ P.J. Goodhew, F.J. Humphreys, "Elektronenmikroskopie Grundlagen und Anwendungen", McGraw-Hill, London, (1991)
- /18/ H. Hantsche, "Röntgenmikroanalyse mit dem Rasterelektronenmikroskop», in «Praxis der Rasterelektronenmikroskopie und Mikrobereichsanalyse», expert verlag, (1994)
- /19/ "Handbook of Auger Electron Spectroscopy", Physical Electronics Industries, Inc., (1976)
- /20/ M. Lavarec, G. Boquet, A. Septier, "Lowering the Secondary Electron Emission Coefficient of Real Surfaces Due to the Primary Electron Bombardment", Institut d'Electronique Fondamentale, Orsay, (1978)
- /21/ B. Schiewe, Vorlesungsmitschrift "Elektronenmikroskopie", TFH-Berlin, (WS 1995)

- /22/ G.L. Weissler, R.W. Carlson, "Vacuum Physics and Technology", Academic Press, (1979)
- /23/ "Korrekturfaktor  $\psi$  für kurze Rohre als Funktion von  $l/d$ ", Berechnungsunterlagen, Katalog Teil 15, VEB Hochvakuum Dresden, (1982)
- /24/ P.A. Readhead, J.P.Hobson, "The Physical Basis of Ultrahigh Vacuum", Chapman and Hall LTD, (1968)
- /25/ A. G. Mathewson, "The Effect of Cleaning and Other Methods on the Vacuum Properties of Technological Materials Used in Ultra-High Vacuum", CERN, (1987)
- /26/ R. Calder, G. Dominichini, N.Hilleret, "Influence of Various Vacuum Surface Treatments on the Secondary Electron Yield of Niobium", Nuclear Instruments and Physics Research B13 631-636, (1986)
- /27/ H.E. Farnsworth, "Atomically Clean Surfaces", Department of Physics, University of Arizona
- /28/ R. Calder, A. Grillot, F. Le Norrand, A. Mathewson, "Cleaning and Surface Analysis of Stainless Steel Ultrahigh Vacuum Chambers by Argon Gas Discharge", Proceedings of the 7th Int. Vacuum Congress, Vienna, (1977)
- /29/ R.V. Stuart, "Vacuum Technology, Thin Films and Sputtering", Academic Press, London, (1982)
- /30/ ASM Handbook, Vol 5, "Surface Engineering", ASM International, (1994)
- /31/ Brian Chapman, "Glow Discharge Processes", John Wiley & Sons, New York, (1980)
- /32/ L. McDonnel, D.P. Woodruff, "A LEED Study of Oxygen Adsorption on Copper", Surface Science 46, (1974)
- /33/ O. Oda, L.J. Hanekamp, G.A. Bootsma, "An AES and LEED Study of Carbon and Oxygen Sorption on Copper Surfaces", Applications of Surface Science 7, (1981)
- /34/ J. A. Basford, Analysis of offgased water: Calibration and techniques, J. Vac. Sci.Technol. A 12(4)
- /35/ M. M. Chevalier, M. A. Tisserand, "L'Oxygène, Propriétés, Dangers, Mesures de Prévention", Institut National de Recherche et de Sécurité
- /36/ L.F. Wagner and W.E. Spicer, "Photoemission Study of the Oxidation of Copper Films", Surface Science Vol 46, 301-307 (1974)
- /37/ J.M. Heras, L. Viscido, "Work Function Changes upon Water Contamination of Metal Surfaces", Applications of Surface Science Vol. 4, 238-241, (1980)
- /38/ E. Haebel, "Couplers for Cavities", CERN Accelerator School, Superconductivity in Particle Accelerators, Hamburg, (1995)
- /39/ Yoshio Murakami, Tetsuo Kurisaki, Yukio Ishibe, Kosuke Okamoto, "Some Considerations on Large-Sized Catalytic Pumps for Nuclear Fusion Apparatus", Japan J. Appl. Phys. Suppl., (1974)
- /40/ E. Haebel, H.P. Kindermann, M. Stirbet, V. Veshcherevich, C. Wyss, "Gas Condensation on Cold Surfaces, a Source of Multipacting Discharges in the LEP2 Power Coupler", 7th Workshop on RF Superconductivity, Gif sur Yvette, (1995)



## Appendix

Scanning electron microscope images of the copper samples after different surface treatments

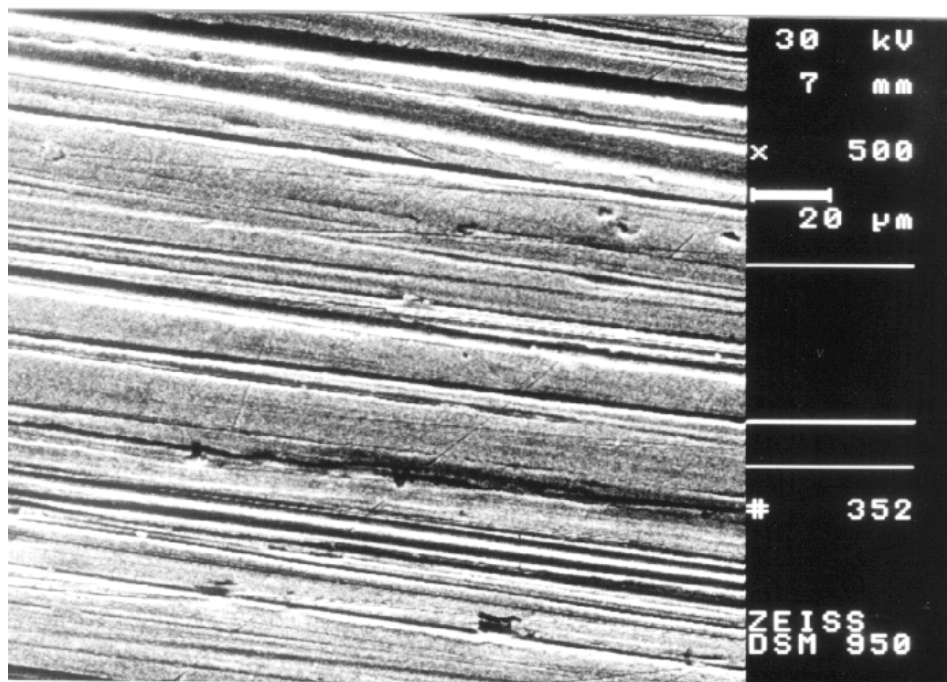


Figure 25; Copper sheet as received from the manufacturer.

Magnification = 500x

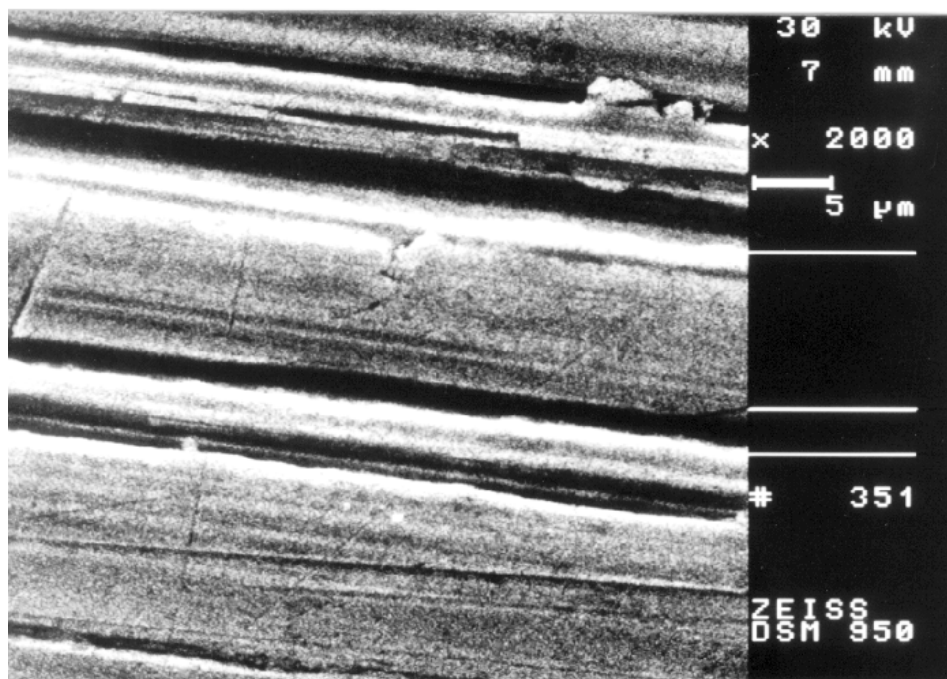


Figure 26; Copper sheet as received from the manufacturer.

Magnification = 2000x

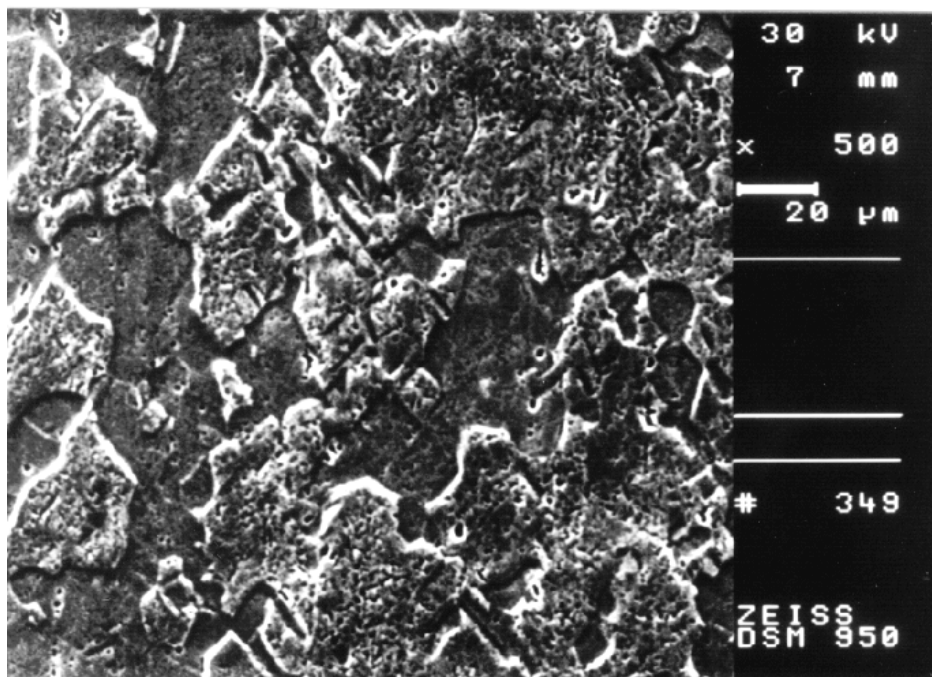


Figure 27; Copper sheet after chemical etching.

Magnification = 500x

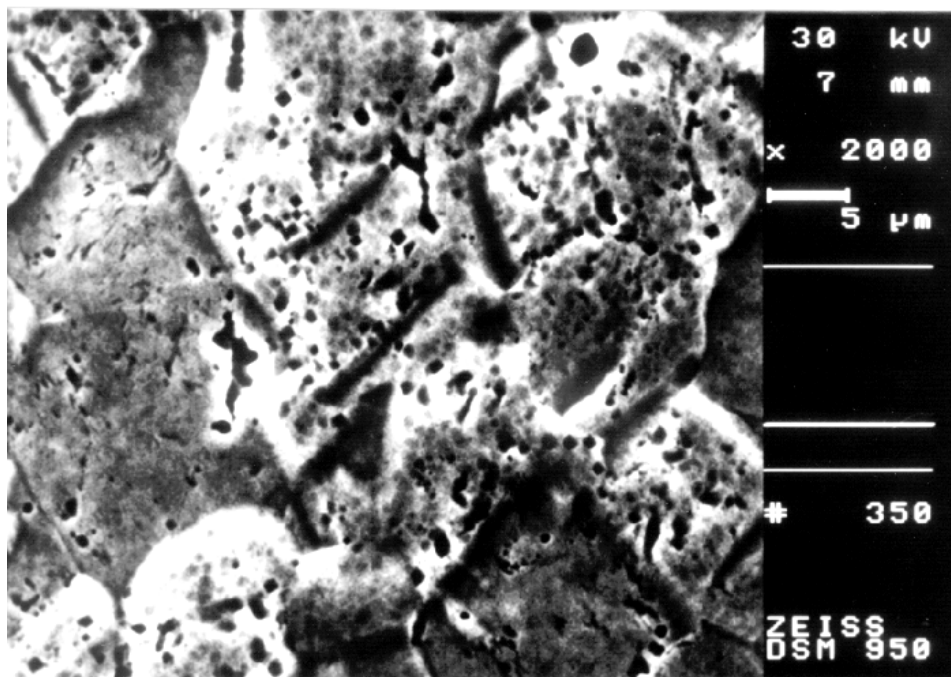


Figure 28; Copper sheet after chemical etching.

Magnification = 2000x

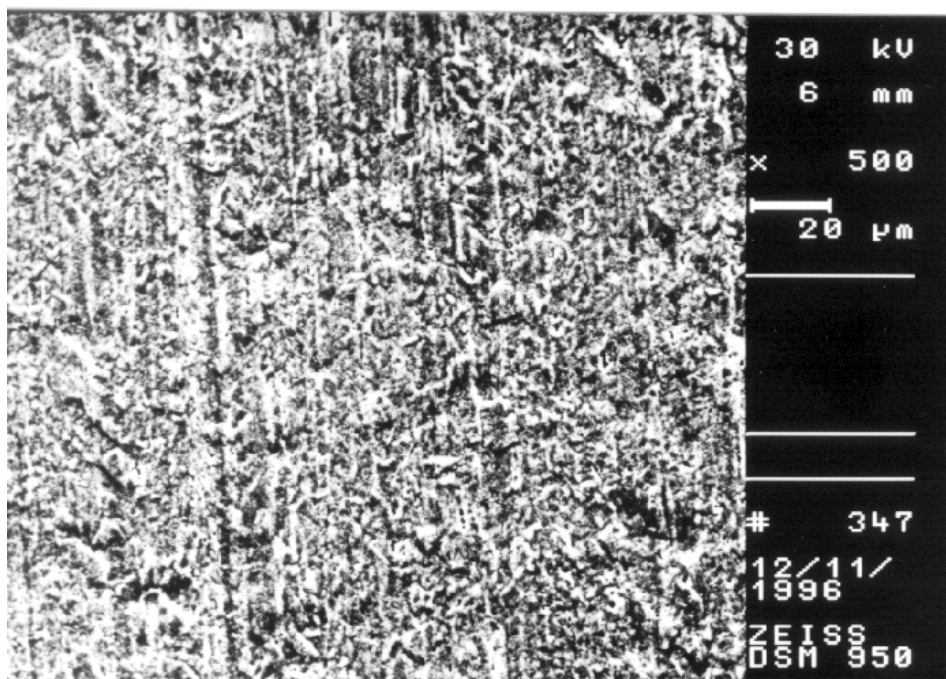


Figure 29; Copper sheet after glow discharge cleaning at  $350^{\circ}\text{C}$  (ion dose =  $2.8 \cdot 10^{18}/\text{cm}^2$ , ion current = 25 mA, dc voltage = 1 kV,  $p = 5 \cdot 10^{-2}$  mbar). Magnification = 500x

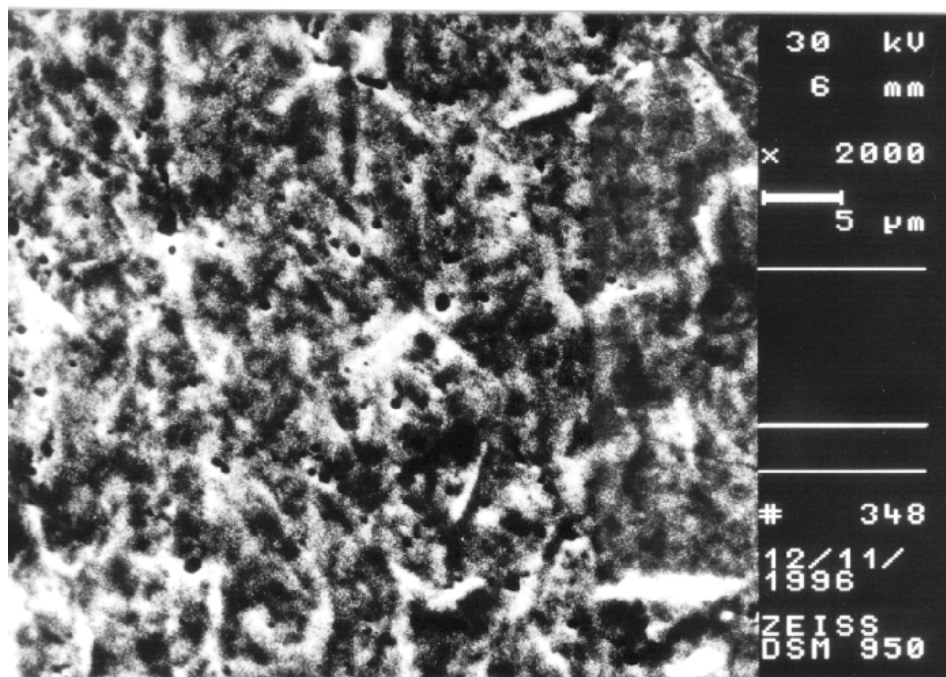


Figure 30; Copper sheet after glow discharge cleaning at  $350^{\circ}\text{C}$  (ion dose =  $2.8 \cdot 10^{18}/\text{cm}^2$ , ion current = 25 mA, dc voltage = 1 kV,  $p = 5 \cdot 10^{-2}$  mbar). Magnification = 2000x

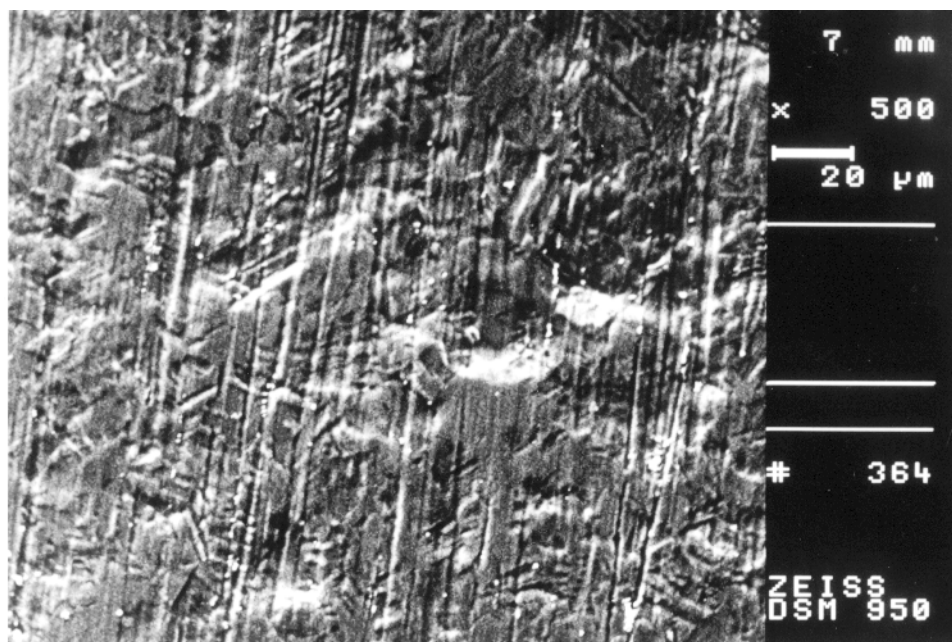


Figure 31; Copper sheet after glow discharge cleaning at ambient temperature (ion dose =  $2.8 \cdot 10^{18}/\text{cm}^2$ , ion current = 25 mA, dc voltage = 1 kV,  $p = 5 \cdot 10^{-2}$  mbar). Magnification = 500x

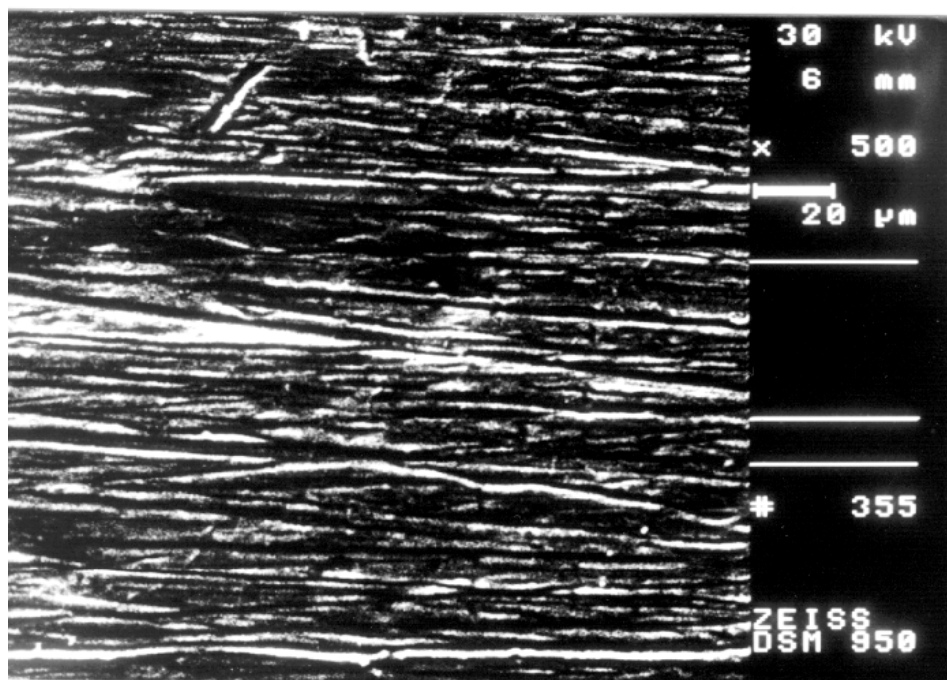


Figure 32; Copper sheet after oxidation at 350°C in air.

Magnification = 500x

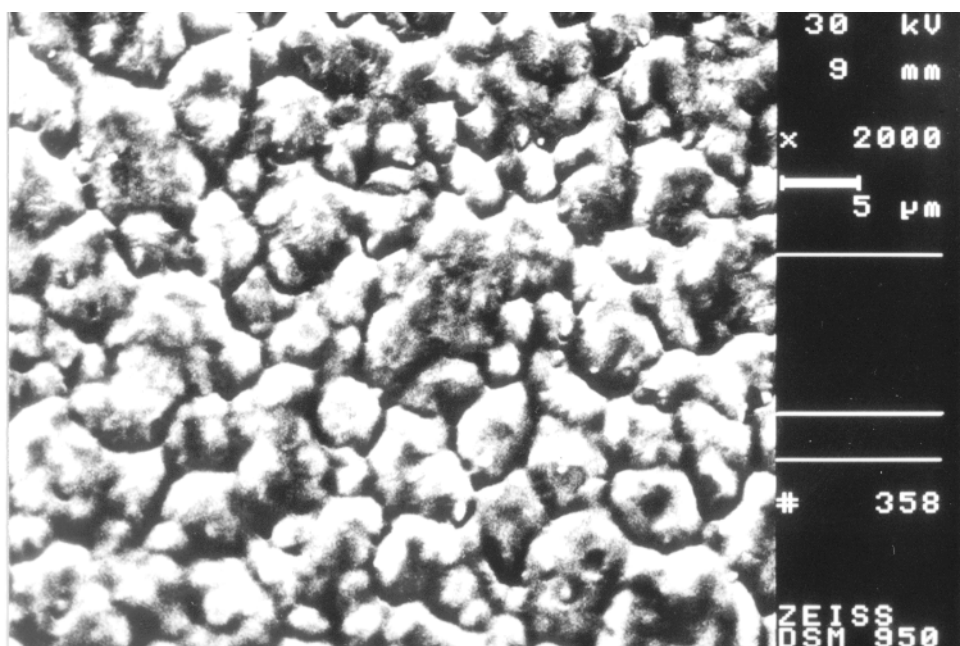


Figure 33; Copper sputter deposited on stainless steel.

Magnification = 500x

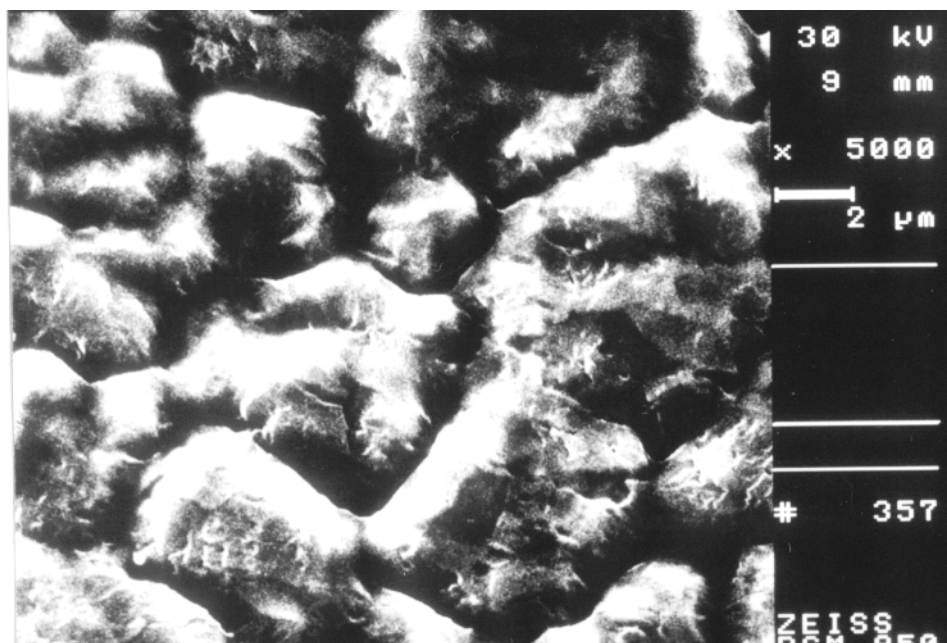


Figure 34; Copper sputter deposited on stainless steel.

Magnification = 2000x



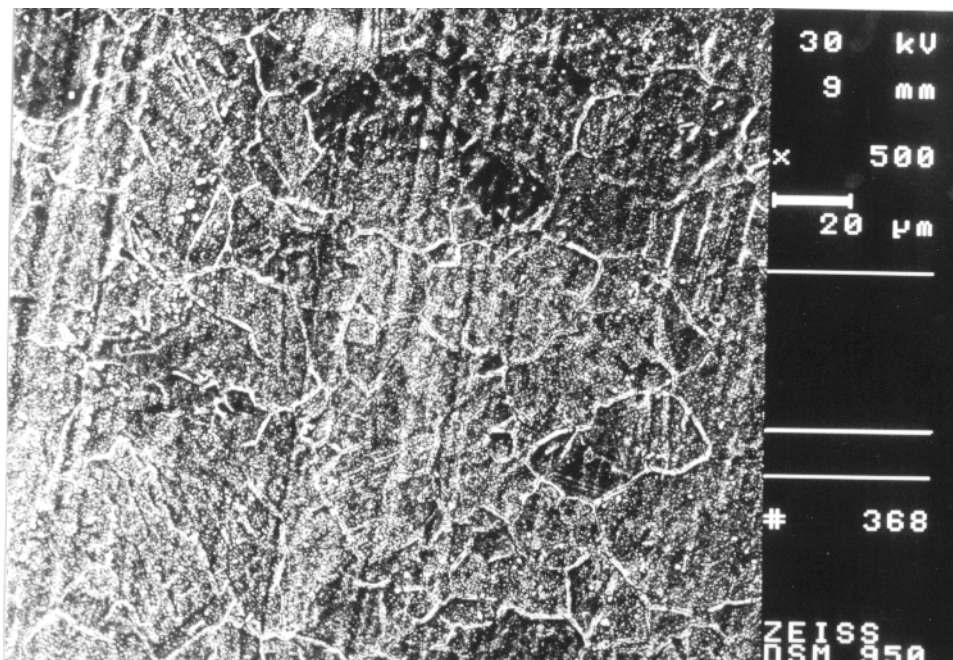


Figure 35; Copper sheet with a changed surface topography due to sputter etching (ion dose =  $10^{19}/\text{cm}^2$ , ion current = 25 mA, dc voltage = 1 kV,  $p = 5 \cdot 10^{-2}$  mbar). Magnification = 500x

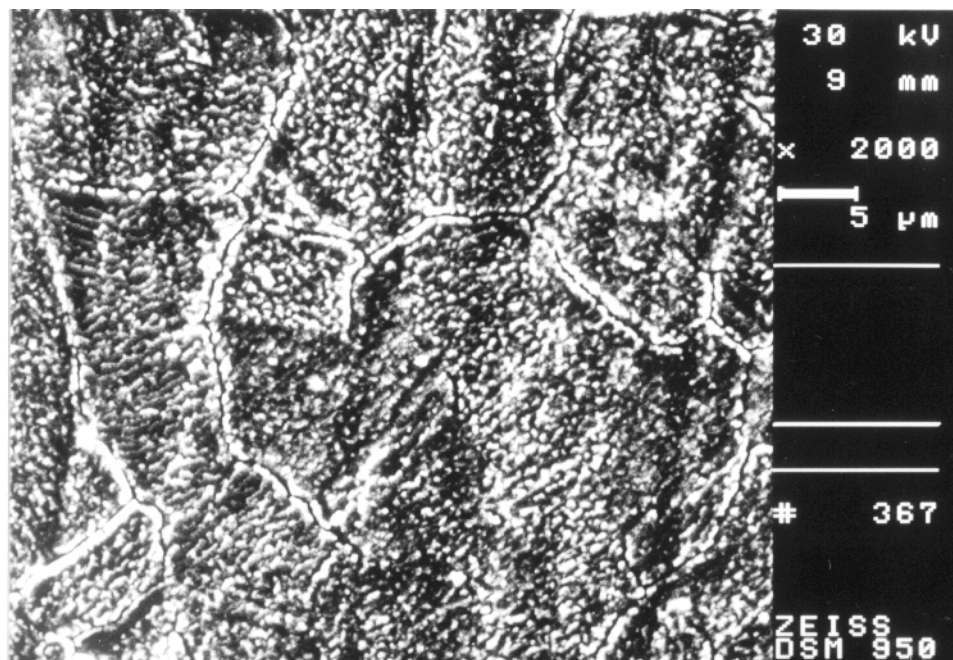


Figure 36; Copper sheet with a changed surface topography due to sputter etching (ion dose =  $10^{19}/\text{cm}^2$ , ion current = 25 mA, dc voltage = 1 kV,  $p = 5 \cdot 10^{-2}$  mbar). Magnification = 2000x

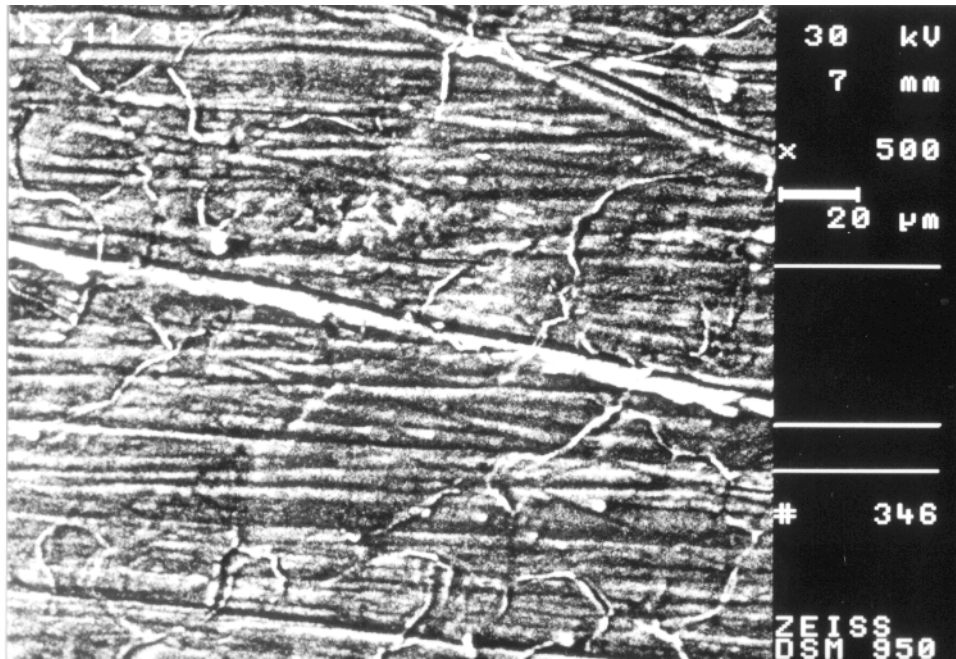


Figure 37: Copper with a strongly changed surface topography due to selective sputter etching (ion dose =  $10^{20}/\text{cm}^2$ , ion current = 25 mA, dc voltage = 1 kV,  $p = 5 \cdot 10^{-2}$  mbar) Magnification = 500x

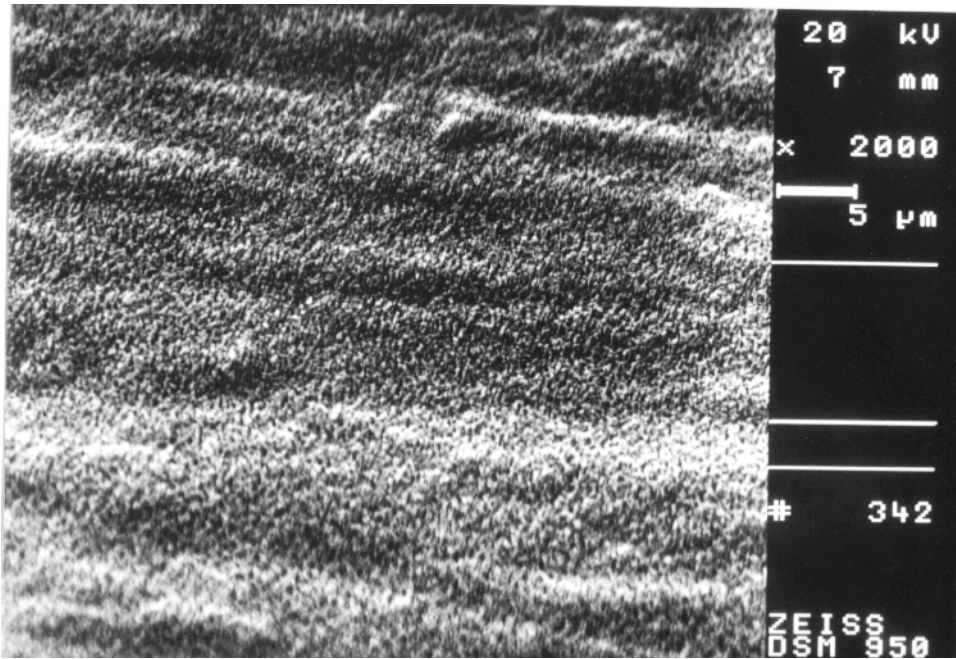


Figure 38: Copper with a strongly changed surface topography due to selective sputter etching (ion dose =  $10^{20}/\text{cm}^2$ , ion current = 25 mA, dc voltage = 1 kV,  $p = 5 \cdot 10^{-2}$  mbar). Magnification = 2000x

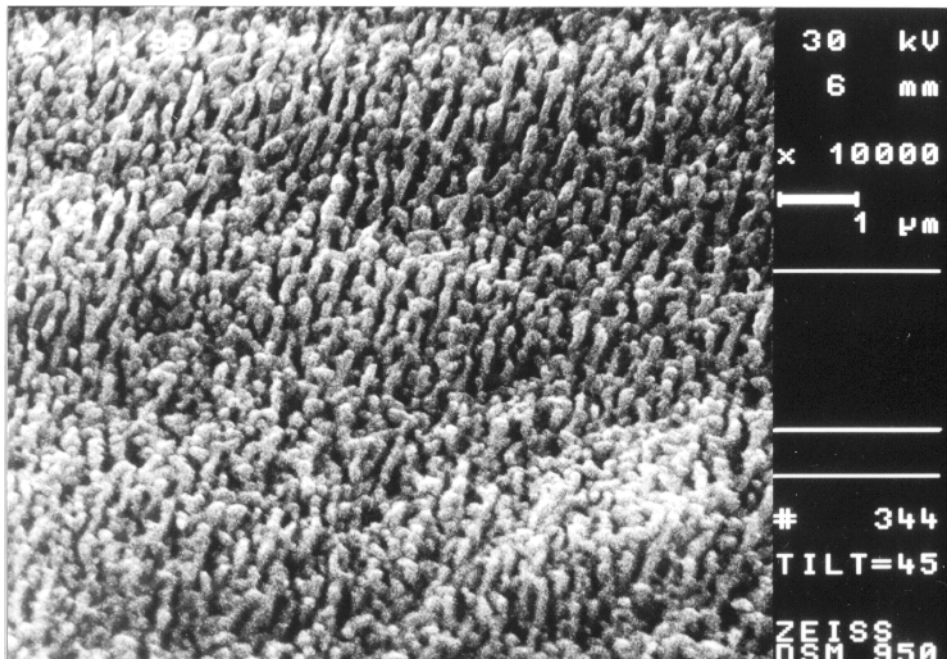


Figure 39: Copper with a strongly changed surface topography due to selective sputter etching (ion dose =  $10^{20}/\text{cm}^2$ , ion current = 25 mA, dc voltage = 1 kV,  $p = 5 \cdot 10^{-2}$  mbar). Magnification = 10 000x

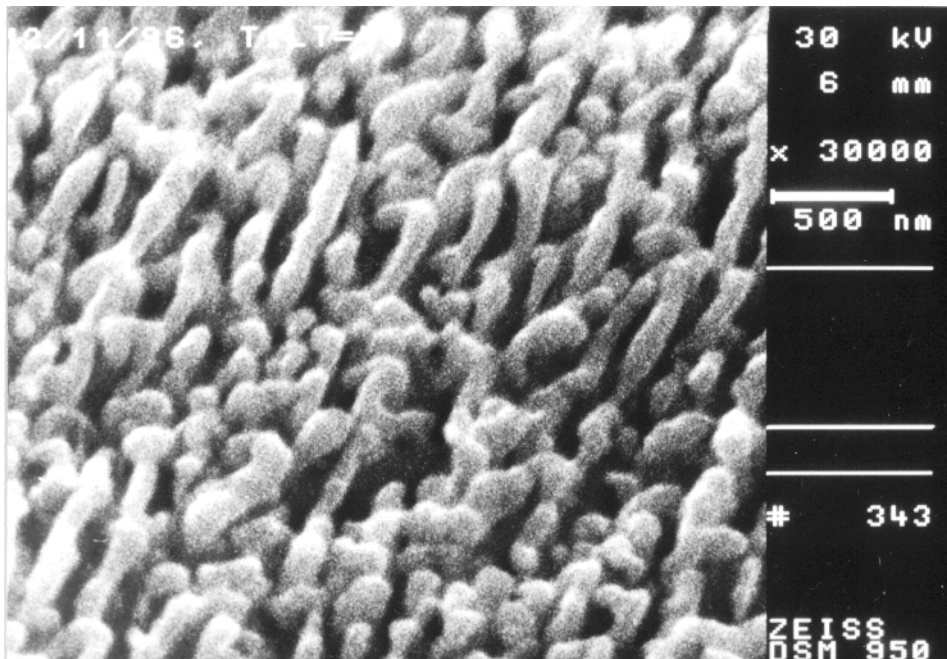


Figure 40: Copper with a strongly changed surface topography due to selective sputter etching (ion dose =  $10^{20}/\text{cm}^2$ , ion current = 25 mA, dc voltage = 1 kV,  $p = 5 \cdot 10^{-2}$  mbar) Magnification = 30 000x



## EDX-Spectra

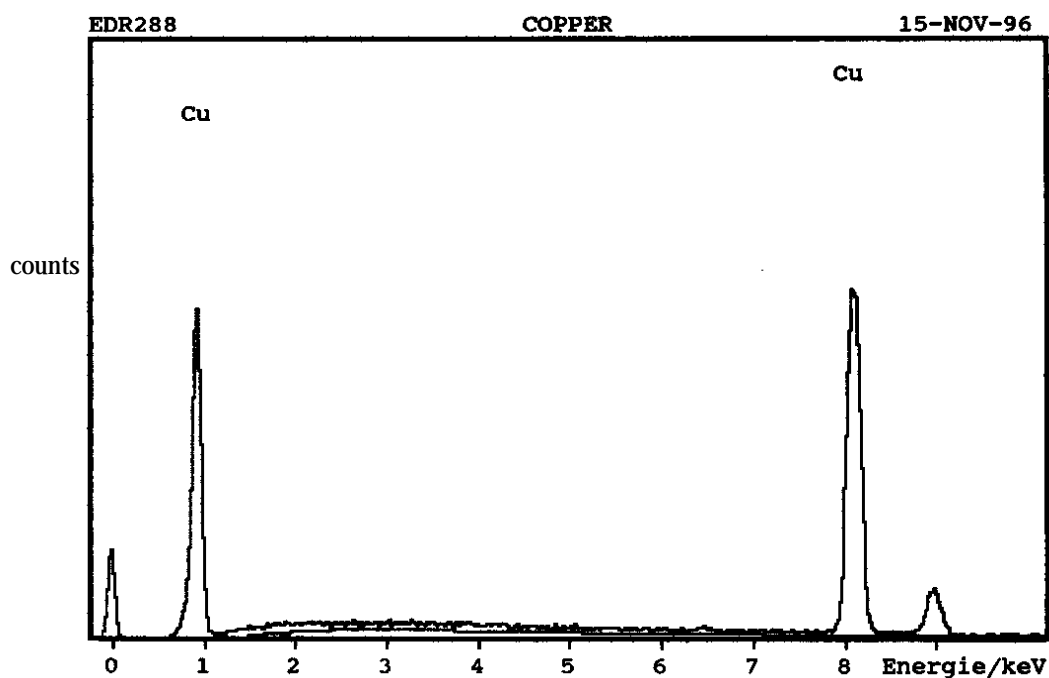


Figure 41; EDX-spectrum of copper after 15 minutes sputter cleaning. Carbon and oxygen which are certainly present on the surface can not be detected because their characteristic X-rays are absorbed by the detector window. No imbedded argon has been detected.

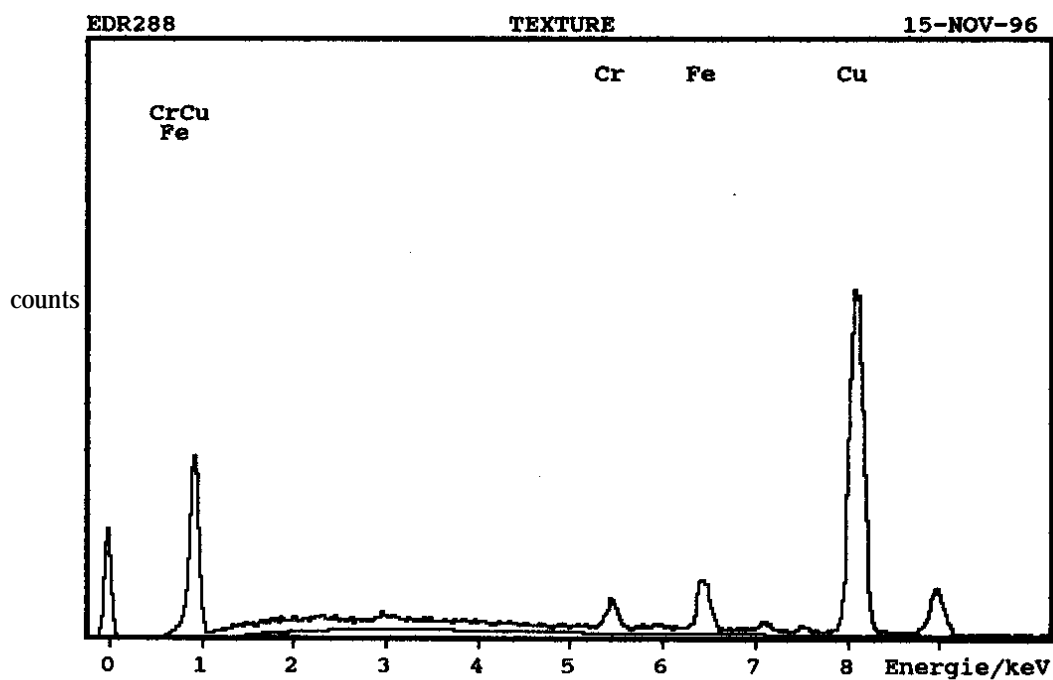


Figure 42; EDX-spectrum of a copper sample after long sputter etching. Iron and chrome originate probably from the sample holder which is at the same potential as the samples during the glow discharge.

## Auger electron spectra

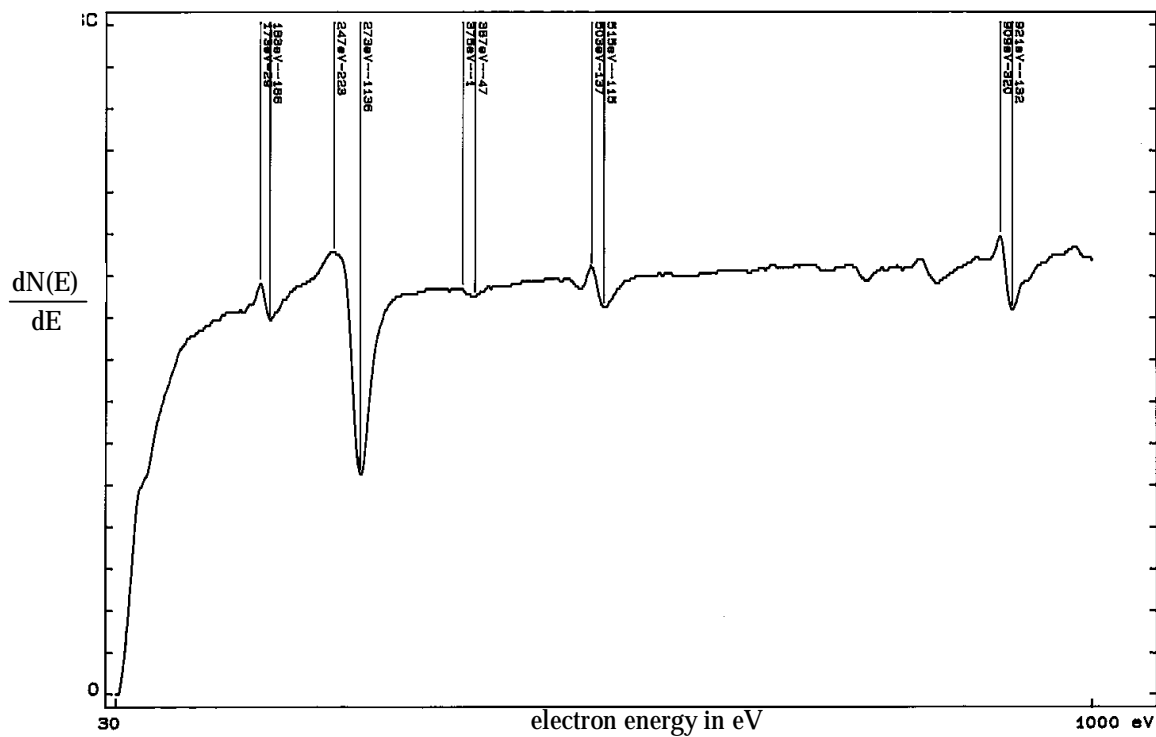


Figure 43; OFHC-copper sample after chemical cleaning. Chlorine (183 eV), carbon (273 eV), nitrogen (387 eV), oxygen (515 eV) and copper (921 eV) are present on the surface

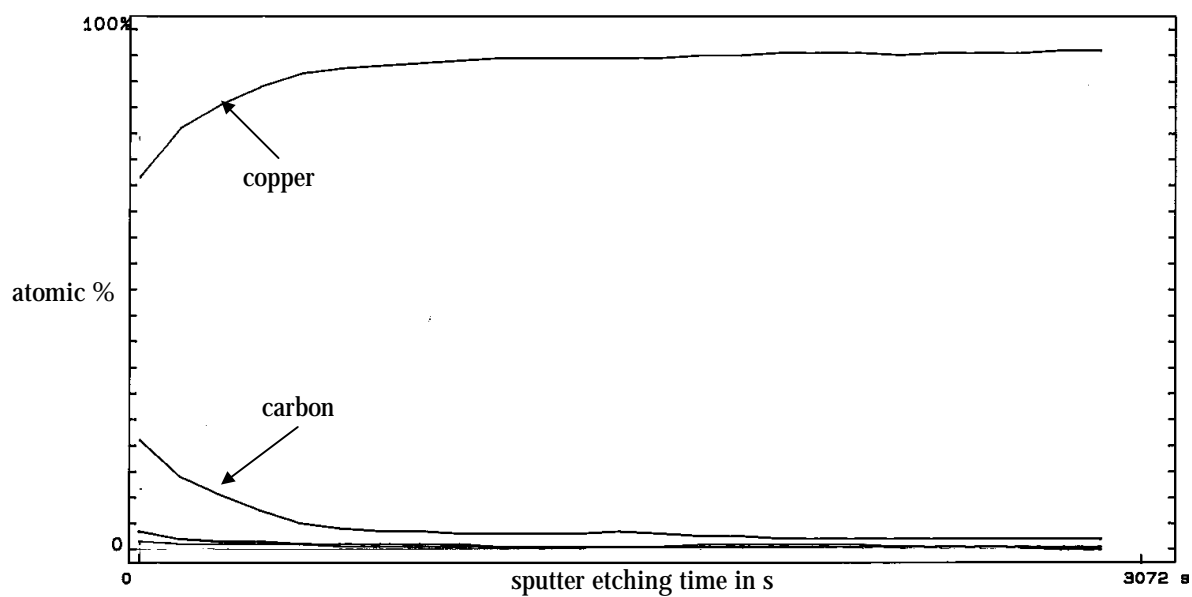


Figure 44; Depth profile of an OFHC-copper sample after chemical cleaning. Carbon is the main contaminant. The investigated depth is 840 Å.

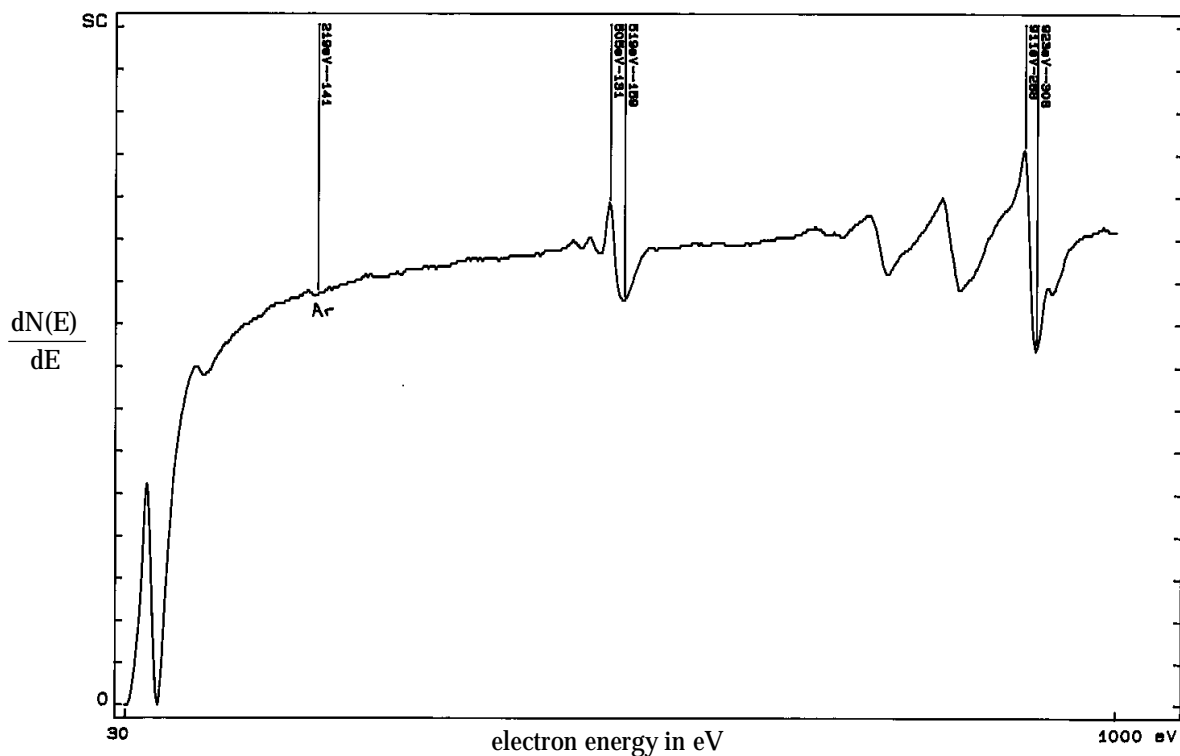


Figure 45; OFHC-copper sample after one hour at 350°C in air in a depth of 3500 Å. Argon (219 eV) is either remaining from a previous glow discharge cleaning or it has been implanted by the ion gun during depth profiling.

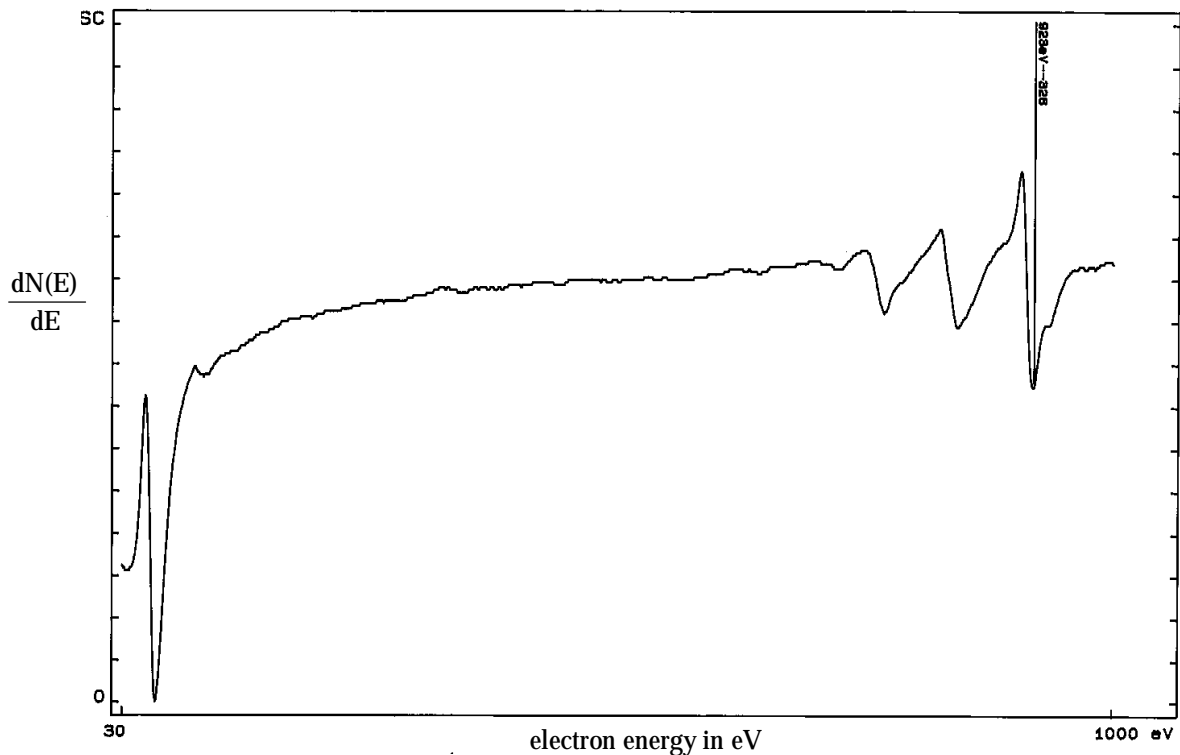


Figure 46; OFHC-copper sample after one hour at 350°C in air. After 7500 Å etching only copper (921 eV) is detected

Cracking pattern of the Balzers Quadrupole Mass Analyser QMA 112 for the exposed gases (secondary electron multiplier voltage = 2 kV)

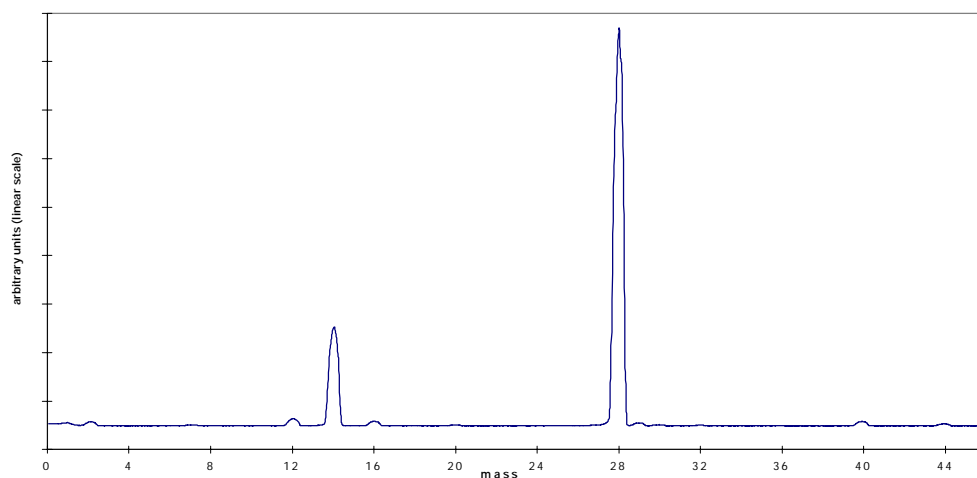


Figure 47; Molecular nitrogen,  $14 \rightarrow N^+$ ,  $28 \rightarrow N_2^+$ ,  $14/28 = 0.25$

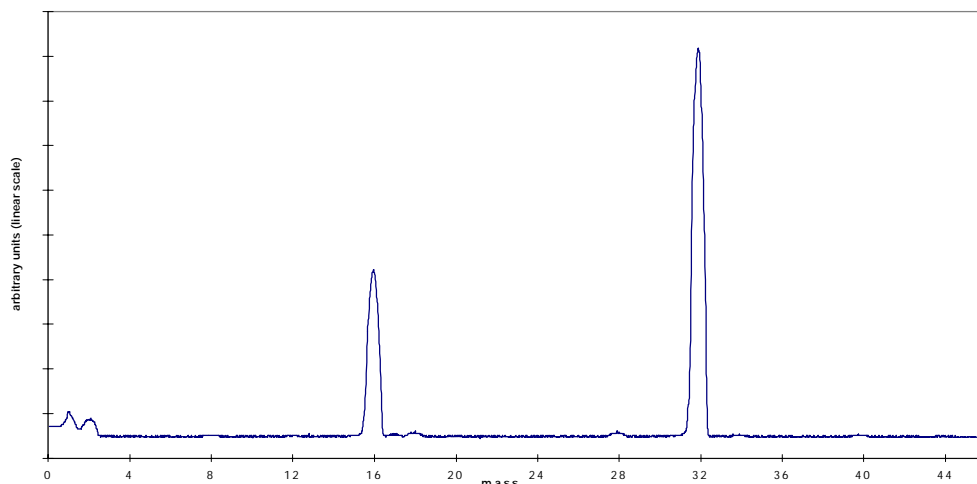


Figure 48; Molecular oxygen,  $16 \rightarrow O^+$ ,  $32 \rightarrow O_2^+$ ,  $16/32 = 0.41$

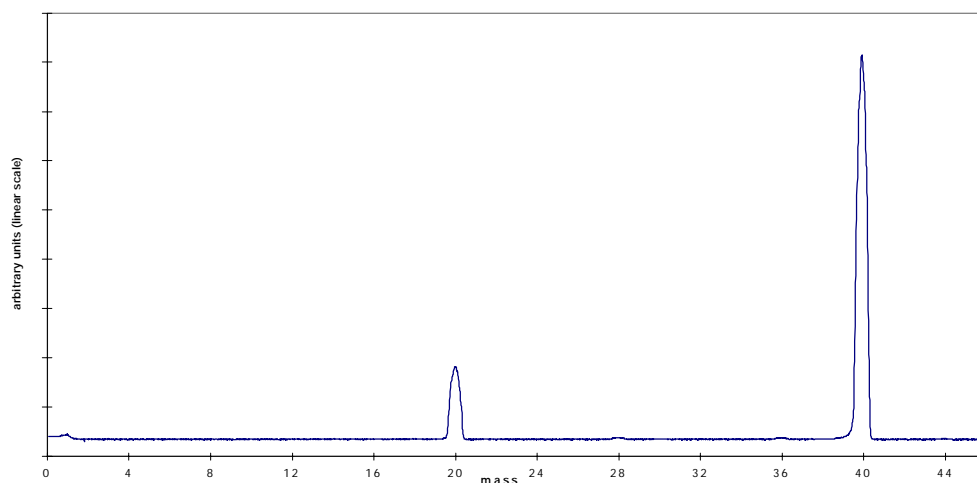


Figure 49; Argon,  $20 \rightarrow Ar^{++}$ ,  $40 \rightarrow Ar^+$ ,  $20/40 = 0.19$

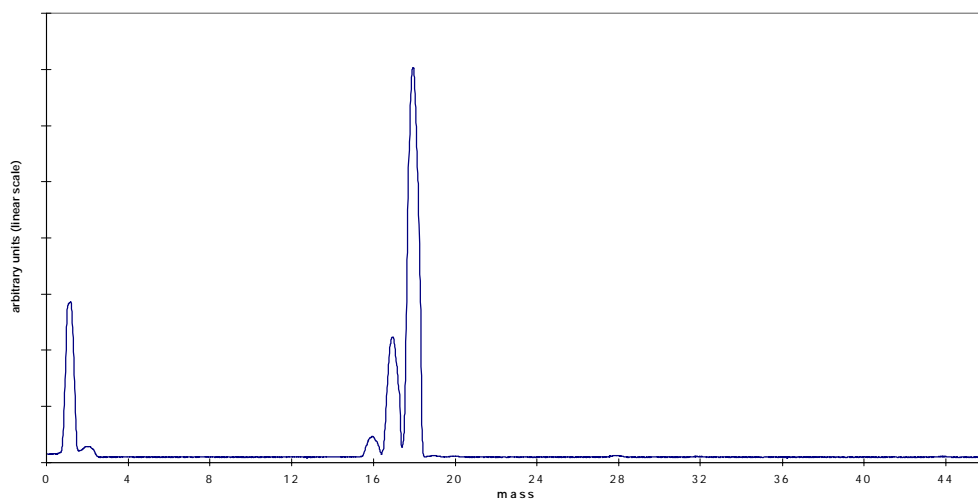


Figure 50; Water vapour,  $1 \rightarrow H^+$ ,  $16 \rightarrow O^+$ ,  $17 \rightarrow OH^+$ ,  $18 \rightarrow H_2O^+$ ,  $1/18 = 0.41$ ,  $16/18 = 0.05$ ,  $17/18 = 0.30$

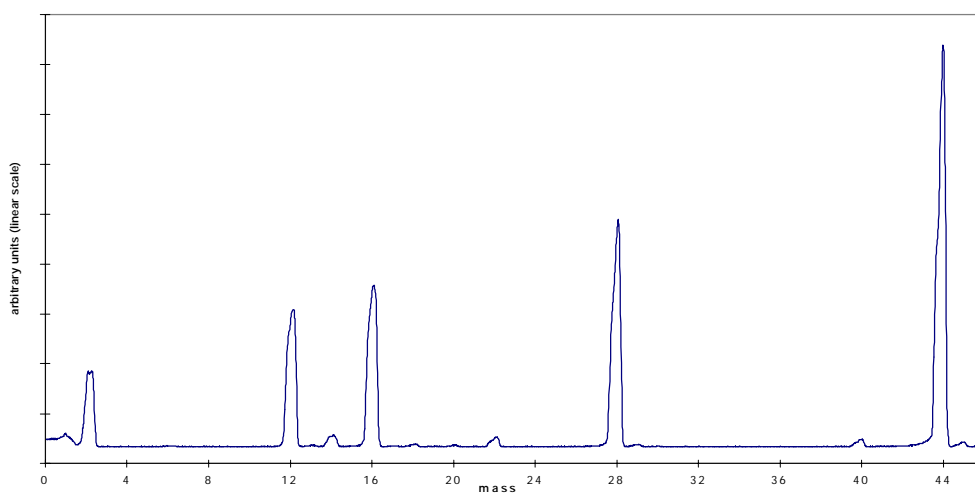


Figure 51; Carbon dioxide,  $12 \rightarrow C^+$ ,  $16 \rightarrow O^+$ ,  $22 \rightarrow CO^{++}$ ,  $28 \rightarrow CO^+$ ,  $44 \rightarrow CO_2^+$ ,  $12/44 = 0.35$ ,  $16/44 = 0.40$ ,  $28/44 \approx 0.5$  (The residual gas contains not only  $CO_2$  but also hydrogen, nitrogen and argon. The peak 28 represents besides  $CO^+$  also  $N_2^+$  and hence the ratio  $28/44$  is not well defined.)

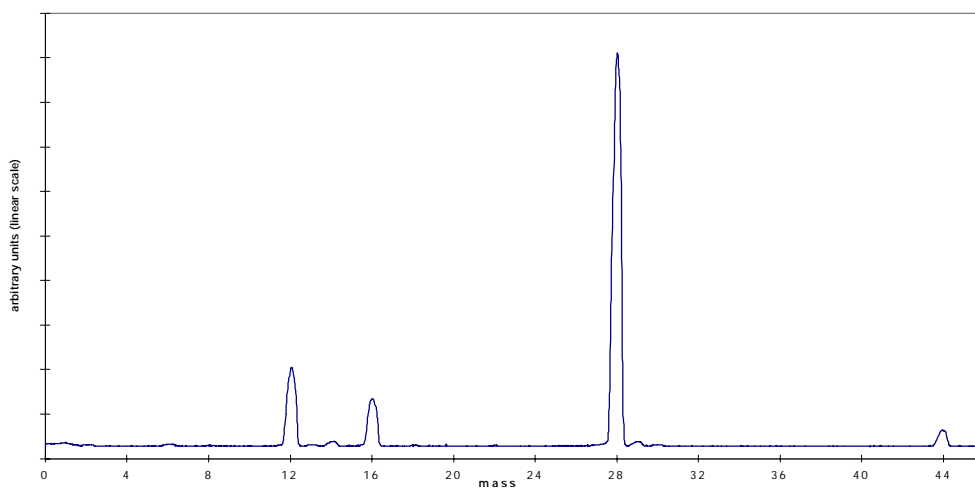


Figure 52; Carbon monoxide,  $12 \rightarrow C^+$ ,  $16 \rightarrow O^+$ ,  $28 \rightarrow CO^+$ ,  $12/28 = 0.18$ ,  $16/28 = 0.13$

The SEY of copper which was exposed to air at 350°C (thick oxide layer) compared with the SEY of copper as received (thin oxide layer) as a function of the primary electron energy after different times of air exposure

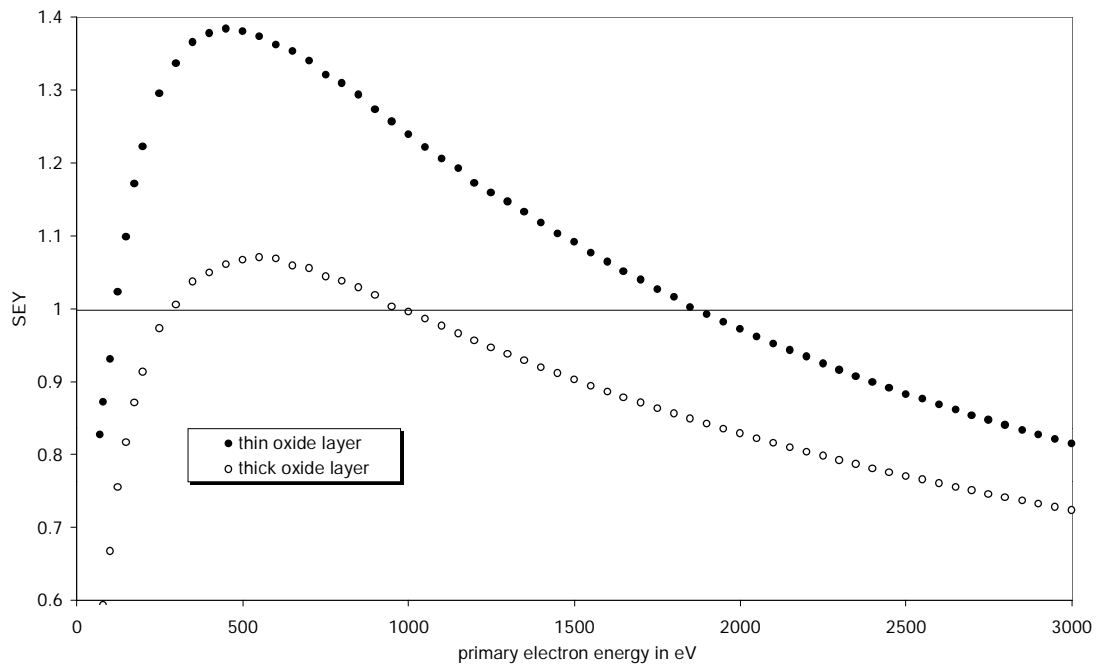


Figure 53; After a 24 hours 350°C bakeout

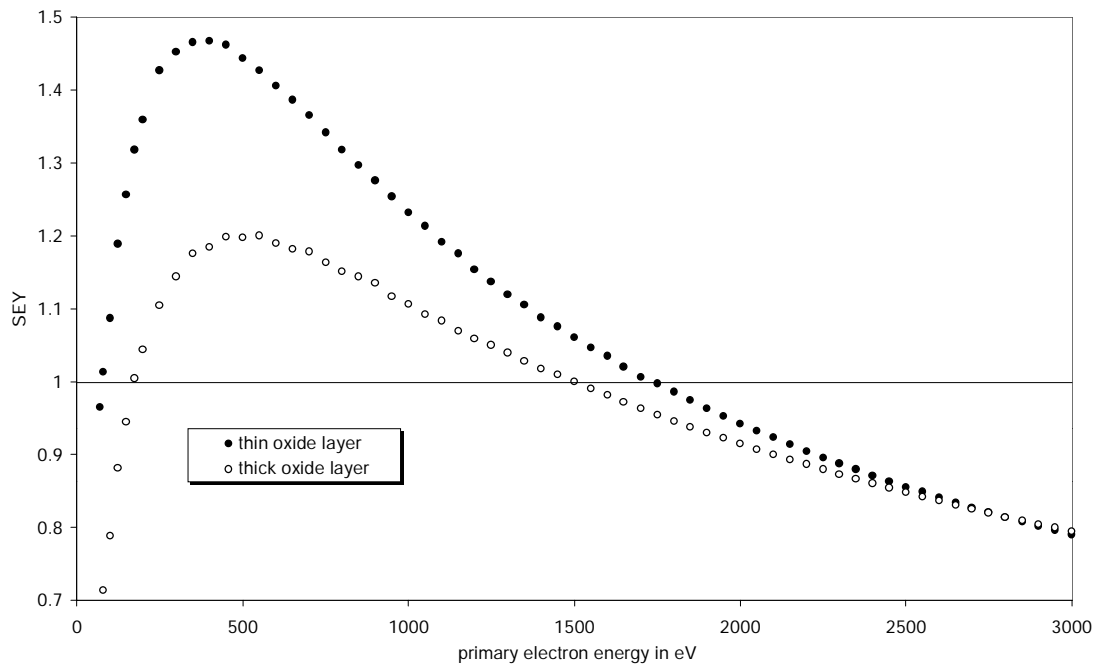


Figure 54; After 30 minutes air exposure

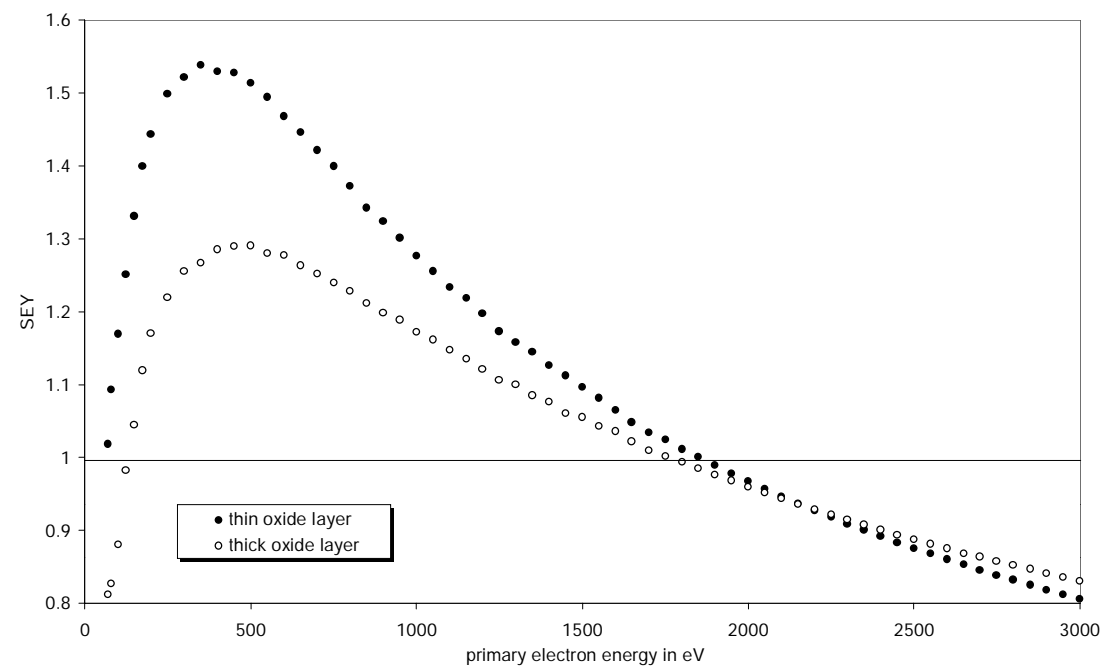


Figure 55; After 90 minutes air exposure

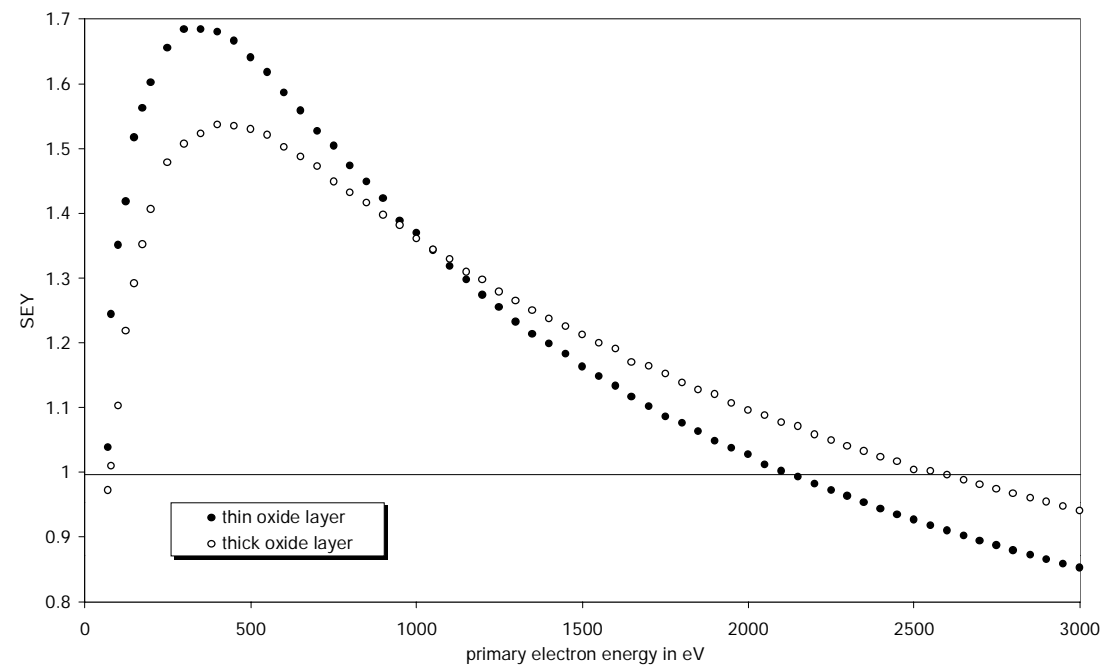


Figure 56; After 4 hours air exposure

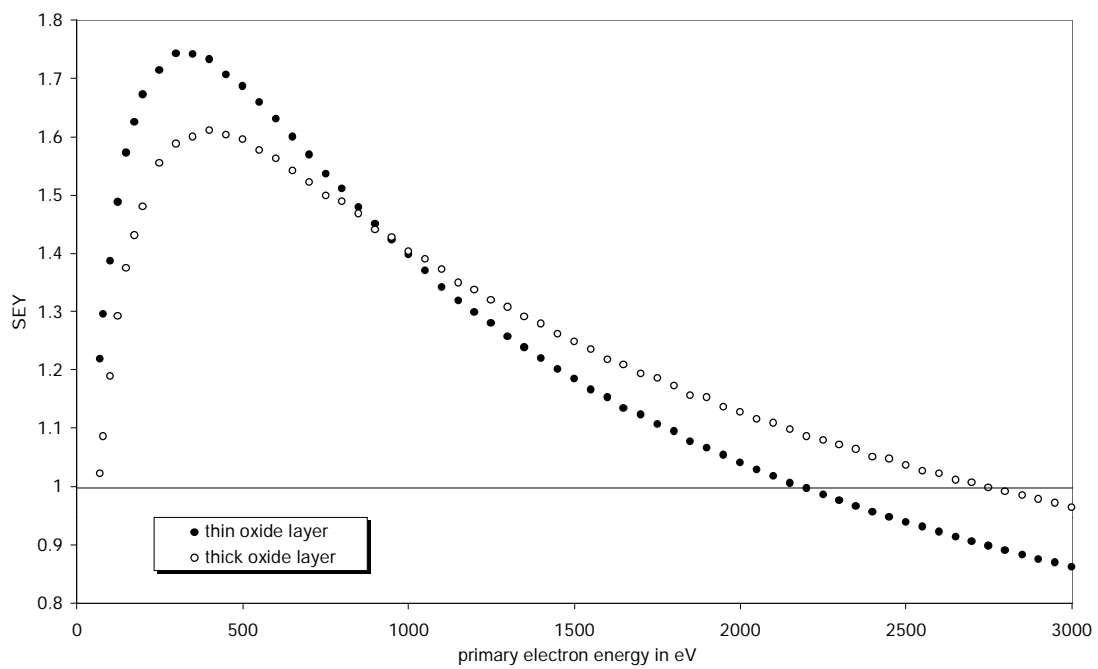


Figure 57; After 8 hours air exposure

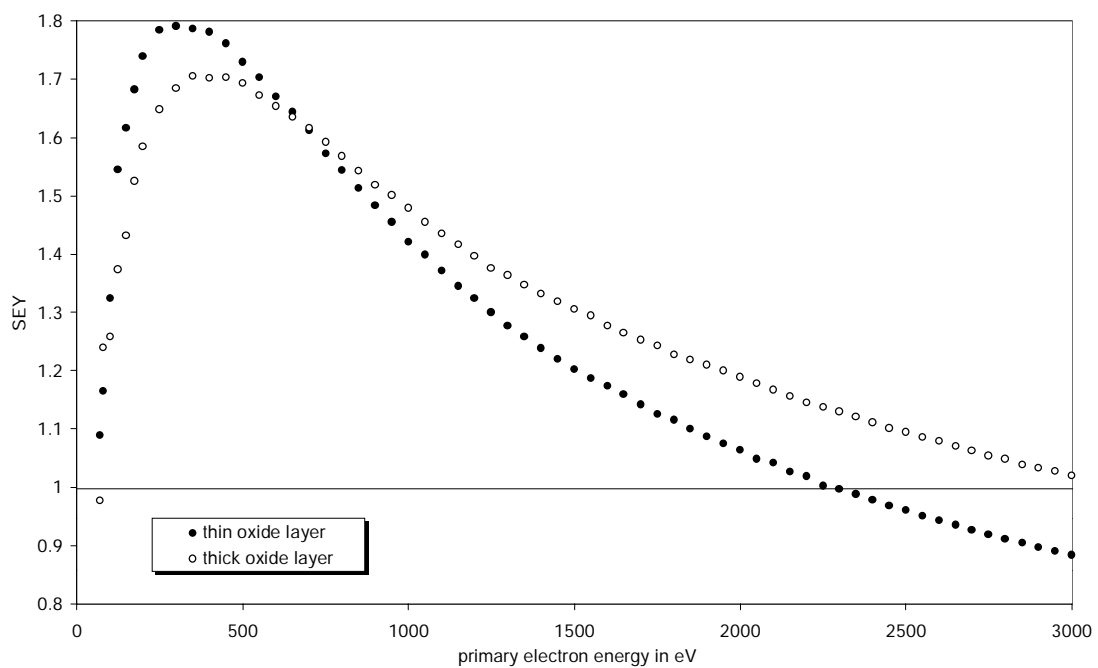


Figure 58; After 19 hours air exposure



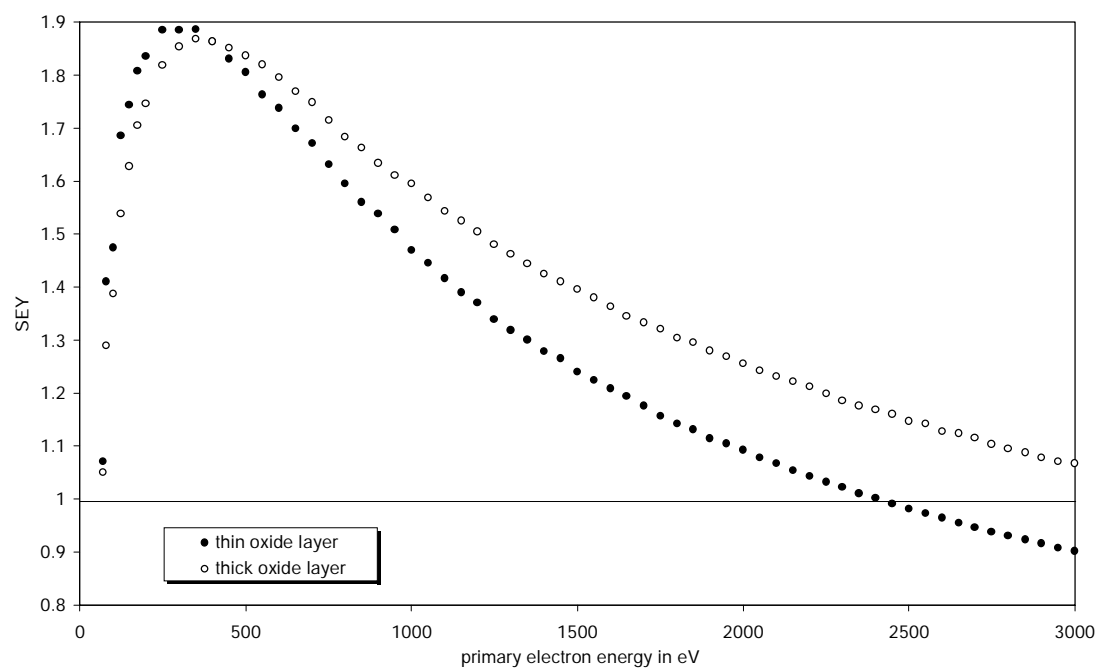


Figure 59; After 42 hours air exposure

## Acknowledgments

I wish to thank Professor Bernd Schiewe from the TFH-Berlin for the supervision of this work.

All experimental work was carried out at the European Laboratory for Particle Physics (CERN) in Geneva and I would like to thank CERN, especially the members of the LHC-vacuum group, for the hospitality and assistance. In particular the help of Jouri Bojko was mostly appreciated.

The Auger analysis of the samples was done by Daniel Latorre from the EST-SM group. Mircea Stirbet from the SL-RF group was responsible for the pre-conditioning of the LEP2 power couplers. I am grateful for his explanations and that he did the test so quickly that the results could be included in this work.

The imaging and the EDX-analysis of the samples were carried out at the Labor für Elektronenmikroskopie of the TFH-Berlin where Jürgen Landskron was a helpful adviser.

I am also thankful to my brother Karl-Martin, Neil Fox and Jean-Luc Dorier for their interest and constructive comments on the manuscript.

Finally, I very much like to thank my supervisor at CERN, Noël Hilleret for his support.

Hiermit versichere ich, daß ich die Diplomarbeit selbständig verfaßt habe und keine anderen als die hier angegebenen Quellen und Hilfsmittel benutzt habe.

Genf, den 10. Februar 1997